THE UNIVERSITY OF CHICAGO

SELF-ORGANIZATION OF THE FISSION YEAST ACTIN CYTOSKELETON

A DISSERTATION SUBMITTED TO
THE FACULTY OF THE DIVISION OF THE BIOLOGICAL SCIENCES
AND THE PRITZKER SCHOOL OF MEDICINE
IN CANDIDACY FOR THE DEGREE OF
DOCTOR OF PHILOSOPHY

GRADUATE PROGRAM IN CELL AND MOLECULAR BIOLOGY

BY
KAITLIN ELISE HOMA

CHICAGO, ILLINOIS
JUNE 2019

Table of Contents

List of Figures

List of Tables

ACKNOWLEDGMENTS

It would have been impossible to complete my PhD without a phenomenal supporting cast. First, I would like to thank David Kovar for his fantastic mentorship and for creating a fun and collaborative lab environment. I cannot emphasize enough how much I enjoyed going to lab every day, which greatly enhanced my graduate school experience. Many thanks also to past and present members of the Kovar lab: Caitlin Anderson, Rachel Brown, Tom Burke, Jenna Christensen, Alyssa Harker, Glen Hocky, Rachel Kadzik, Yujie Li, Patrick McCall, Alisha Morganthaler, Meghan O'Connell, Cristian Suarez, Jon Winkelman, and Dennis Zimmermann. It was a pleasure to work alongside so many hardworking and innovative scientists, and our lively discussions about the minutiae of actin were my favorite part of graduate school. We went on countless adventures over the years and I'm happy to have made so many friends along the way. I would specifically like to thank Jenna Christensen for paving the way for my projects, her guidance and willingness to train me, and her support and friendship during my time in Chicago and beyond, as well as Cristian Suarez for sharing his wisdom during what seemed like daily discussions about my projects. Thanks also to Ashley Rich for being an exemplary member of the graduate student community and for her companionship and support every step of the way. Finally, thanks to Kristine Gaston for keeping me on track for six years.

I am very fortunate to also have a strong support system outside of lab. Thanks to my parents, Mike and Betsy Homa, for their unconditional and enduring support from day one. I definitely would not be here without the support of Dylan Richter, who provides me with endless encouragement and entertainment every single day. I would also like to thank his family, who has always treated me like one of their own, as well as all of my friends, near and far, who have supported me along the way.

PREFACE

This dissertation is a compilation of three distinct manuscripts. Chapter 2, "Cooperation between tropomyosin and α-actinin inhibits fimbrin association with actin filament networks in fission yeast," was recently resubmitted to *eLife*. Additional contributors to Chapter 2 are Jenna R. Christensen, Alisha N. Morganthaler, Rachel R. Brown, Cristian Suarez, Alyssa J. Harker, Meghan E. O'Connell, and David R. Kovar. The manuscripts that make up Chapters 3 and 4 are currently in preparation. Additional contributors to Chapter 3, "Arp2/3 complex- and formin-mediated actin networks tune actin-binding protein sorting in fission yeast," are Cristian Suarez, Glen M. Hocky, and David R. Kovar. Additional contributors to Chapter 4, "Formin Cdc12's specific actin assembly properties are tailored for cytokinesis in fission yeast," are Erin M. Neidt, Tamara C. Bidone, Vilmos Zsolnay, Gregory A. Voth, and David R. Kovar. Prefaces at the beginning of each chapter indicate the specific work performed by the contributors listed above.

ABSTRACT

The actin cytoskeleton is a large and dynamic network that mediates many important cellular processes, including polarity, endocytosis, motility, and cytokinesis. In an extremely crowded cytoplasm, cells must simultaneously assemble multiple distinct filamentous actin (F-actin) networks with the proper architecture and dynamics at the correct time and place. How a cell initiates and maintains these distinct F-actin structures to drive essential cellular functions is a fundamental question in cell biology. In cells, actin assembly factors initiate F-actin assembly from monomeric globular actin subunits (G-actin). The organization of these filaments into higher-order networks with specific architectures and dynamics is regulated by the coordinated efforts of actin-binding proteins (ABPs) that nucleate, crosslink, sever, stabilize, and cap actin filaments. Therefore, the accurate localization of particular ABPs to specific F-actin networks is paramount, as the identity of each F-actin network is defined by the subgroup of ABPs with which it associates. However, the mechanistic principles guiding the sorting of ABPs to distinct F-actin networks remain largely unclear.

Previous work from our lab revealed that competitive and cooperative interactions between ABPs drive their sorting to specific F-actin networks in fission yeast. In particular, fimbrin, a crosslinking protein found in actin patches, competes with tropomyosin, a side-binding protein that localizes to the contractile ring, for binding F-actin both in vitro and fission yeast cells [27, 162]. Here, we investigated other potential competitive interactions between ABPs by conducting a survey in fission yeast. We discovered a competitive interaction between fimbrin and α-actinin, a bundling protein found in the contractile ring. Fimbrin and α-actinin compete for binding F-actin *in vitro*, in actin patches, and in the contractile ring in fission yeast cells. Additionally, tropomyosin synergizes with α-actinin to inhibit fimbrin's association with F-actin.

While competitive and cooperative interactions between ABPs certainly tune their sorting to distinct F-actin networks, how ABP sorting is initially established is currently un-

known. Our longstanding hypothesis is that actin assembly factors build actin filaments with specific characteristics that are preferred by certain ABPs, thereby recruiting them to particular F-actin networks and triggering the cascade of ABP sorting. We used fluorescence microscopy in fission yeast and *in vitro* reconstitution to investigate how actin assembly factors Arp2/3 complex and formin Cdc12 influence the localization of ABPs fimbrin and tropomyosin. We show that in fission yeast, fimbrin is preferentially recruited to actin patches (assembled by Arp2/3 complex), while tropomyosin prefers to localize to the contractile ring (assembled by formin Cdc12). Interestingly, we also see that actin filaments assembled by different actin assembly factors are not sufficient to induce ABP sorting *in vitro*. Instead, F-actin with distinct architectures and competition between ABPs are both necessary to recapitulate fimbrin's preferred association with Arp2/3 complex-mediated actin filaments and tropomyosin's localization to formin Cdc12-generated F-actin.

In addition to driving ABP sorting, formins generate straight actin filaments that regulate fundamental processes such as cell division and polarity. While formins assemble F-actin via a well-conserved molecular mechanism, diverse cell types require many distinct formin isoforms to carry out specific cellular functions. Therefore, we sought to understand whether a specific formin is tailored for a particular cellular role by its actin assembly properties. We engineered formin chimera fission yeast strains in which the actin assembly domains of the contractile ring formin Cdc12 were replaced by the actin assembly domains of functionally diverse formins. These formin chimeras produce viable cells, but exhibit a range of cytokinesis defects and delays in contractile ring assembly. We determined that formin chimeras with nucleation efficiencies similar to Cdc12 are generally less defective in cytokinesis than those that are poor F-actin nucleators. Additionally, we used a computational model to isolate specific formin actin assembly properties and found that the probability and timing of contractile ring formation are both critically impacted by variations in formin nucleation efficiency.

CHAPTER 1

INTRODUCTION

1.1 The importance of cellular self-organization

Cells come in all shapes and sizes and are composed of a complex and rapidly diffusing mixture of proteins, nucleic acids, lipid vesicles, and other molecules that are organized into large, dynamic structures such as membrane-bound compartments and organelles, protein assemblies, and phase-transitioning droplets. Despite the vast number of component parts, cells exhibit remarkable stability and organization. How these macroscopic cellular structures are built and maintained remains a fundamental question in cell biology, but it is clear that organization of a cell's interior is paramount for the successful completion of essential cellular processes. For example, cell division relies on the equal distribution of cellular components to two daughter cells, while membrane trafficking involves the transport of cargo across long distances throughout the cell. Different cell types display distinct morphological features and can range from 300 nm (*Mycoplasma*, the smallest bacterial cell [145] to several inches in diameter (the giant coenocyte *Caulerpa taxifolia* [144]), but the scale of individual cellular components is much smaller. Given this difference in scale, how do cells achieve organization at the whole cell level?

Two general and very different principles exist to describe how macromolecular cellular components are generated: self-assembly and self-organization [82, 115]. Self-assembly is a spontaneous process that involves the physical interactions of molecules into a static equilibrium structure [93]. A well-studied example of self-assembly is the formation of viral capsids and bacteriophages from protein components via protein-protein interactions. A hallmark of self-assembly is that the resulting structure is stable, exhibiting little exchange of matter or energy with the environment. In contrast, self-organization in cell biology is defined as the capacity of a macromolecular structure, such as an organelle, to determine its own

structure based on the physical interactions of its component parts [115]. For a process to be considered self-organization, it must meet three main criteria: 1) the resulting cellular structure must be dynamic, 2) the cellular structure must exchange matter and energy with its environment, and 3) a generally stable, steady-state configuration must be produced from dynamic component parts [115]. Self-organization is a general phenomenon that plays an important role in life sciences as well as chemistry and material sciences. In cell biology, self-organization is responsible for biogenesis of the nucleolus, generation of polarized stacks of Golgi membranes, and assembly of the actin and microtubule cytoskeletons.

This dissertation will focus on the assembly and maintenance of the actin cytoskeleton, which fulfills all the requirements of a self-organizing system. First, the actin cytoskeleton is extremely dynamic, with actin filaments constantly growing, disassembling, and undergoing turnover. Dynamic actin filaments also build more stable, higher order networks that continually exchange actin subunits and associated proteins with the cytoplasm. A fundamental question in cell biology is how a single basic actin cytoskeletal building block can generate many structurally and functionally diverse actin networks, and the key to understanding this phenomenon lies in its ability to self-organize. The actin cytoskeleton plays a central role in determining cell shape and polarity, providing structural support, and mediating essential cellular processes such as cell division and motility, revealing the physiological relevance of actin cytoskeleton self-organization. Here, we study the assembly and dynamics of actin cytoskeleton self-organization in the fission yeast *Schizosaccharomyces pombe*, as it has a simplified actin cytoskeleton with a limited number of component parts.

1.2 Assembly of actin filament networks

1.2.1 Actin

Actin is one of the most well-conserved and abundant proteins across diverse life forms, accounting for over 10% of total protein in many cell types. Archaea, bacteria, and eukaryotes all utilize actin molecules that are structurally similar and functionally related [58]. Many multicellular organisms, including humans and plants, express multiple actin genes that encode actin isoforms specialized for different functions in specific tissues. In contrast, some single-celled eukaryotes, such as budding yeast and fission yeast, produce one actin protein from a single actin gene that assembles all of the actin networks necessary to support life. The extreme conservation of the actin gene family can be attributed to constraints imposed by the self-association of actin to form polymers as well as its association with many binding partners. As a central player in many essential cellular functions, actin engages in more protein-protein interactions than any other known eukaryotic protein [58].

The fundamental building block of the actin cytoskeleton is the globular actin monomer (G-actin), a 375-residue polypeptide that folds into a flat protein with four subdomains. Actin monomers also contain a medial nucleotide-binding cleft that binds adenosine triphosphate (ATP), ADP-Pi, or adenosine diphosphate (ADP) (Figure 1.1A) [168]. However, in the cytoplasm, the vast majority of G-actin is tightly bound to ATP. Actin monomers spontaneously polymerize under physiological conditions to form dynamic actin filaments (F-actin) (Figure 1.1B). F-actin polymerization begins with a lag period due to the rate-limiting nucleation step, where multiple actin monomers must come together to form stable oligomers [31, 46, 155]. This lag arises from the formation of actin dimers and trimers, which are energetically unstable and dissociate quickly (Figure 1.2A). Once a stable nucleus is formed, G-actin adds to both ends of the filament, albeit at different rates. F-actin elongation occurs preferentially at the fast-growing barbed end of the filament ($k+ = 11.6\ \mu M^{-1}s^{-1}$) compared

to the slower-growing pointed end (k+ = 1.3 $\mu M^{-1}s^{-1}$) [138], generating polar actin filaments (Figure 1.1B). The conformational changes associated with addition of actin monomers to the growing filament promotes ATP hydrolysis, leading to ADP-Pi and later ADP after slow phosphate release [22]. ADP-actin dissociates more easily from both filament ends, thereby completing the F-actin growth cycle.

While F-actin assembles spontaneously in a test tube, cellular actin behaves quite differently. Cytoplasmic actin concentrations range from ~50-200 μM, approximately half of which remains unpolymerized at any given time. Thus, the concentration of cellular G-actin greatly exceeds the critical concentration necessary for F-actin assembly. However, most cytoplasmic unpolymerized actin is bound to profilin [78], a small monomer-binding and sequestering protein that sterically inhibits F-actin nucleation but allows monomer addition at the barbed end of existing filaments [140, 141]. Profilin is just one example of an actin-binding protein (ABP) that regulates the polymerization of cellular actin and controls actin assembly in time and space. Many additional ABPs work together to maintain a cytoplasmic pool of G-actin, nucleate and elongate F-actin, and build higher order actin networks by crosslinking, severing, stabilizing, and capping actin filaments.

1.2.2 Actin assembly factors

To overcome cellular mechanisms that prevent spontaneous F-actin nucleation, actin assembly factors are targeted to specific subcellular sites to restrict actin assembly in time and space. The three main classes of eukaryotic actin assembly factors are discussed in more detail below.

1.2.2.1 Arp2/3 complex

The actin-related protein-2/3 (Arp2/3) complex is an evolutionarily ancient complex of seven protein subunits that is essential in many eukaryotes. Two subunits, actin-related proteins

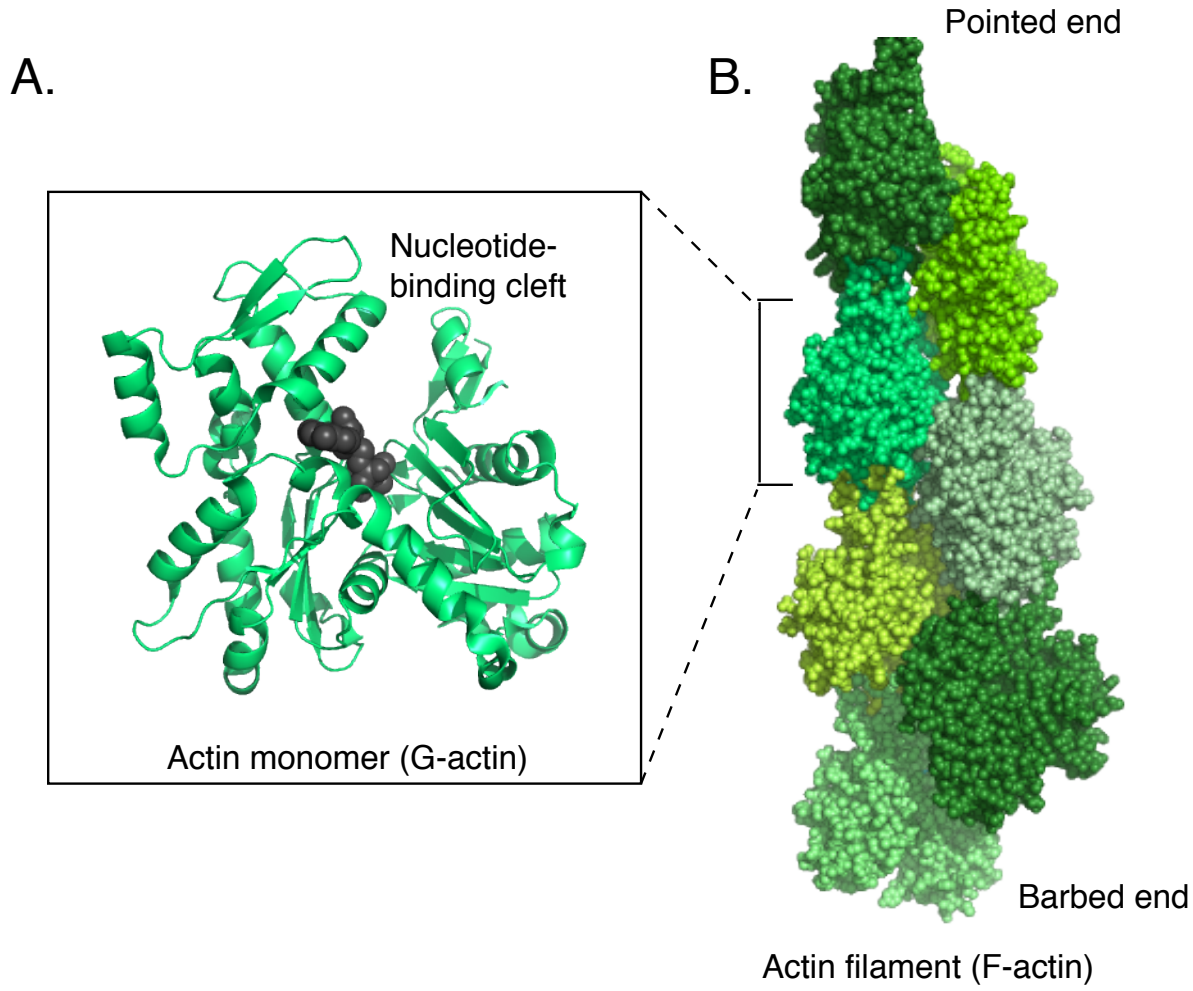

Figure 1.1: **Actin monomers (G-actin) polymerize to form actin filaments (F-actin). (A)** Structure of a globular actin monomer (PDB: 1NWK) with the nucleotide-binding cleft in the ATP-bound state (grey). **(B)** G-actin polymerizes to form a polar actin filament (PDB:6BNO) with a slow-growing pointed end and a fast-growing barbed end.

2 and 3 (Arp2 and Arp3), closely resemble actin monomers and mimic an actin dimer [119]. To nucleate F-actin, Arp2/3 complex binds to the side of an existing actin filament (the mother filament), where Arp2 and Arp3 act as a seed for new filament growth (the daughter filament). Arp2/3 complex anchors the pointed end of the daughter filament while the barbed end is free to grow, creating a branch at a fixed angle of 70 degrees to the mother filament (Figure 1.2B) [55].

Arp2/3 complex is inherently inactive and must be activated by a nucleation-promoting factor (NPF) prior to branch formation. Different families of NPFs activate Arp2/3 complex depending on the subcellular context [150], the most well-studied of which is the Wiscott-Aldrich Syndrome Protein (WASP) family that includes WASP, N-WASP, SCAR/WAVE, and WASH [92]. Two models have been proposed to describe the mechanism by which NPF activation leads to Arp2/3 complex-mediated F-actin nucleation. First, the NPF could add a third actin monomer to the Arp2/Arp3 dimer mimic to stabilize the nucleus [106, 36]. Alternatively, nucleation could be stimulated by a conformational change in Arp2/3 complex induced by the NPF [55]. The dense, branched actin filaments generated by Arp2/3 complex are tailored for force generation, optimizing them to push the membrane forward in the lamellipodium at the leading edge of motile cells and promote the internalization of vesicles at sites of endocytosis [172, 187]. Additionally, Arp2/3 complex-mediated nucleation is often exploited by pathogens that express NPFs on their surface to hijack the host's F-actin and facilitate their cell-to-cell spreading [183].

1.2.2.2 Formin

Formins are a large, highly conserved family of multidomain proteins that associate with the barbed end of F-actin. Formins are widely expressed and most eukaryotic species express multiple formin isoforms that often mediate specific cellular processes in distinct cell types. All formins are characterized by their formin homology 1 and 2 (FH1 and FH2) domains

[137]. The FH2 domain homodimerizes to form a donut-shaped structure that nucleates actin filaments *de novo* (Figure 1.2C), presumably by interacting with and stabilizing F-actin intermediates (G-actin dimers and trimers) [17]. After filament nucleation, FH2 dimers maintain processive association with the growing barbed end of the filament, while the FH1 domain "arms" contain polyproline-rich regions that bind profilin-actin to facilitate addition of G-actin to the barbed end [136] (Figure 1.4). Many formins use this mechanism to increase the F-actin elongation rate far beyond that of actin alone.

In addition to the FH1FH2 domain that mediates actin assembly, formins contain less well-conserved regulatory and localization domains [23]. Many formins are autoinhibited by an interaction between their Diaphanous inhibitory domain (DID) and Diaphanous autoregulatory domain (DAD), and this autoinhibition is released upon binding of the DID to a Rho family GTPase [3, 101, 132, 133]. Interestingly, while all formins utilize the same general mechanism to assemble F-actin, their *in vitro* actin nucleation, elongation, and association rates vary widely [154]. Some formins also exhibit additional behaviors, such as F-actin bundling and depolymerization [59]. In contrast to Arp2/3 complex, formins elongate longer, unbranched actin filaments that are suited for contractile actin networks such as the contractile ring and stress fibers, as well as actin networks under tension. More recently, formins have also been implicated in actin-microtubule crosstalk [12, 65].

1.2.2.3 WH2 domain-containing nucleators

WASP homology 2 (WH2) domain-containing nucleators are a more recently discovered and less well-understood class of actin nucleators that nucleate actin filaments by a variety of different mechanisms and have distinct cellular functions. The WH2 domains within these proteins contain an actin monomer-binding motif that mediates F-actin nucleation and sometimes elongation [142]. For example, Spire proteins, present in higher eukaryotes and characterized in *Drosophila*, contain four WH2 domains that each bind an actin monomer

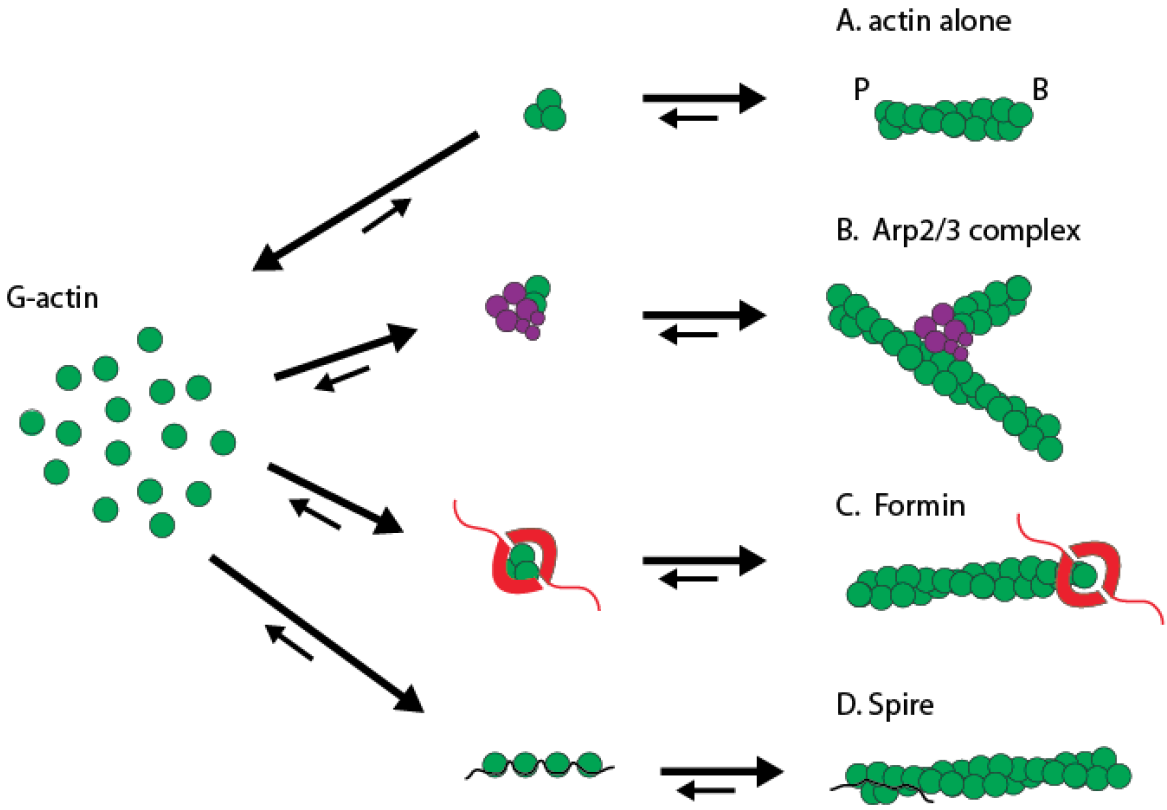

Figure 1.2: **Mechanisms of F-actin nucleation.** Pathways to F-actin nucleation. **(A)** Spontaneous F-actin nucleation is energetically unfavorable because G-actin dimers and trimers are unstable. **(B)** The Arp2/3 complex mimics an actin nucleus to template new filament growth as a branch from an existing filament. **(C)** Formins nucleate and stabilize actin nuclei and elongate straight actin filaments by maintaining a processive association with the F-actin barbed end. **(D)** Spire proteins associate with four actin monomers via four tandem WH2 domains to build a scaffold for polymerization of an unbranched actin filament.

to generate a G-actin string that elongates to form an actin filament [143] (Figure 1.2D). Additionally, Cobl is a vertebrate-specific nucleator that arranges its three WH2 domains to form a nucleus of three actin monomers, but the exact mechanism by which Cobl carries out its biological function is unclear [2]. What is clear is that F-actin nucleation via WH2 domains is an effective way to generate actin filaments, thus it is unsurprising that this method has been adopted by pathogens. Recent evidence suggests that bacterial effectors such as VopL and VopF use WH2 domains to directly nucleate actin filaments in order to disrupt the host cytoskeleton [151]. Understanding the mechanisms behind F-actin nucleation by WH2 domain-containing proteins will be critical in combating infection by these bacterial pathogens.

1.3 Regulation of F-actin network assembly in space and time

While much is understood about how actin assembly factors function on a mechanistic level, how these assembly factors are regulated to assemble F-actin at the correct time and place with the proper size and architecture remains unclear. Arp2/3 complex and formin are both intrinsically inactive and must associate with upstream activators prior to F-actin assembly. Therefore, it has been largely accepted that upstream signalling cascades activate assembly factors at specific times and places, thereby controlling where and when actin is assembled [60]. As was previously mentioned, the upstream activator of Arp2/3 complex is often a WASP family NPF, which itself is activated by a Rho GTPase [100, 174]. Formin autoinhibition is also relieved by direct interaction with a Rho GTPase [182, 132]. Though activation of actin assembly factors by GTPases at the right time and place is important for generating F-actin, it has recently become clear that signalling cascades alone are not sufficient to generate diverse actin networks at the correct time and place within a crowded cytoplasm.

1.3.1 Assembly factors compete for actin monomers

Previous work from our lab supports an updated model for actin network regulation, whereby competition between diverse actin networks for a limited pool of actin monomers influences the density and size of each network [19, 170, 171]. If homeostatic actin networks compete for G-actin, one prediction is that disruption of one actin network will lead to a corresponding increase in actin monomer consumption by the remaining F-actin networks. In support of this model, numerous studies over the last decade report that modification of the amount of actin in a single actin network affects the size and density of other actin structures [19, 170, 52, 184, 75]. In particular, treatment of fission yeast cells with the Arp2/3 complex inhibitor CK-666 depletes actin patches, leading to a 20-fold increase in the amount of "ectopic" actin incorporated into formin-mediated actin structures [19]. Similarly, consumption of G-actin by Arp2/3 complex is increased by 50% following the genetic inhibition of both fission yeast formins and disappearance of all formin-mediated actin networks [19]. Additionally, increasing the amount of cytoplasmic G-actin results in a greater number of Arp2/3 complex-mediated actin patches but not an increased patch size, indicating that other factors must be involved in regulating F-actin network size. Competition for G-actin has been shown to play a role in other systems as well, as Arp2/3 complex competes with actomyosin systems in epithelial cells [104]. In this case, pharmacological inhibition of non-muscle myosin II with blebbistatin leads to a 50% increase in the concentration of cytoplasmic G-actin, which is quickly incoporated into Arp2/3 complex-mediated branched networks at the leading of the cell to stimulate spontaneous polarity and migration [104].

If F-actin networks compete for a limited pool of G-actin, there must be cellular mechanisms in place to tune this competition to spatially and temporally favor distribution of actin monomers to specific actin networks. In fission yeast cells, 50% of cellular actin is incorporated into Arp2/3 complex-mediated actin patches, which is not surprising given that fission yeast expresses 15-fold more Arp2/3 complex molecules than formin molecules [159, 19, 191].

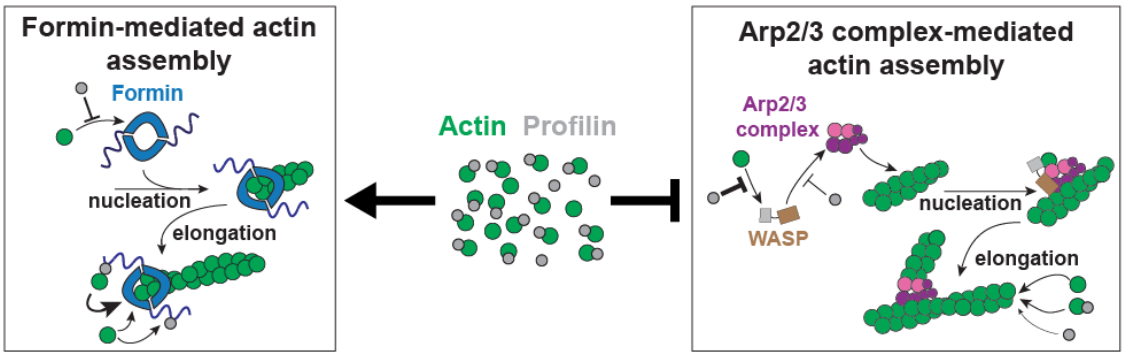

Figure 1.3: **Profilin mediates internetwork competition for G-actin.** Cartoon illustrating how profilin promotes formin-mediated actin assembly and inhibits Arp2/3 complex activity. Adapted with permission from [170].

Thus, a small number of formins must compete with numerous Arp2/3 complexes to assemble actin cables and the contractile ring. As mentioned previously, the monomer-binding protein profilin enhances formin-mediated actin assembly by binding to the proline-rich formin FH1 domain and facilitating monomer addition to the barbed end (Figure 1.3) [148, 90, 89]. More recently, profilin has been implicated as an inhibitor of Arp2/3 complex activity, as it competes with Arp2/3 complex activators for association with actin monomers [170, 152], decreasing the rate at which Arp2/3 complex can nucleate branched filaments in both fission yeast and mammalian cells (Figure 1.3). Thus, profilin acts as a molecular switch that mediates internetwork competition. In accordance with this model, overexpression of profilin favors the formation of formin-mediated contractile rings [19, 170]. The regulation of profilin localization and/or activity is likely important for controlling the balance between Arp2/3 complex- and formin-mediated F-actin networks in fission yeast and beyond.

1.4 Actin-binding proteins regulate F-actin assembly and organization into higher-order networks

Localization of actin assembly factors to specific subcellular compartments confines F-actin assembly in time and space. However, higher-order actin networks are composed of more than just actin filaments. Actin-binding proteins (ABPs) work together to define the characteristics of each network by modulating how actin filaments interact with one another as well as their size, organization, structure and flexibility [139]. The aforementioned actin monomer-binding protein profilin is just one example of an ABP that plays a pivotal role in regulating F-actin assembly. There are hundreds of eukaryotic ABPs that are responsible for crosslinking, severing, bundling, capping, and depolymerizing actin filaments (Figure 1.4). These ABPs can be divided into groups based on their function, so I will focus on the four types of ABPs most relevant to this work.

1.4.1 Crosslinking proteins

Crosslinked actin filaments are an integral feature designed to stabilize and provide rigidity to virtually all higher-order F-actin networks, including filopodia [87], stress fibers [69], actin patches [197], lamellipodia [164], and the contractile ring. While some formins and other proteins not canonically known as crosslinking proteins can create linkages between actin filaments, most of these direct associations are mediated by ABPs belonging to the crosslinking/bundling protein family. While the term "crosslinker" is a catch-all term that describes any protein that mediates a physical connection between actin filaments, many crosslinkers can also be classified as bundlers, which create multiple connections between two parallel actin filaments. For the sake of simplicity, I will use the terms crosslinking and bundling interchangeably, even though some crosslinking proteins are not considered to be bundling proteins.

Crosslinking proteins mediate physical linkages between actin filaments by binding multiple filaments simultaneously (Figure 1.4). Some crosslinkers, including α-actinin and spectrin, accomplish this task through dimerization of two monomers that each contain a single actin-binding domain [108, 179, 160, 193]. In contrast, fimbrin and fascin are examples of bundling proteins that contain multiple actin-binding modules in each molecule [108, 11]. This dissertation will focus on two well-characterized bundling proteins in fission yeast, fimbrin and α-actinin. Fimbrin crosslinks short, branched filaments in actin patches to form the dense F-actin network required to mediate endocytic vesicle internalization, while α-actinin localizes to the contractile ring and serves as a dynamic bundling protein that allows F-actin sliding throughout contractile ring assembly and constriction.

1.4.2 Filament side-binding proteins

Actin filament side-binding proteins serve as "gatekeepers" that can dictate how other ABPs access specific actin networks [58]. Tropomyosin is a well-characterized, coiled-coil side-binding protein that binds head-to-tail with other tropomyosin molecules to form a polymer along the length of actin filaments [61]. Tropomyosin is best known for its role in regulating contraction of skeletal muscle, where it facilitates the coordinated movement of myosin heads [53, 99, 165]. However, tropomyosin is also important for actin network organization in other cell types. Mammals express over 40 tropomyosin isoforms that localize to specific subcellular compartments to mediate how ABPs, in particular cofilin and myosin, access specific F-actin networks [37, 131, 167]. Fission yeast expresses a single tropomyosin gene, *cdc8*, that produces two protein variants, acetylated and unacetylated Cdc8. Like other tropomyosins, fission yeast Cdc8 has been shown to inhibit the activities of cofilin Adf1 and myosin-I while promoting formin Cdc12 and myosin-II activities [162, 161, 28].

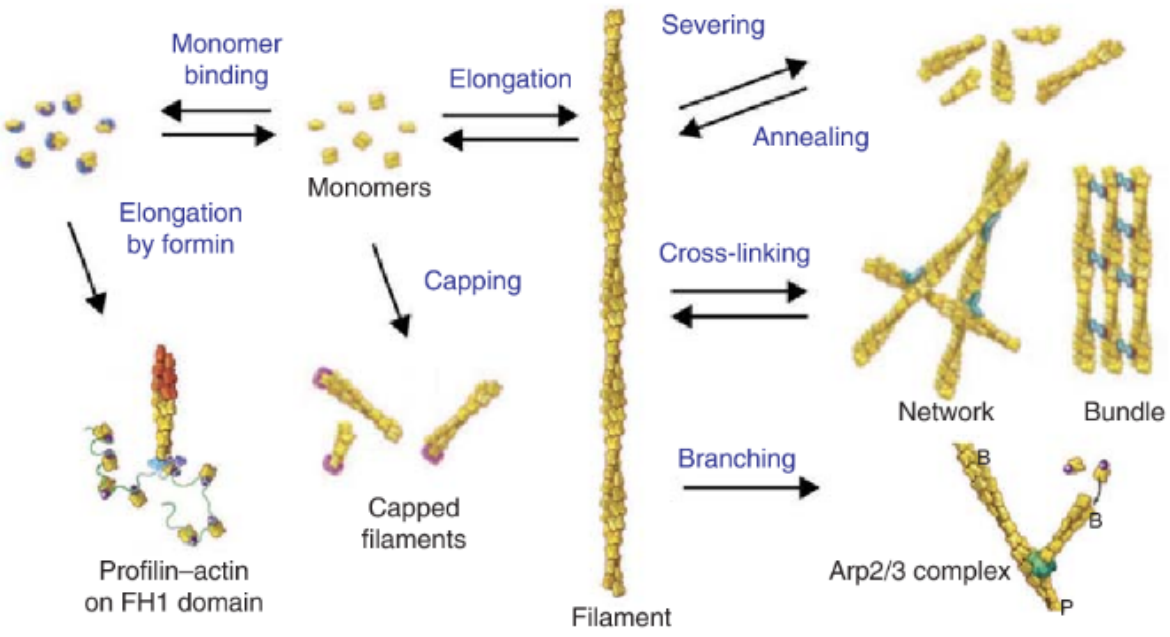

Figure 1.4: **Actin-binding proteins.** Diagram of the many roles of actin-binding proteins, including monomer-binding, elongation, capping, severing, and crosslinking. Adapted with permission from [139].

1.4.3 Severing proteins

Actin networks are incredibly dynamic, with F-actin constantly assembling and disassembling. Actin filament disassembly must be properly regulated to promote rapid F-actin turnover and to maintain a pool of assembly-competent G-actin (Figure 1.4) [19]. The majority of *in vivo* F-actin disassembly is carried out by two families of actin severing/depolymerizing proteins whose main cellular role is to sever actin filaments, gelsolin and Actin Depolymerizing Factor (ADF)/cofilin. This dissertation will focus on ADF/cofilin, which is essential for F-actin severing during cell motility and cytokinesis and exhibits a unique F-actin severing mechanism. Cofilin binds cooperatively to the sides of actin filaments and has a higher affinity for ADP-actin than ATP-actin. F-actin saturated with cofilin is stable, but actin filaments sparsely decorated by cofilin are severed at boundaries between bare filament and cofilin-associated stretches [41, 127], likely because of the differences in filament stiffness be-

tween these sites. Cofilin's affinity for ADP-actin promotes the disassembly and recycling of older actin, which maintains the cytoplasmic G-actin pool. Fission yeast expresses a single cofilin, ADF1, that functions as the primary severing protein in both actin patches and the contractile ring [121, 26, 123].

1.4.4 Capping proteins

Cells need to maintain actin filaments of different lengths to carry out specific cellular functions. While many eukaryotic proteins exhibit actin filament-capping behavior, including capping protein, gelsolin, and tropomodulin, capping protein protein is expressed in virtually all eukaryotic cells and is extremely important for regulating F-actin dynamics [39]. Capping protein forms a dimer of structurally similar α- and β-subunits that tightly binds actin filament barbed ends [88]. The relatively high concentration of cellular capping protein ensures that F-actin is capped within seconds, thereby limiting the number of free barbed ends to prevent excess actin assembly and maintain the actin monomer pool (Figure 1.4). Fission yeast capping protein cooperates with cofilin and profilin to play an integral role in regulating F-actin dynamics.

1.5 Localization of actin-binding proteins to the proper F-actin networks

To build distinct F-actin networks within a crowded cytoplasm, cells need to activate actin assembly factors at the correct time and place and ensure that the appropriate subset of actin-binding proteins (ABPs) localizes to each network. The number of ABPs expressed in eukaryotic cells ranges from tens to hundreds, and each ABP must associate with one or more actin networks that are simultaneously present, a process we have termed ABP "sorting". A variety of non-mutually-exclusive mechanisms have been proposed to explain how ABPs

are recruited to particular F-actin networks at the right time and place, each of which falls into one of two general categories: extrinsic and intrinsic factors.

1.5.1 Extrinsic factors

Extrinsic factors that contribute to ABP sorting include any external signals acting on an ABP. Just as upstream signals activate actin assembly factors to generate F-actin at a particular time and place, the model of extrinsic regulation posits that upstream signals could control ABP localization to distinct actin networks. Examples of such upstream signals include post-translational modifications or ions that mediate ABP activity or expression in different cell cycle stages or subcellular compartments [124, 156, 44], as well as mechanical stresses applied to actin filaments. While some ABP activity is ion-dependent or modulated by post-translational modifications, little is known about how these factors actually influence ABP association with specific actin networks. For example, budding yeast fimbrin Sac6 is phosphorylated in a cell cycle-dependent manner, enhancing its ability to bind F-actin [111]. However, it is unclear how this phosphorylation promotes Sac6's proper localization to actin cables. An interesting possibility is that extrinsic signals may govern how ABPs interact with actin filaments, while intrinsic factors direct ABPs to specific F-actin networks.

1.5.2 Intrinsic factors

The intrinsic regulation model of ABP sorting revolves around qualities inherent to ABPs themselves that influence how, where, or when ABPs associate with F-actin or F-actin networks. Important intrinsic factors that could affect ABP sorting include the type, number, orientation, and spacing of actin-binding modules, as all ABPs must associate with F-actin. Indeed, it has been demonstrated that the actin-binding domains alone of α-actinin and filamin are sufficient to localize to the proper cellular actin networks in *Dictyostelium* [181]. These intrinsic features could alter 1) an ABP's affinity for a specific type of actin (ATP state,

length), 2) an ABP's preference for a specific F-actin architecture (branched vs. straight filaments), or 3) the kinetics of an ABP's association with F-actin. Additionally, intrinsic factors could modify actin filaments to make them more amenable for ABP-binding by changing the twist and/or flexibility of individual filaments or altering characteristics of higher-order F-actin works, such as the spacing, orientation, or density of filaments within the network.

Previous work from our lab revealed that intrinsic factors mediate the segregation of ABPs to distinct stretches of bundled F-actin. Two crosslinking proteins, fascin and α-actinin, sort themselves into mutually exclusive domains on the same bundle [186]. Fascin is a compact protein that generates bundles with a narrow 8 nm spacing, while α-actinin creates more widely spaced bundles, with filaments roughly 40 nm apart. Interestingly, espin and fimbrin, also compact crosslinking proteins, sort to the fascin-coated domain of the bundle, which suggests that filament spacing may be a key mechanism of ABP sorting in bundled networks [186]. The ability to reconstitute this ABP sorting from purified proteins *in vitro* highlights the importance of intrinsic regulation, as no extrinsic signalling is required to generate mutually exclusive domains of fascin and α-actinin.

The formation of domains of crosslinking proteins depends on another important intrinsic property exhibited by many ABPs: cooperativity. Cooperativity occurs when the binding of one molecule increases the likelihood that another will bind, and ABPs demonstrate cooperativity by a variety of different mechanisms. Crosslinking proteins generate bundles with a specific spacing that is optimal for recruiting additional crosslinkers with that spacing, as described for fascin and α-actinin above [186]. The end-to-end association of tropomyosin makes it an extremely cooperative molecule, as cytoplasmic tropomyosin molecules are recruited to the actin-bound tropomyosin cable. Finally, cofilin-binding changes the twist of an actin filament to favor binding of additional cofilin molecules. While these intrinsic factors certainly facilitate ABP sorting to different F-actin networks, many types of extrinsic and

intrinsic regulation are likely important for organizing the actin cytoskeleton.

1.5.3 Competition between actin-binding proteins tunes their sorting to distinct actin networks

While much is known about individual ABPs and how they associate with F-actin, how ABPs behave in concert and affect each other's sorting is less clear. Recent evidence suggests that competition between ABPs for binding F-actin drives their sorting to different actin networks. Work from many labs characterized the competition between capping protein and formin, two barbed end-binding proteins [62, 90, 16, 157, 198]. Once either capping protein or formin becomes associated with a barbed end, it prevents the other from affecting polymerization [90]. However, more recent evidence suggests that formin and capping protein may actually bind the barbed end simultaneously, creating a "decision complex" that allows fine-tuning of filament length [16, 157]. Further study will elucidate how cells balance formin and capping protein activities to promote actin assembly at the proper time and place.

Previous work from our lab revealed that fimbrin Fim1, a crosslinking protein that localizes primarily to actin patches, competes with tropomyosin Cdc8 to inhibit its association with F-actin both *in vitro* and in fission yeast cells [27, 162]. Live cell imaging combined with *in vitro* bulk biochemistry also showed that Cdc8 protects F-actin from cofilin-mediated severing [162]. Thus, another important role for Fim1 is to promote severing by preventing Cdc8's association with actin patches. Furthermore, Cdc8 differentially regulates three fission yeast myosins: Myo1 (a class I myosin that activates Arp2/3 complex in actin patches), Myo51, and Myo52 (class V myosins that localize to the contractile ring and actin cables, respectively) [28]. Cdc8 was shown to promote motor activity of Myo51 and Myo52 at formin-mediated actin networks but block Myo1-binding at actin patches. However, Fim1 restores Myo1 association with Arp2/3 complex-mediated filaments in actin patches by antagonizing Cdc8 [28].

Subsequent work from our lab sought to understand the mechanism by which Fim1 inhibits Cdc8 association with F-actin [27]. Using three-color TIRFM with labeled ABPs, we saw that while Cdc8 readily associates with single actin filaments, Fim1 actively displaces Cdc8 from these filaments as it bundles them [27]. We suspect that Cdc8's cooperative binding contributes to its rapid displacement from F-actin bundles, as it appears to be stripped away from actin filaments in a cooperative manner. Since Cdc8's competition with cofilin Adf1 has been well-documented [162], we also investigated the mechanism of this interaction. Supporting previous findings, we showed that Cdc8 inhibits the initial association of Adf1 with F-actin, but Adf1 still displaces Cdc8 from older actin at later timepoints [27]. Interestingly, Fim1 also displays a mutually exclusive binding pattern with Adf1, despite both being actin patch-associated proteins. Although Adf1 excludes Fim1 from single filaments and Fim1 excludes Adf1 from bundled regions, this competitive interaction actually leads to a more densely bundled network, as cofilin severing events within F-actin bundles rapidly generate new, elongating barbed ends [27]. Thus, competition between Adf1 and Fim1 causes them to synergize and initiates rapid actin assembly. Not surprisingly, the synergistic interaction between Adf1 and Fim1 allows them to better compete with Cdc8, as Cdc8 is completely prevented from associating with actin filaments in the presence of both Adf1 and Fim1 [27]. Together, these results suggest that a complicated web of competitive interactions between ABPs drives their sorting to distinct F-actin networks. Each pair of ABPs exhibits a distinct pairwise interaction that could mediate their own sorting or influence how still other ABPs associate with F-actin. Future work will aim to understand the molecular mechanisms that govern how hundreds of ABPs localize to distinct F-actin networks on a cellular scale.

1.5.4 Actin assembly factors influence the ABP composition of F-actin networks

To carry out a particular cellular function, a cell must build a specific actin network by 1) localizing the actin assembly factor to the correct place, 2) activating the actin assembly factor at the correct time, and 3) recruiting the proper set of ABPs. As a result, one previously discussed model of F-actin network regulation is that diverse actin networks are properly formed simply by activating the actin assembly factor at the correct time and place. Different actin assembly factors generate F-actin with specific characteristics, such as architecture or twist, that are instrumental in recruiting specific "upstream" ABPs [114]. These upstream ABPs help determine the ABP composition of each network by recruiting additional "downstream" ABPs while inhibiting the association of others.

It has long been suggested that the actin assembly factor defines the subset of ABPs that is recruited to a particular F-actin network. The intracellular bacterial pathogen *Listeria monocytogenes* expresses ActA, an Arp2/3 complex activator, on its surface to hijack the host's actin cytoskeleton and propel itself through the cytoplasm by generating burts of F-actin assembly [176]. Additionally, this motility was recapitulated upon incubation of ActA-coated polystyrene beads in cellular extracts [21], and it was later determined that only seven proteins are sufficient to generate actin tails capable of promoting bead motility similar to that of *Listeria in vivo* [103]. Together, these studies reveal that the presence of an assembly factor alone can lead to the formation of an F-actin network with a specific architecture that carries out a particular function.

The role of actin assembly factors in establishing the ABP composition of each network became more clear when recent work demonstrated that beads coated with the budding yeast Arp2/3 complex activator Las17 form comet tails when incubated in budding yeast extracts that recruit the subset of ABPs found in actin patches [113]. Similarly, when incubated

in mitotic cell extracts, beads coated with budding yeast formin Bni1 generate an actin cable-like network that associates with the ABPs that normally localize to budding yeast actin cables [112]. These results suggest that the actin assembly factor alone is sufficient for generating an F-actin network capable of recruiting the appropriate subset of ABPs.

Finally, work in fission yeast has also suggested that actin assembly factors are important for ABP sorting. Fission yeast expresses a single tropomyosin isoform, Cdc8, that is present in two forms: acetylated, which associates with the formin Cdc12-mediated contractile ring, and unacetylated, which localizes to actin cables that are assembled by formin For3 [163, 32]. Interestingly, when the cellular localizations of Cdc12 and For3 are swapped, acetylated Cdc8 maintains its association with F-actin assembled by Cdc12, while unacetylated Cdc8 continues to localize to For3-mediated F-actin [74]. Thus, the localization of both forms of Cdc8 to a specific actin network is completely dependent on which formin builds the F-actin in that network.

1.6 Fission yeast as a model organism

Although ABP sorting is a challenge faced by all cell types, understanding how diverse actin networks maintain specificity in a crowded cytoplasm is particularly difficult in mammalian cells, as they build up to 20 different types of actin networks and express multiple isoforms of actin and hundreds of ABPs. Because the complexity of higher eukaryotes makes it difficult to assess the molecular mechanisms of actin cytoskeleton organization, we instead use model organisms to investigate how ABPs sort to the proper actin networks. As previously mentioned, this dissertation will focus on the self-organization of the actin cytoskeleton in the fission yeast *Schizosaccharomyces pombe*, a powerful model for studies of eukaryotic cells. A small genome with low redundancy optimizes fission yeast for genetic screens, leading to the identification of many important players in the regulation and organization of the actin cytoskeleton. Additionally, the fission yeast genome is easily engineered due to the

efficiency of homologous recombination, which affords us the opportunity to fluorescently tag endogenous proteins. Finally, localization studies in fission yeast are aided by powerful imaging techniques that permit high spatial and temporal resolution tracking of protein dynamics.

Fission yeast is also an ideal model to study actin organization, as it contains a simplified actin cytoskeleton with a single isoform of actin and ~40 ABPs. Furthermore, vegetative fission yeast cells build only three distinct actin networks, each assembled by a distinct actin assembly factor: endocytic actin patches (Arp2/3 complex), polarizing actin cables (formin For3), and the contractile ring (formin Cdc12) (Figure 1.5). This simplified actin cytoskeleton allows us to probe how a single actin network is generated at the proper time and place, while the presence of three distinct F-actin networks allows us to explore how ABPs sort between them. While this dissertation will focus on actin patches and the contractile ring, all three fission yeast F-actin networks are briefly described below.

1.6.1 Actin patches

Actin patches assemble at the growing tips of interphase cells and at the midzone of dividing cells to mediate endocytosis at those sites (Figure 1.5) [9, 48]. Assembly of yeast actin patches occurs in a strictly ordered fashion, with proteins that promote membrane invagination arriving first, followed by adaptor proteins and regulators of actin assembly [159]. Internalization of endocytic vesicles in fission yeast depends on Arp2/3 complex-mediated actin assembly. Several Arp2/3 complex activators, including WASP homolog Wsp1 and type I myosin Myo1, localize to the base of the invaginating membrane to stimulate F-actin assembly and cooperate with BAR proteins to promote membrane tubulation [159, 98, 177].

Although the mechanism by which Arp2/3 complex-mediated actin assembly results in vesicle internalization is unclear, more is known about the components involved in building the actin network. Mathematical models predict that actin patches are composed of ~150

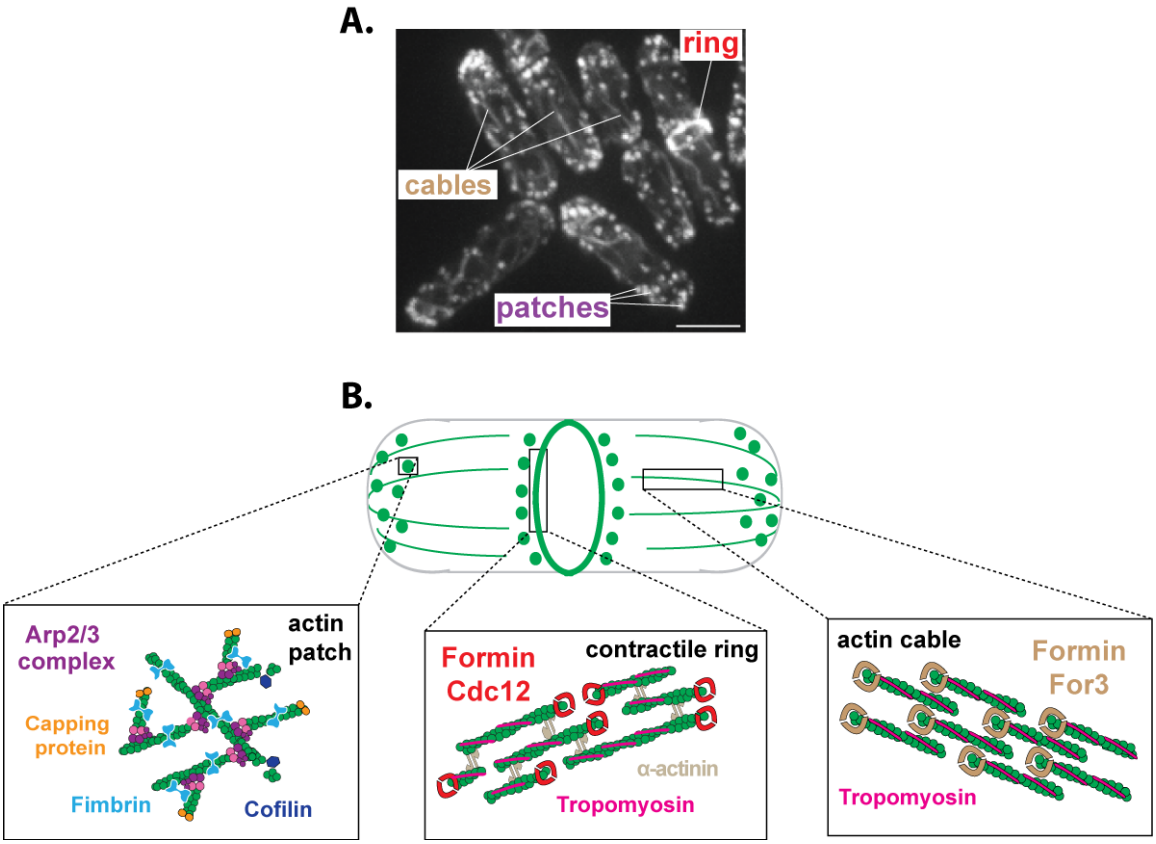

Figure 1.5: **Actin networks in fission yeast.** **(A)** Fluorescence micrograph of fission yeasts cells expressing GFP-CHD (calponin homology domain of Rng2) to label F-actin networks. Adapted with permission from [91]. **(B)** Cartoon of the three primary F-actin networks in vegetative fission yeast cells and the associated actin-binding proteins relevant to this work.

actin filaments that are kept short (100-200 nm or 40-60 subunits) due to rapid capping by capping protein [159, 13]. These short, branched filaments are crosslinked by fimbrin Fim1 (Figure 1.5B), which strengthens the network and inhibits tropomyosin Cdc8's association with actin patches to promote severing by cofilin Adf1 as discussed previously [159, 162]. Additional ABPs associate with actin patches to regulate vesicle internalization and filament debranching during patch disassembly [51].

1.6.2 Actin cables

Actin cables serve as polarized tracks for type V myosin-based transport of cargo to the growing tips of fission yeast cells. Actin cables are composed of short bundles of parallel actin filaments assembled by the formin For3, which associates with the cortex at cell tips to nucleate and elongate F-actin until it is propelled inward by retrograde flow with the growing cable (Figure 1.5B) [122, 79, 43, 180]. This inward movement partially inactivates For3 to keep filaments short, with barbed ends oriented toward the cortex [107]. In general, less is known about the assembly and ABP composition of actin cables compared to actin patches and the contractile ring. Actin cables are historically difficult to image in live cells (Figure 1.5A), making it hard to identify the group of ABPs that associates with them. Tropomyosin Cdc8 and coronin Crn1 localize to actin cables, but the ABP responsible for bundling filaments in cables has not yet been established. It is also possible that actin cable ABPs are present at low concentrations, increasing the difficulty of their detection.

1.6.3 The contractile ring

Much of what is known about how actomyosin rings drive cytokinesis was discovered in yeast, as a number of genetic screens in budding and fission yeasts allowed for identification of important and conserved players [10]. Along with computational modeling, these genetic screens have lead to the development of two different and potentially complementary

mechanisms of fission yeast ring assembly. The first, called Search, Capture, Pull, and Release (SCPR) [178, 192], involves the assembly of ~65 pre-ring cytokinesis nodes composed of type-II myosin Myo2, formin Cdc12, and additional scaffolding and signaling proteins, such as anillin-like Mid1, IQGAP Rng2, and F-BAR protein Cdc15 [190, 29]. These nodes assemble at the cell midzone immediately prior to the onset of mitosis, at which time Cdc12 nucleates actin filaments that elongate to make contact with Myo2 in nearby nodes (Search and Capture). Myo2 exerts a pulling force on F-actin, driving node coalescence and thus ring compaction (Pull). These node-node contacts are released by cofilin-mediated F-actin severing (Release), and repeated cycles of this process generate a constricting contractile ring [30, 166, 123]. The dynamic crosslinking protein α-actinin Ain1 is thought to be responsible for bundling F-actin into short, anti-parallel bundles (Figure 1.5B) [189, 80]. This SCPR mechanism is the prevailing model for contractile ring assembly in wild-type fission yeast cells.

An additional, non-mutually exclusive mechanism of fission yeast contractile ring assembly is known as the leading cable model, which was proposed to explain the formation of contractile rings in *mid1*Δ fission yeast cells that lack cytokinesis nodes [72, 25]. The leading cable model involves the septation initiation network (SIN), which is a conserved signaling pathway that triggers contractile ring assembly and septation at the end of anaphase [188]. In the absence of pre-ring nodes, actomyosin cables grow from a single cortical spot (the "leading cables") and coalesce to form contractile rings that are often misplaced and disorganized [25]. The SCPR and leading cable models could both contribute to contractile ring assembly under normal cellular conditions, as contractile rings fail to form entirely in the absence of both SIN activity and Mid1. It has also been posited that F-actin generated by Cdc12 outside the cell midzone can incorporate into the contractile ring [71].

1.7 Single molecule Total Internal Reflection Fluorescence Microscopy (TIRFM)

In addition to cell biological techniques that allow us to observe and manipulate F-actin networks in fission yeast, we can reconstitute actin networks *in vitro* using purified proteins in order to determine the components that are necessary and sufficient for building distinct actin networks. Much of the *in vitro* reconstitution discussed throughout this dissertation utilizes an optical technique known as Total Internal Reflection Fluorescence Microscopy (TIRFM). TIRFM is a type of microscopy that relies on a special objective that allows for a low incidence angle of the incoming excitation laser, leading to total internal reflection of the laser within the glass coverslip [45, 8]. This process produces an exponentially decaying evanescent wave that excites fluorophores only within ~200 nm of the coverglass, which greatly increases the signal-to-noise ratio, as background fluorescence beyond the ~200 nm threshold is significantly reduced (Figure 1.6) [8]. Thus, TIRFM is especially useful for visualization of single molecules and is used in our lab as a sensitive probe to study how ABPs interact with actin filaments. By introducing purified proteins into the TIRFM chamber, we can watch actin filaments assemble in real time and investigate the kinetics of single molecule ABP association with F-actin. Unlike bulk *in vitro* techniques such as fluorescent pyrene assays, TIRFM also allows us to distinguish between nucleation and elongation of actin filaments and measure F-actin elongation rates. Thus, we can take advantage of TIRFM to investigate the molecular mechanisms of F-actin network assembly.

1.8 Summary

It is apparent that the process of building and maintaining diverse actin networks in a crowded cytoplasm is extremely complex, with contributions from many different and complementary mechanisms. Cells must localize actin assembly factors to the correct place,

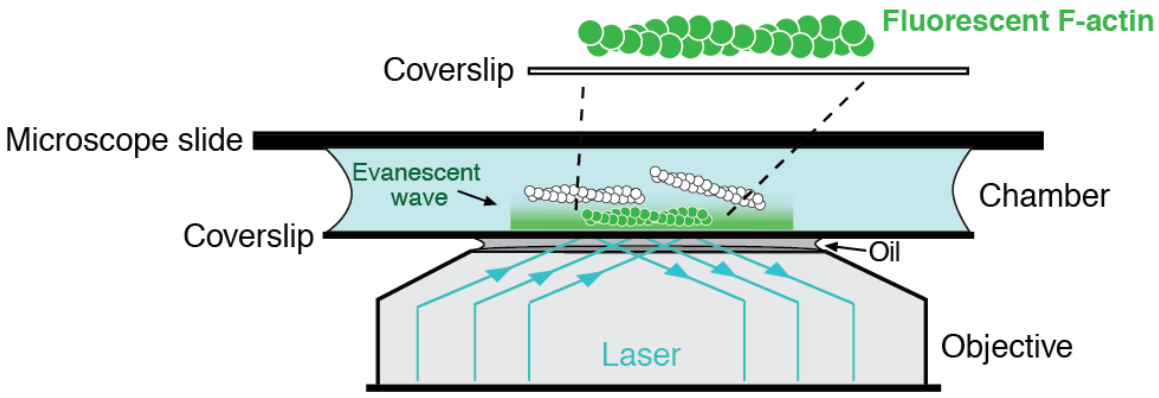

Figure 1.6: **Total Internal Reflection Fluorescence Microscopy (TIRFM).** Schematic of Total Internal Reflection Fluorescence Microscopy (TIRFM) of single fluorescent actin filaments. Flourophores in the flow chamber are illuminated by a laser at a critical angle that enables total internal reflection of the laser within the glass coverslip. This incident light generates an exponentially decaying evanescent wave that only excites fluorescent molecules close to the probe surface (within 200 nm), allowing imaging with high signal-to-noise ratio and reduced background fluorescence [45, 8].

activate them at the correct time, and regulate actin assembly to ensure proper distribution of actin monomers to different networks. We suspect that actin assembly factors nucleate and elongate actin filaments with distinct characteristics that are recognized by specific ABPs, and that the dynamic interplay between ABPs drives their sorting to particular F-actin structures. Using a combination of *in vivo* cell biology and *in vitro* reconstitution techniques, this work addresses how actin assembly factors and ABPs mediate actin cytoskeleton self-organization in fission yeast.

CHAPTER 2

COOPERATION BETWEEN TROPOMYOSIN AND α-ACTININ INHIBITS FIMBRIN ASSOCIATION WITH ACTIN FILAMENT NETWORKS IN FISSION YEAST

Preface

The work in the following chapter was performed in collaboration with Jenna Christensen, a previous graduate student in our lab. Jenna initiated the project by performing the experiments in Figures 2.1, 2.2, 2.3, 2.7, and 2.9 and completing the analysis. We collaborated on the microscopy and analysis for Figure 2.4, and I performed the microscopy in Figure 2.5 and 2.8 while Jenna did the analysis. I did both the microscopy and analysis for Figure 2.6. Additional experimental assistance for Figure 2.10 was provided by Alisha Morganthaler (low-speed sedimentation in Figure 2.10A-B), Alyssa Harker (TIRFM shown in Figure 2.10E), and Cristian Suarez (quantification in Figure 2.10F-G). Jenna performed the TIRFM and analysis in Figure 2.10C-D, while Rachel Brown performed the low-speed sedimentation and analysis in Figure 2.11. Additionally, I developed the assay and performed the TIRFM and analysis for Figure 2.12, and Jenna and I collaborated to complete the manuscript together. Finally, Meghan O'Connell assisted with the creation of fission yeast strains and performed preliminary experiments that were essential for establishing our experimental approaches, but were not included in this chapter.

2.1 Abstract

We previously discovered that competition between fission yeast actin binding proteins (ABPs) for association with F-actin facilitates their sorting to different F-actin networks. Specifically, competition between endocytic actin patch ABPs fimbrin Fim1 and cofilin Adf1

enhances each other's activities, and also rapidly displaces tropomyosin Cdc8 from actin patches. However, these interactions do not explain how Fim1 is prevented from associating strongly with other F-actin networks such as the contractile ring. Here, we identified the contractile ring ABP α-actinin Ain1 as an important sorting factor. Fim1 competes with Ain1 for association with F-actin, which is dependent upon their F-actin residence time. Remarkably, although Fim1 outcompetes both contractile ring ABPs Ain1 and Cdc8 individually, Cdc8 enhances the F-actin bundling activity of Ain1, and Ain1 generates F-actin bundles that Cdc8 can bind, even in the presence of Fim1. Therefore, the combination of Ain1 and Cdc8 is capable of inhibiting Fim1 association with F-actin networks.

2.2 Introduction

As in many cell types, the unicellular fission yeast assembles diverse actin filament (F-actin) networks within a crowded cytoplasm to facilitate different cellular functions such as cytokinesis (contractile ring), endocytosis (actin patches) and polarization (actin cables). These F-actin networks each possess a defined set of actin binding proteins (ABPs) that regulate the formation, organization, and dynamics of the actin filaments within the network. However, the mechanisms by which specific sets of ABPs sort to particular F-actin networks are less clear. We hypothesize that a combination of competitive and cooperative interactions between different ABPs for association with F-actin is critical for establishing and maintaining their sorting. We previously identified competitive binding interactions between three fission yeast ABPs with distinct network localizations—fimbrin Fim1 and ADF/cofilin Adf1 (endocytic actin patches) and tropomyosin Cdc8 (cytokinetic contractile ring) (hereafter called Fim1, Adf1 and Cdc8)—that help facilitate their sorting to the proper F-actin networks [27, 162]. Specifically, synergistic activities between Fim1 and Adf1 rapidly displace Cdc8 from F-actin networks such as actin patches [27, 162]. However, these interactions do not explain how Fim1 is prevented from strongly associating with other F-actin networks

such as the contractile ring. Therefore, we sought to determine whether other ABPs at the contractile ring prevent Fim1 association. In this study, we demonstrate that Fim1 competes with the contractile ring ABP α-actinin Ain1 (hereafter called Ain1) for association with F-actin, and that their ability to compete is dependent upon their residence time on F-actin. Additionally, we show that although Fim1 outcompetes both Cdc8 and Ain1 individually, Cdc8 and Ain1 have synergistic effects. Cdc8 enhances Ain1-mediated F-actin bundling, and Ain1 facilitates association of Cdc8 with Fim1-bound F-actin. These combined effects allow the combination of Cdc8 and Ain1 to successfully compete with Fim1 for association with F-actin.

2.3 Results

2.3.1 F-actin crosslinking proteins fimbrin Fim1 and α-actinin Ain1 compete at the contractile ring and at actin patches

We previously found that fimbrin Fim1 and ADF/cofilin Adf1 synergize to displace tropomyosin Cdc8 from F-actin [27], which helps explain why Fim1 is highly concentrated on actin patches whereas Cdc8 is not [162]. Conversely, despite Fim1 being a dominant competitor for F-actin [27, 162], Fim1 is present at much lower concentrations at the contractile ring, an F-actin network where Cdc8 is abundant [6, 121, 189]. We hypothesized that competition with additional contractile ring ABPs may prevent Fim1 from strongly associating with the contractile ring. As Fim1 is highly concentrated in actin patches, we speculated that depletion of actin patches by the Arp2/3 complex inhibitor CK-666 [19, 128] would result in a rapid increase of free Fim1 in the cytoplasm that might subsequently allow Fim1 to outcompete its contractile ring ABP competitors. Upon treating fission yeast cells expressing the general F-actin marker Lifeact-GFP with CK-666, we observed a depletion of actin patches and the formation of excessive formin-mediated 'ectopic' actin cables and contractile ring material

(Figure 2.1A) [19].

In control (DMSO-treated) fission yeast cells, Fim1-GFP localizes predominantly to actin patches, with only a small amount associating with the contractile ring (Figure 2.1B, left) [189]. However, in cells treated with CK-666, Fim1-GFP strongly associates with the contractile ring and to a subset of ectopic F-actin (Figure 2.1B, right). The localization of most contractile ring ABPs, including formin Cdc12, type II myosin Myo2, myosin regulatory light chain Rlc1, the IQGAP Rng2, and tropomyosin Cdc8, is unaffected by CK-666 treatment, (Figures 2.2 and 2.3). Conversely, less α-actinin Ain1 associates with the contractile ring in cells treated with CK-666 (Figure 2.1C, Figure 2.2). Therefore, we hypothesized that Fim1 and Ain1 are competitors, and that enhanced Fim1 association with the contractile ring in cells treated with CK-666 displaces Ain1. We tested this hypothesis by observing Ain1 localization in a strain lacking Fim1 (*fim1-1*Δ, Ain1-GFP). In *fim1-1*Δ cells, similar amounts of Ain1-GFP are associated with the contractile ring in control and CK-666-treated cells (Figure 2.1D), suggesting that the absence of competitor Fim1 allows Ain1 to remain associated with the contractile ring in the presence of CK-666. At all stages of contractile ring assembly and constriction, Fim1 similarly localizes to the contractile ring and displaces Ain1 following CK-666 treatment (Figure 2.4), though it is most prominent in stages with fully-developed contractile rings (stages 2 and 3).

If competition between Fim1 and Ain1 is a primary driver of their sorting to distinct F-actin networks, we expected that Ain1-GFP might erroneously localize to actin patches in the absence of Fim1. However, Ain1-GFP is observed at actin patches in less than 1% of *fim1-1*Δ cells (Figure 2.1D, 2.5C). It is possible that a combination of the low number of Ain1 molecules ($\sim$3,600 $\pm$ 500 [191]), and the high density of F-actin in actin patches (5,000-7,000 actin molecules in each of 30-50 actin patches [159, 191]), may dilute the Ain1-GFP signal beyond detection. Therefore, increasing the concentration of Ain1-GFP could allow observable Ain1-GFP at actin patches, but only in a *fim1-1*Δ background. To in-

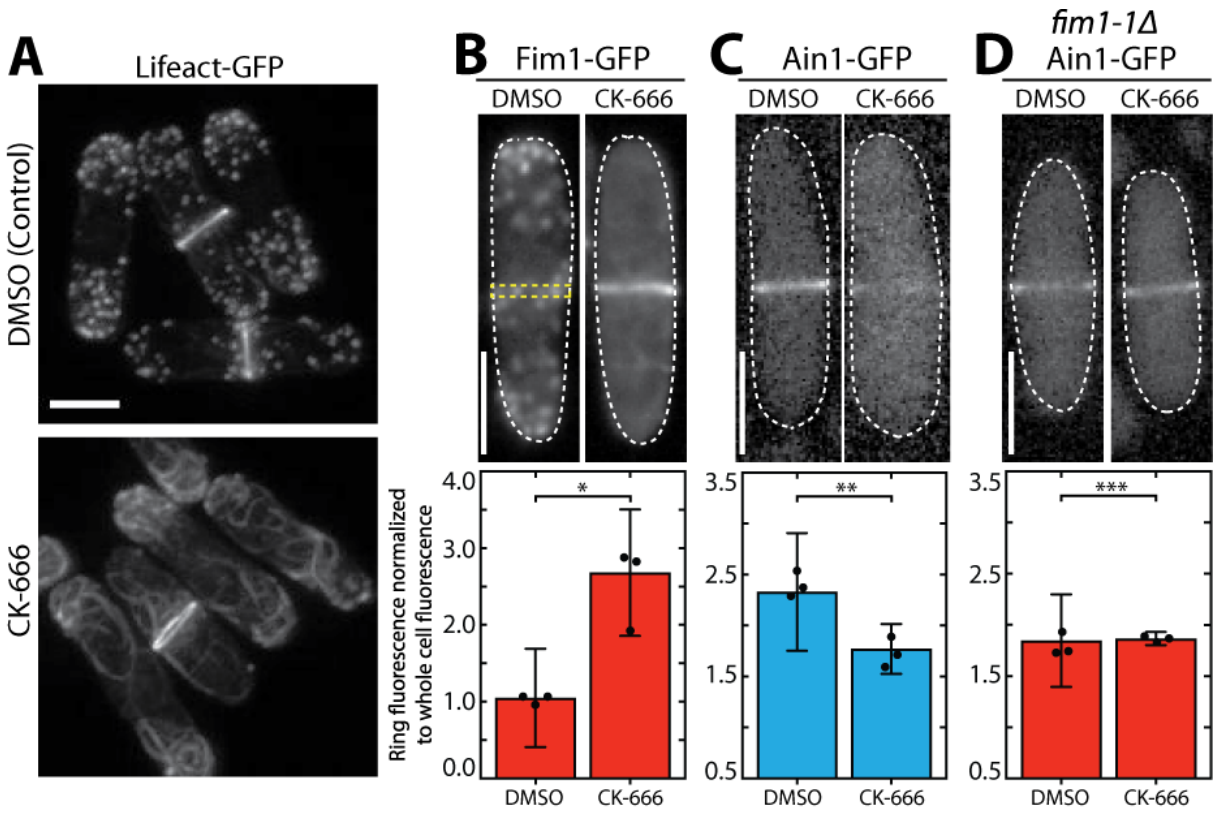

Figure 2.1: **Fimbrin Fim1 and α-actinin Ain1 compete for association with the contractile ring. (A)** Fluorescence micrographs of fission yeast cells expressing Lifeact-GFP following treatment with DMSO (control, top) or 200 μM Arp2/3 complex inhibitor CK-666 (bottom). **(B-D, top panels)** Fluorescence micrographs of fission yeast cells expressing Fim1-GFP **(B)**, Ain1-GFP **(C)**, or Ain1-GFP in a *fim1-1*Δ background **(D)**, following treatment with DMSO (left) or 200 μM CK-666 (right). Dotted lines outline cells. Yellow dotted line denotes representative region used to quantify fluorescence value in cells lacking a visible contractile ring. Scale bars, 5 μm. **(B-D, bottom panels)** Mean Fim1-GFP **(B)** or Ain1-GFP **(C,D)** fluorescence at the contractile ring normalized to whole cell fluorescence. Error bars=s.d. Filled circles indicate means of experimental replicates. n$\geq$18 cells from three independent experiments. Two-tailed t-tests for data sets with unequal variance yielded p-values *p=$8.57\text{x}10^{-20}$, **p=$1.75\text{x}10^{-6}$, ***p=0.81.

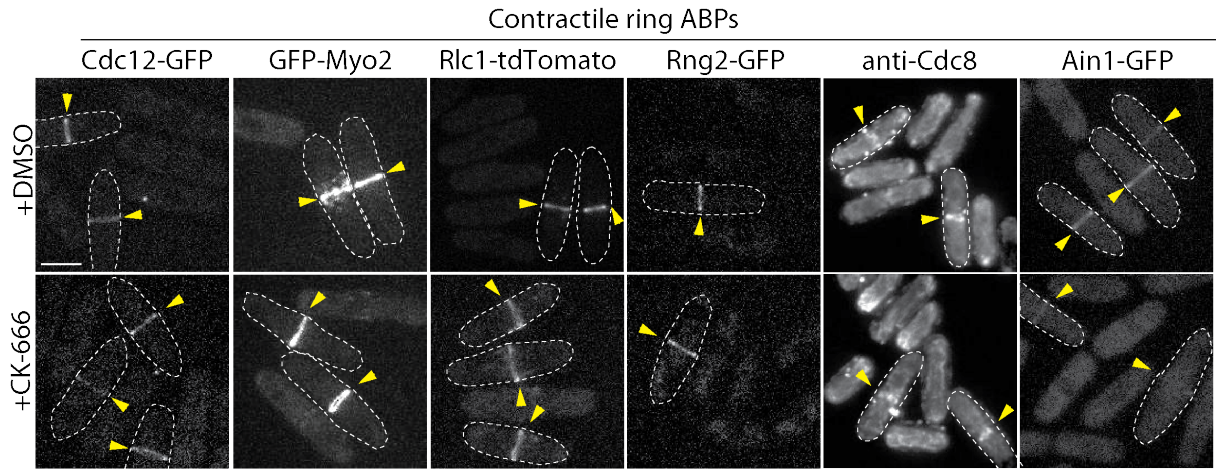

Figure 2.2: **Contractile ring ABP localization following CK-666 treatment.** Fluorescent micrographs of fission yeast cells either immuno-stained (anti-Cdc8) or expressing the indicated fluorescently-tagged contractile ring ABPs from their endogenous locus: formin Cdc12-GFP, type II-myosin motor GFP-Myo2, myosin regulatory light chain Rlc1-tdTomato, IQGAP Rng2-GFP, and α-actinin Ain1-GFP. Cells were treated with DMSO (control) or 200 μM Arp2/3 complex inhibitor CK-666. Yellow arrowheads denote contractile rings. Dotted lines outline individual cells for clarity. Scale bar, 5 μm.

crease the expression of Ain1-GFP, we introduced an additional copy of Ain1-GFP at the *leu1-32* locus under the medium-strength 41Xnmt promoter [102]. We first quantified the cellular expression of endogenously tagged Ain1-GFP and the overexpressed Ain1-GFP constructs used in this study. We observed that while most Ain1-GFP constructs are expressed similarly to endogenously-tagged Ain1, the amount of Ain1-GFP overexpressed under the 41Xnmt promoter is almost two-fold higher (Figure 2.6). As predicted, despite this two-fold increase in expression, Ain1-GFP localizes to actin patches in only 10% of WT cells expressing endogenous Fim1 (Figure 2.5A,C). In contrast, overexpressed Ain1-GFP associates with ~67% of actin patches in *fim1-1*Δ cells (Figure 2.5B,C). Therefore, Fim1 and Ain1 appear to compete for association with F-actin at both actin patches and the contractile ring.

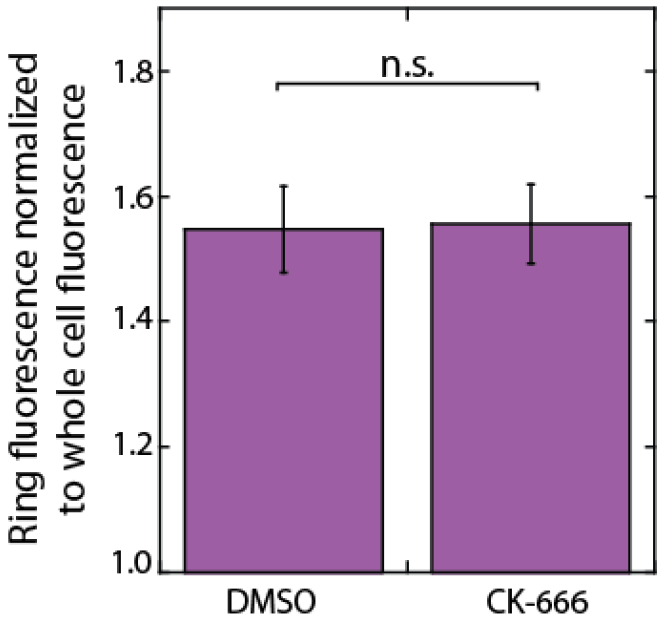

Figure 2.3: **Tropomyosin Cdc8 does not leave the contractile ring following CK-666 treatment.** Mean anti-Cdc8 contractile ring fluorescence normalized to total cell fluorescence. Error bars=s.e. A two-tailed t-test for data sets with unequal variance yielded p-value=0.9338. n$\geq$10 cells.

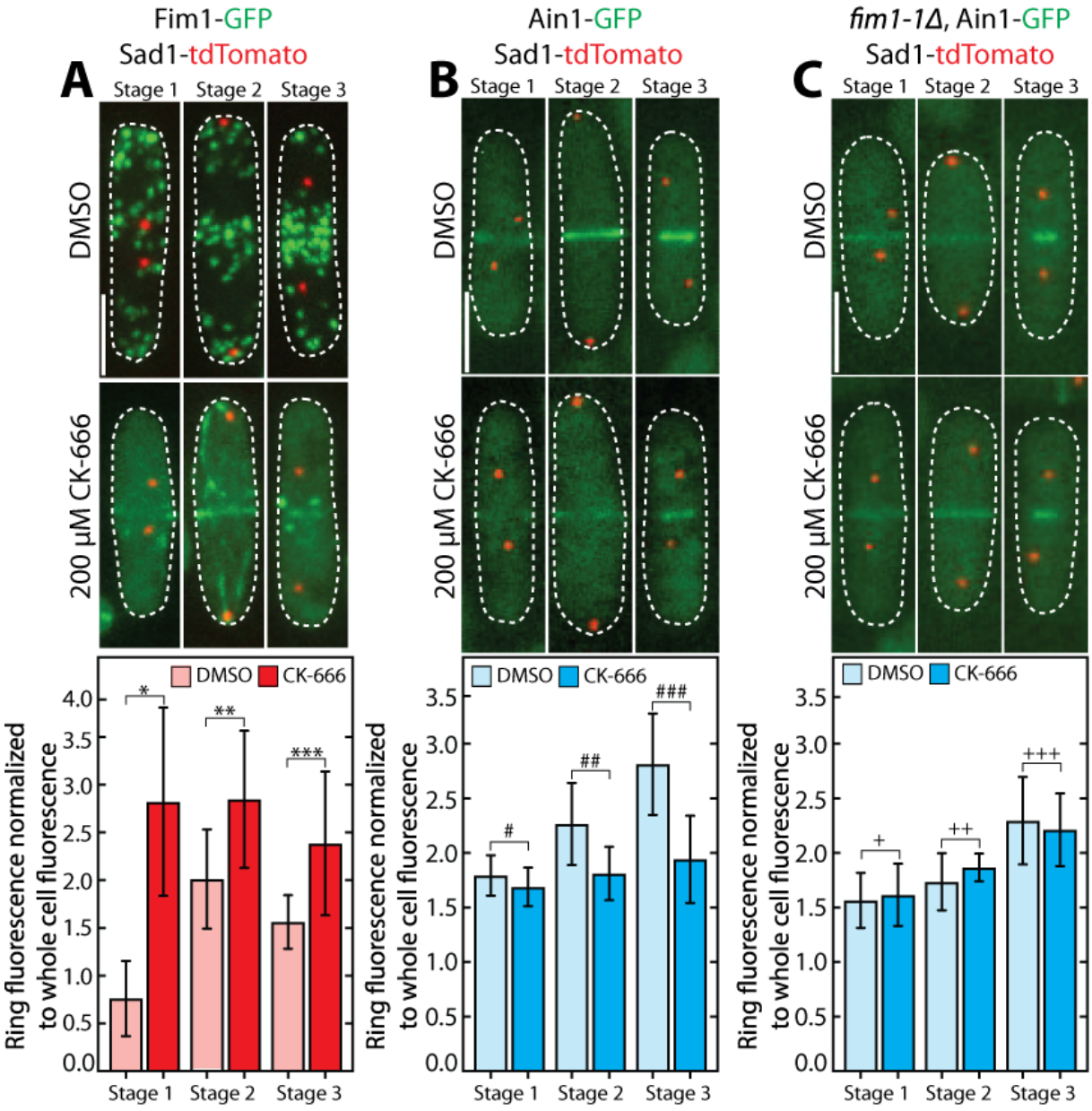

Figure 2.4: **Fimbrin Fim1 displaces α-actinin Ain1 from the contractile ring following CK-666 treatment. (A-C, top)** Fluorescent micrographs of fission yeast cells expressing spindle pole body marker Sad1-tdTomato and Fim1-GFP **(A)**, Ain1-GFP **(B)**, or Ain1-GFP in a *fim1-1*Δ background **(C)**, following treatment with DMSO (control, top) or 200 μM Arp2/3 complex inhibitor CK-666 (bottom). Scale bar, 5 μm. **(A-C, bottom)** Mean Fim1-GFP **(A)** or Ain1-GFP **(B-C)** contractile ring fluorescence normalized to whole cell fluorescence for cells in stage 1 (contractile ring formation), stage 2 (contractile ring dwell), or stage 3 (contractile ring constriction) of cytokinesis following treatment with DMSO (control) or 200 μM CK-666. Error bars=s.d. Two-tailed t-test for data sets with unequal variance yielded p-values *p=.024, **p=.034, ***p=.13, $^{\#}$p=.38, $^{\#\#}$p=.094, $^{\#\#\#}$p=.061, $^{+}$p=.53, $^{++}$p=.87, and $^{+++}$p=.55.

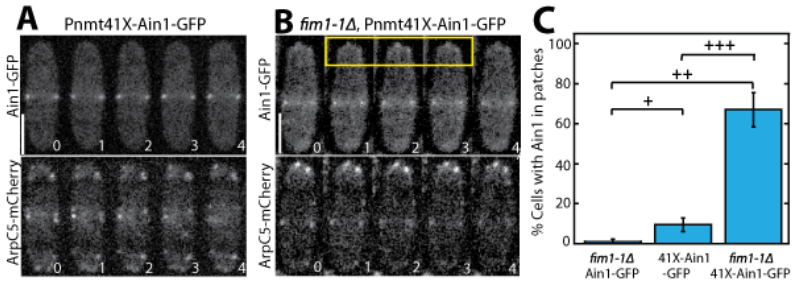

Figure 2.5: **Fimbrin Fim1 and α-actinin Ain1 compete for association with actin patches. (A-B)** Time-lapse fluorescent micrographs of fission yeast cells expressing ArpC5-mCherry (bottom) and overexpressing GFP-tagged α-actinin Ain1 from the 41Xnmt promoter (top) for 20 hours in a wild-type **(A)** or *fim1-1*Δ background **(B)**. Yellow box highlights Ain1-GFP localization at actin patches. Scale bars, 5 μm. Time in sec. **(C)** Percentage of cells in which Ain1-GFP is observed in actin patches. Error bars=s.e. Two-tailed t-tests for data sets with unequal variance yielded p-values $^{+}$p=0.113, $^{++}$p=0.002, $^{+++}$p=0.012. n=3 experimental replicates.

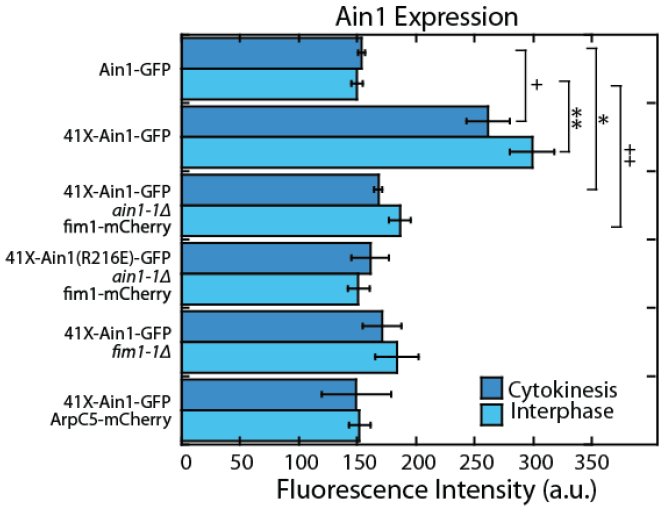

Figure 2.6: **Cellular expression of GFP-tagged α-actinin Ain1 constructs.** Fluorescence intensity of GFP-tagged Ain1 constructs for cells in cytokinesis (with contractile ring) or interphase (no contractile ring). Error bars=s.e. A single factor ANOVA yielded p-values of .0052 and $2.02\text{x}10^{-5}$ for cytokinesis and interphase, respectively. Pairwise two-tailed t-tests for data sets with unequal variance were conducted to determine which strain(s) contributed to the significant ANOVA results, where each strain was compared to the Ain1-GFP control. The two-tailed t-tests resulted in significant p-values of *p=.029, **p=.017, $^{+}$p=.029, and $^{++}$p=.039. n=3 experimental replicates of >50 cells each.

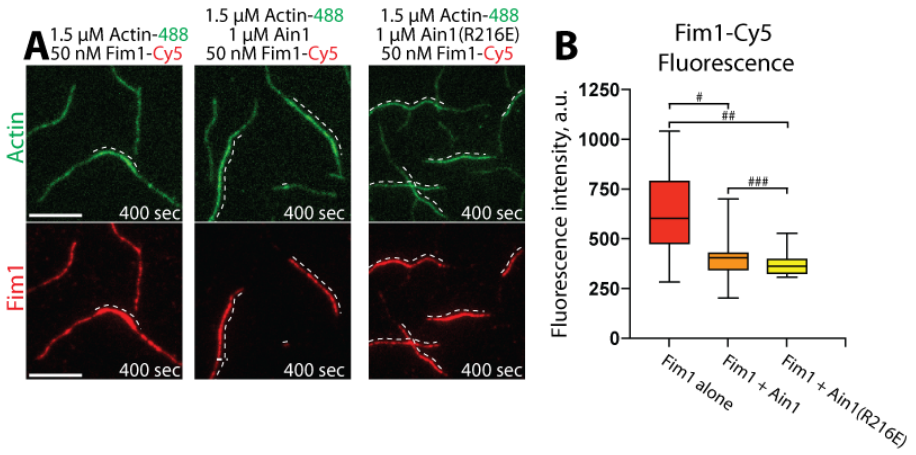

Figure 2.7: **Fimbrin Fim1 and α-actinin Ain1 compete for F-actin binding *in vitro*.** **(A-B)** Two-color TIRFM of 1.5 μM Mg-ATP actin (15% Alexa 488-labeled) with 50 nM fimbrin Fim1 (Cy5-labeled) alone, or with either 1 μM wild-type α-actinin Ain1 or mutant Ain1(R216E). Scale bars, 5 μm. Dotted lines denote bundled regions. **(B)** Box plots of the amount of Fim1-Cy5 fluorescence on two-filament F-actin bundles in either the absence (red) or presence of Ain1 (orange) or Ain1(R216E) (yellow). Error bars=s.e. Two-tailed t-tests for data sets with unequal variance yielded p-values $^{\#}$p=3.90x10^{-4}, $^{\#\#}$p=1.97x10^{-5}, $^{\#\#\#}$p=0.18. Two independent experiments were performed for each condition. In total, n$\geq$16 two-filament bundle measurements were taken for each condition.

2.3.2 Less dynamic α-actinin Ain1 associates with actin patches

Ultrastructural and mutational studies of fimbrin/plastin and α-actinin from several organisms demonstrate that they bind to a similar site on F-actin [50, 49, 67, 68, 110]. However, while fission yeast fimbrin Fim1 is relatively stable on single filaments (k_{off} = 0.0400 $\pm$ 001 s^{-1}) and very stable on F-actin bundles (k_{off} = 0.023 $\pm$ 0.003 s^{-1}) [161], α-actinin Ain1 has not been observed to associate with single actin filaments and is extremely dynamic on F-actin bundles (k_{off} = 3.33 s^{-1} on two-filament and three-filament bundles) [102]. Therefore, we hypothesized that Fim1's longer residence time on F-actin bundles may explain its ability to outcompete Ain1 for a similar F-actin binding site. To test this possibility, we took advantage of the Ain1 mutant Ain1(R216E), which is five- to ten-fold less dynamic on F-actin bundles (k_{off} = 0.67 s^{-1} and k_{off} = 0.33 s^{-1} on two- and three-filament bundles, respectively) [102], and assessed its ability to compete with Fim1 *in vitro* and *in vivo*.

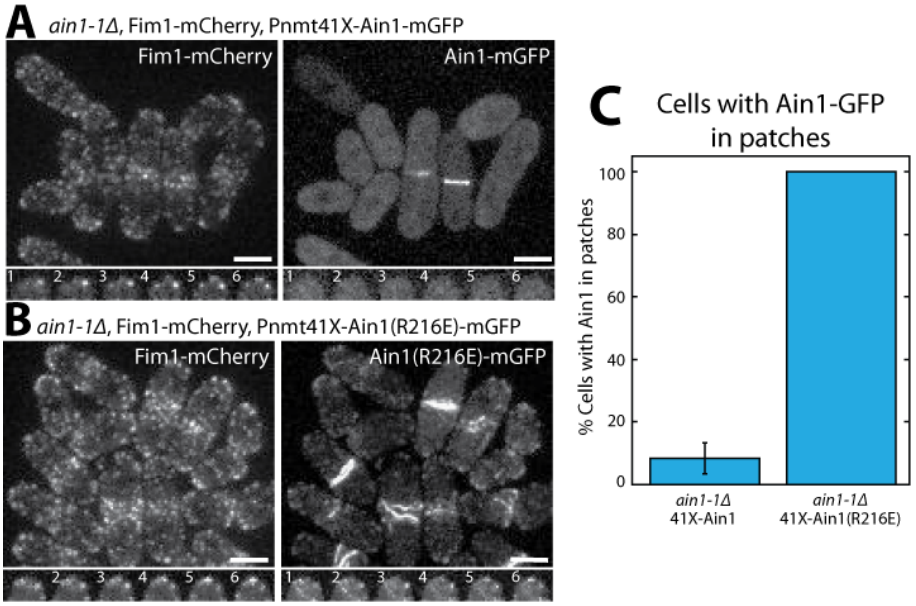

Figure 2.8: **Fimbrin Fim1 and α-actinin Ain1 competition at actin patches is driven by their residence time on F-actin. (A-B, top)** Fluorescence micrographs of fission yeast cells in an *ain1-1*Δ background overexpressing GFP-tagged wild-type Ain1 **(A)** or mutant Ain1(R216E) **(B)** from the 41Xnmt1 promoter. Scale bars, 5 μm. **(A-B, bottom)** Timelapse (in sec.) of cell taken from a single Z-plane. **(C)** Percentage of cells in which Ain1-GFP is observed in actin patches. Error bar=s.e.m. Two-tailed t-test for data sets with unequal variance yielded p-value=0.0029.

We utilized multi-color TIRF microscopy (TIRFM) to directly visualize the association of fluorescently labeled Fim1 with actin filaments *in vitro* in either the presence or absence of unlabeled Ain1. Compared to 50 nM Fim1-TMR alone, which fully decorates actin bundles, less Fim1-TMR associates with two-filament F-actin bundles in the presence of either 1 μM wild-type Ain1 or Ain1(R216E) (Figure 2.7A,B). However, there is little difference in the amount of Fim1-TMR associated with two-filament F-actin bundles in the presence of wild-type Ain1 or mutant Ain1(R216E).

Although we did not detect that Ain1(R216E) competes with Fim1 better than does wild-type Ain1 *in vitro* (Figure 2.3), the less dynamic Ain1(R216E) mutant is better than wild-type Ain1 at associating with Fim1-bound actin patches *in vivo* (Figure 2.4). In fission yeast cells expressing endogenously-tagged Fim1-mCherry, overexpressed wild-type Ain1-

GFP localizes to actin patches in only ~9% of cells (Figure 2.8A,C), whereas overexpressed mutant Ain1(R216E)-GFP localizes to actin patches in 100% of cells (Figure 2.8B,C). The disparity between Ain1(R216E)'s ability to compete with Fim1 *in vitro* versus *in vivo* potentially suggests that slight differences in dynamics may have a bigger effect in a cellular context. In particular, the dynamics of ABPs such as Ain1 may be finely tuned to allow for proper sorting given the large number of actin interacting proteins, with a small change in dynamics skewing the sorting to a dramatic degree. Alternatively, it is possible that our simplified *in vitro* system does not fully mimic *in vivo* conditions.

2.3.3 Tropomyosin Cdc8 and α-actinin Ain1 do not compete for association with actin filaments

We previously reported that tropomyosin Cdc8, an F-actin side-binding protein that associates with the contractile ring, is displaced from F-actin by fimbrin Fim1 *in vitro* and is thereby prevented from associating with actin patches in fission yeast cells [27, 162]. Although fimbrin/plastin and α-actinin isoforms bind to a similar site on F-actin, Cdc8 and α-actinin Ain1 both associate with the contractile ring. Therefore, we considered whether Ain1 also displaces Cdc8 from F-actin, or if they can simultaneously associate with F-actin. In multi-color *in vitro* TIRFM assays, Cdc8 is not displaced from Ain1- or Ain1(R216E)-bundled F-actin networks (Figure 2.9A,B), but it is displaced from Fim1-bundled networks (Figure 2.9C; [27, 162]). Thus, Ain1 and Cdc8 are capable of co-existing on the same F-actin network *in vitro* as they do at the contractile ring in cells.

2.3.4 Tropomyosin Cdc8 enhances the bundling activity of α-actinin Ain1

Compared to fimbrin Fim1, α-actinin Ain1 is a relatively weak F-actin bundling protein [1, 102, 117]. Remarkably, low-speed sedimentation (Figure 2.10A,B) and TIRFM assays (Figure 2.10C,D) revealed that tropomyosin Cdc8 significantly enhances the bundling ability

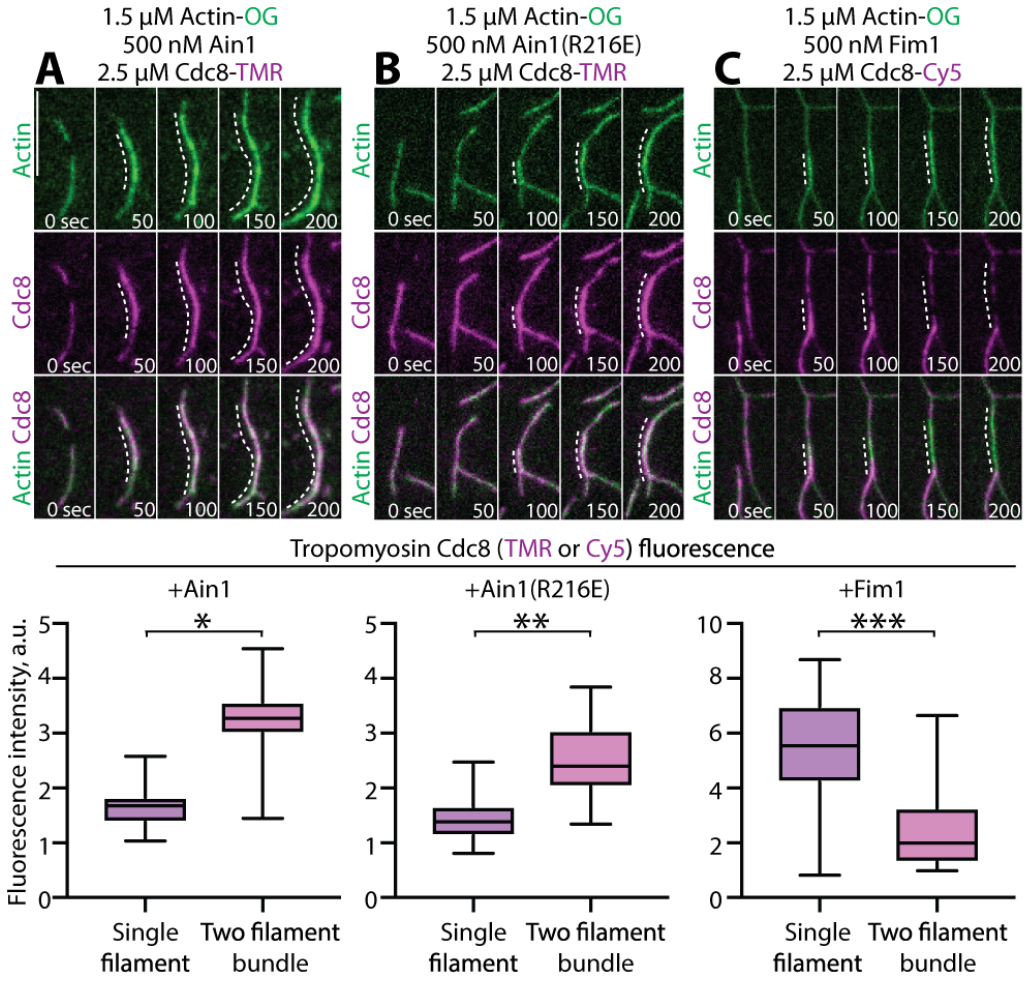

Figure 2.9: **α-actinin Ain1 does not displace tropomyosin Cdc8 from F-actin bundles *in vitro*.** **(A-C, top)** Two-color TIRFM of 1.5 μM Mg-ATP actin (15% Alexa 488-labeled) with 2.5 μM tropomyosin Cdc8 (TMR-labeled) and unlabeled 500 nM **(A)** wild-type α-actinin Ain1, **(B)** mutant Ain1(R216E), or **(C)** fimbrin Fim1. Scale bar, 1 μm. Dotted lines denote bundled regions. **(A-C, bottom)** Dot plots of the amount of Cdc8-TMR or Cdc8-Cy5 fluorescence on single filaments or two-filament bundles in the presence of Ain1 **(A)**, Ain1(R216E) **(B)** or Fim1 **(C)**. Error bars=s.e.m. Two-tailed t-tests for data sets with unequal variance yielded p-values *p=$8.24\text{x}10^{-18}$, **p=$5.47\text{x}10^{-12}$, ***p=$5.72\text{x}10^{-11}$.

of Ain1. In single-color TIRFM assays with unlabeled ABPs, 500 nM Cdc8 increases Ain1-mediated F-actin bundling 10-fold over Ain1 alone (Figure 2.10D). This surprising finding suggests that the combination of Ain1 and Cdc8 may allow for significant F-actin bundling to occur in the context of the contractile ring despite Ain1's poor bundling ability alone.

Cdc8's enhancement of Ain1-mediated F-actin bundling could potentially arise from Cdc8 increasing the number of Ain1 binding events on F-actin. To test this possibility, we analyzed the single molecule dynamics of Ain1 by performing TIRFM experiments with sparsely-labeled (0.5% TMR-labeled) Ain1 on uncoated versus Cdc8-coated F-actin. Three-fold more Ain1 binding events were observed on Cdc8-coated F-actin compared to uncoated F-actin (Figure 2.10E-G), suggesting that Cdc8 enhances the binding of Ain1 to F-actin, thereby increasing the F-actin bundling ability of Ain1.

2.3.5 Tropomyosin Cdc8 and α-actinin Ain1 cooperate to displace fimbrin Fim1 from actin filaments

On their own, both α-actinin Ain1 and tropomyosin Cdc8 are outcompeted by fimbrin Fim1 for binding to F-actin. Furthermore, there are ~86,500 Fim1 polypeptides in the cell, but only ~3,600 Ain1 molecules [191], raising the question as to why Fim1 is not associated more strongly with the contractile ring in wild-type cells. Given that Cdc8 enhances the bundling ability of Ain1, we speculated that the combination of Cdc8 and Ain1 might inhibit Fim1's association with actin filaments. To test this possibility, we first performed low speed F-actin sedimentation assays in the presence of Cdc8 and either Fim1, Ain1, or both (Figure 2.11A,B). Almost two-fold more Cdc8 pellets with Ain1-mediated F-actin bundles than Fim1-mediated bundles (Figure 2.11B). Additionally, an intermediate amount of Cdc8 pellets in the presence of both Fim1 and Ain1, suggesting that Ain1 allows Cdc8 to better associate with F-actin in the presence of Fim1.

To directly investigate the effect of Ain1 and Cdc8 cooperation on competition with

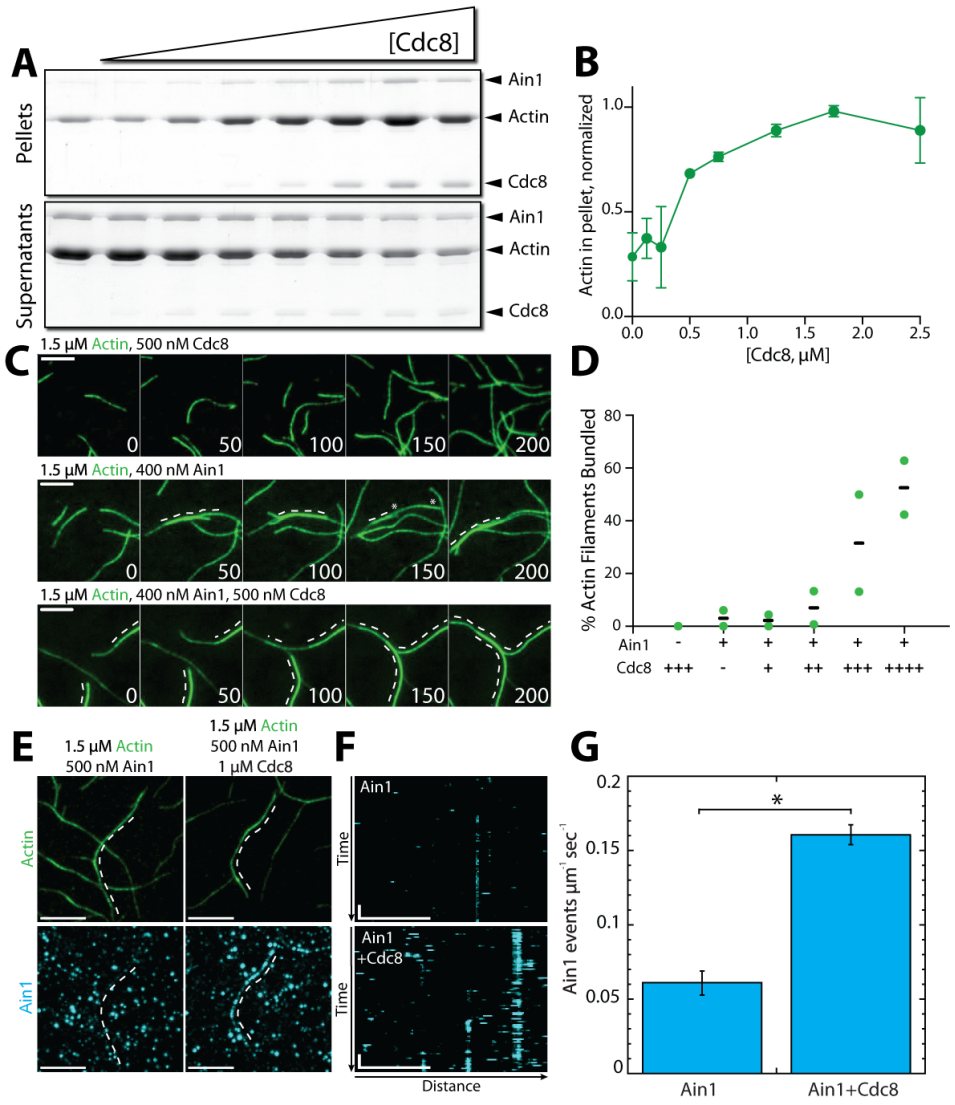

Figure 2.10: **Tropomyosin Cdc8 enhances α-actinin Ain1-mediated F-actin bundling *in vitro*.** **(A-B)** Low speed (10,000 x g) sedimentation assays of 5 μM Mg-ATP preassembled actin filaments, 500 nM Ain1, and increasing concentrations of Cdc8 (0-5 μM). **(A)** Coomassie blue-stained gel of pellets and supernatants from a representative experiment. **(B)** Quantification of actin extracted from the pellet as a function of Cdc8 concentration. Error bars=s.d, n=2. **(C-D)** TIRFM of 1.5 μM Mg-ATP actin (15% Alexa 488-labeled) in the presence of 500 nM Cdc8 **(C, top)**, 400 nM Ain1 **(C, middle)** or both **(C, bottom)**. Dotted lines indicate the bundled region. Scale bars, 5 μm. **(D)** Quantification of the percent of bundled F-actin with 500 nM Cdc8 alone, 400 nM Ain1 alone, or 400 nM Ain1 with 50 nM, 125 nM, 250 nM or 500 nM Cdc8. Black lines indicate averages and green circles indicate values from independent TIRFM experiments. n=2 independent experiments for each condition. **(E-G)** Spot density TIRFM experiments of 1.5 μM Mg-ATP actin (15% Alexa 488-labeled) and 500 nM Ain1 (0.5% TMR-labeled) alone or with 1 μM unlabeled Cdc8.

Figure 2.10: (continued) **(E, top)** Representative image of Alexa-488-labeled F-actin bundles. **(E, bottom)** Representative max projection of Ain1 spots on corresponding F-actin bundles. **(F)** Kymographs of bundle from **(E)** over time. Scale bar, 5 μm. Time bar, 11 sec. **(G)** Ain1 spot density (Ain1 events/μm/sec). Two-tailed t-tests for data sets with unequal variance yielded p-value *p=0.026. Error bars=s.e.m. n=2 independent experiments.

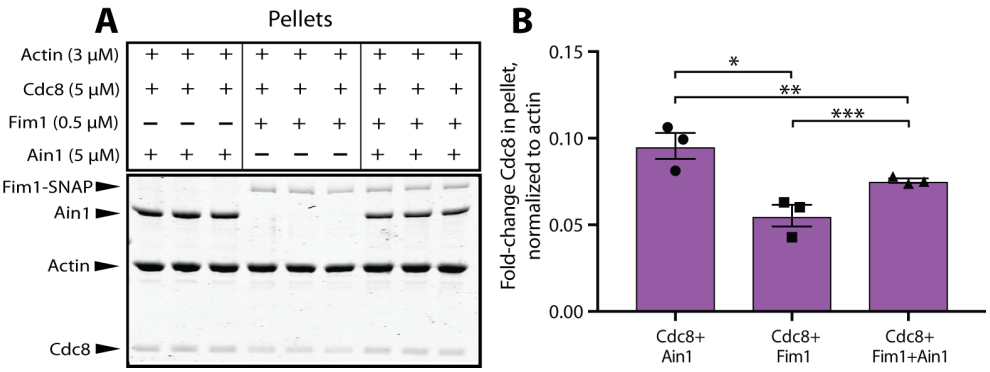

Figure 2.11: **α-actinin Ain1 facilitates the association of tropomyosin Cdc8 with bundled F-actin in the presence of fimbrin Fim1 *in vitro*.** **(A-B)** Low speed sedimentation comparing Cdc8 in the pellet with F-actin bundled by Fim1 (left), Ain1 (middle), or both (right). **(A)** Coomassie blue-stained gel of representative triplicate samples of 3 μM Mg-ATP pre-assembled actin filaments incubated and centrifuged with fixed concentrations of Cdc8 (5 μM), Fim1 (0.5 μM), and Ain1 (5 μM). **(B)** Fold change of Cdc8 in the pellet from conditions presented in **(A)**. Error bars=s.e.m., n=3. Filled shapes indicate individual values from each of three replicates as seen in **(A)**. Two-tailed t-tests for data sets with unequal variance yielded p-values *p=0.0450, **p=0.629, ***p=0.0348.

Fim1, we performed four-color TIRFM with fluorescently labeled ABPs and quantified Fim1 association with F-actin in the presence of Cdc8 and/or Ain1. In the absence of Ain1, Cdc8 is displaced from F-actin bundles by Fim1 in a cooperative manner, with most F-actin bundles completely devoid of Cdc8, concurrent with regions of high Fim1 localization (Figure 2.12A; [27]). Conversely, in reactions containing Ain1, over 100-fold more Cdc8 is associated with F-actin bundles (Figure 2.12B,C). Furthermore, ~40% less Fim1 is observed to associate with these bundles (Figure 2.12B,D), suggesting that the combination of Ain1 and Cdc8 is capable of inhibiting Fim1 association with F-actin networks. Additionally, in the presence of Cdc8, Fim1 and Ain1 sort into mutually exclusive domains along F-actin bundles (Figure 2.12B), similar to what has been observed previously between human Fascin1 and α-actinin-4 [186]. We speculate that competition for the same binding site allows Ain1 to prevent long stretches of Fim1 from forming that might be capable of displacing Cdc8. Thus, Fim1 poorly associates with F-actin in the presence of both Cdc8 and Ain1 because 1) Cdc8 and Ain1 prevent Fim1 from cooperatively associating with F-actin and 2) Cdc8 and Ain1 synergize to compete with Fim1. The synergy between Cdc8 and Ain1 may explain why Fim1 only poorly associates with contractile rings in fission yeast cells (Figure 2.12E).

2.4 Discussion

We have discovered that fimbrin Fim1 is inhibited from associating with actin filaments by the combined efforts of contractile ring ABPs α-actinin Ain1 and tropomyosin Cdc8. Though we have demonstrated that competition between ABPs is one key mechanism that drives their sorting to different F-actin networks, we suspect that there are several non-mutually exclusive mechanisms that mediate the sorting of Fim1 and other ABPs to the correct F-actin network. Specifically, our data suggest that Fim1's association with the contractile ring is inhibited by both (1) a preferred association with actin patches, and (2) competition with Cdc8 and Ain1.

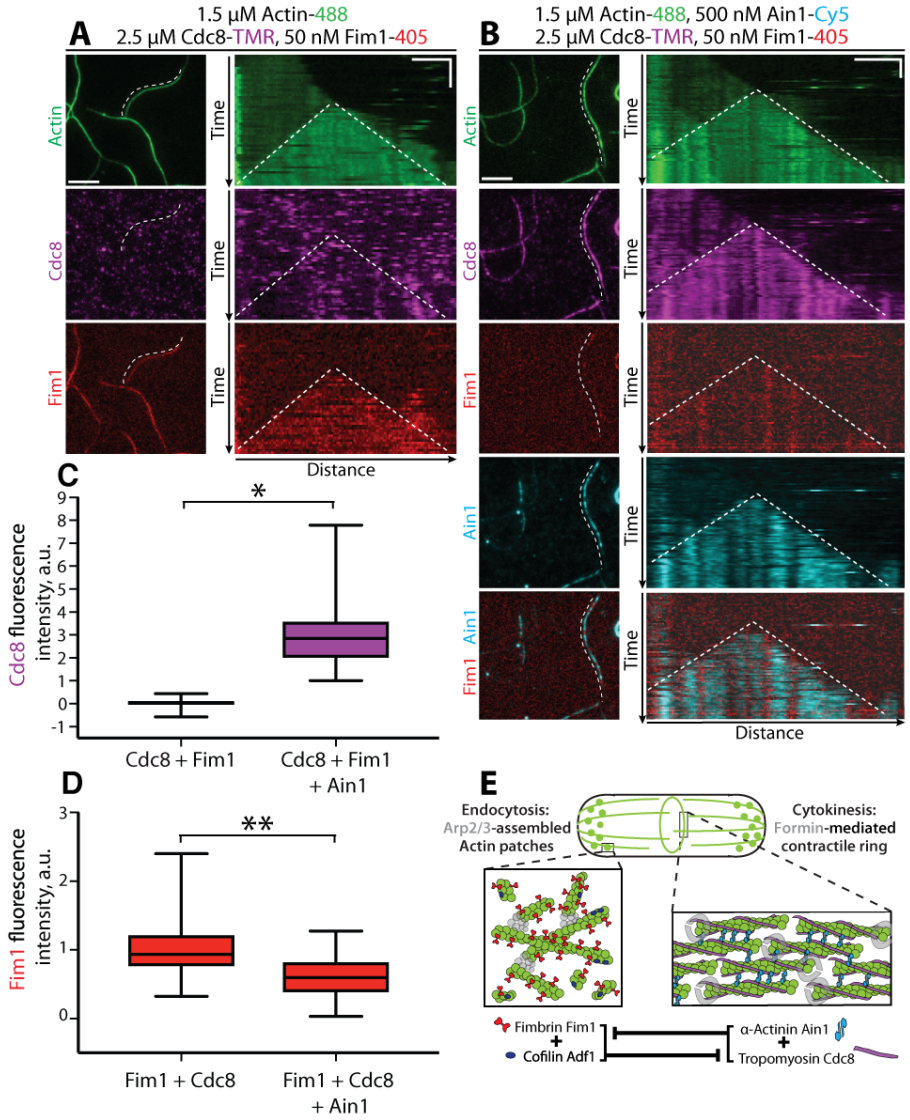

Figure 2.12: **Tropomyosin Cdc8 and α-actinin Ain1 cooperate to compete with fimbrin Fim1 for association with F-actin *in vitro*.** **(A-C)** Four-color TIRFM of 1.5 μM Mg-ATP actin (15% Alexa 488-labeled) with 50 nM fimbrin Fim1 (Alexa 405-labeled) and 2.5 μM tropomyosin Cdc8 (TMR-labeled) in the **(A)** absence or **(B)** presence of 500 nM α-actinin Ain1 (Cy5-labeled). **(A-B, left)** Representative TIRF field. Dotted lines denote bundled regions. Scale bar, 5 μm. **(A-B, right)** Kymographs of actin, Fim1, and Cdc8 during bundle formation. Dotted lines denote bundled regions. Scale bars, 3 μm. Time bar, 1 minute. **(C-D)** Box plots of the amount of Cdc8-TMR **(C)** or Fim1-Cy5 fluorescence **(D)** on two-filament bundles in experiments with Cdc8 and Fim1, or Cdc8, Fim1 and Ain1. Two-tailed t-tests for data sets with unequal variance yielded p-values *p=$3.88\text{x}10^{-16}$ and **p=$7.09\text{x}10^{-7}$. n$\geq$30 measurements from two independent experiments.

Figure 2.12: (continued) **(E)** Model of the involvement of ABP competition in ABP sorting in the fission yeast cell. In endocytic actin patches, fimbrin Fim1 and cofilin Adf1 enhance each other's activities, resulting in the displacement of tropomyosin Cdc8 from the F-actin network [27]. In the contractile ring, α-actinin Ain1 and tropomyosin Cdc8 work together to prevent fimbrin Fim1 association with the F-actin network.

2.4.1 A 'sink' model for Fim1 association with actin patches

If fimbrin Fim1 preferentially associates with actin patches over other F-actin networks, actin patches could act as a "sink" for Fim1, thereby sequestering Fim1 and limiting the concentration of free Fim1 capable of associating with other F-actin networks. Indeed, although only small amounts of Fim1 are present on the contractile ring of wild-type cells [121, 189], depletion of actin patches (the "sink") by the Arp2/3 complex inhibitor CK-666 results in significantly more Fim1 associating with the contractile ring (Figure 2.1B). However, a sink model alone likely cannot account for Fim1's primary localization to actin patches. Only 30% (~25,000) of the ~86,500 total Fim1 molecules in a fission yeast cell associate with ~50 actin patches [159, 191]. Therefore, 70-75% of Fim1 molecules are either cytoplasmic or associated with another F-actin network. We suspect that other mechanisms (conformational changes in the actin filament, ABP dynamics, post-translational modifications) may dictate both Fim1's preferential association with actin patches, as well as the observed competitive and cooperative interactions amongst Fim1, α-actinin Ain1, and tropomyosin Cdc8.

2.4.2 Conformational changes in the actin filament

Actin forms a flexible polymer capable of adopting a variety of conformations [50, 129], and different F-actin conformations have been demonstrated to both result from or influence the association of ABPs [114, 134, 146]. Fimbrin Fim1's inherent preference for actin patches could result from a preference for either a branched F-actin network or for a particular twist or conformational change imparted by Arp2/3 complex-mediated actin assembly. We suspect that conformational changes in the actin filament may also affect the observed increase of

α-actinin Ain1-mediated bundling in the presence of Cdc8 (Figure 2.10A-D). Tropomyosins have been found to increase the persistence length of F-actin [47, 73], suggesting that they are capable of altering the conformation of an actin filament. Therefore, Cdc8 may mediate a slight conformational change more amenable to Ain1 binding, increasing the density of Ain1 on the actin filaments and the corresponding degree of bundling. Tropomyosin's increase of the persistence length of F-actin may have an additional effect on actin bundling by promoting bundle stability and inter-filament contacts.

2.4.3 ABP dynamics affect their ability to compete

We discovered that the contractile ring ABP α-actinin Ain1 competes with fimbrin Fim1, and that dynamic association of both Ain1 and Fim1 with actin filaments affects their ability compete at different F-actin networks. In particular, we found that a less dynamic mutant Ain1(R216E) mislocalizes to F-actin patches in the presence of Fim1. However, in addition to ectopic localization to actin patches, cells expressing Ain1(R216E) also have cytokinesis defects [102]. These findings may explain why fission yeast requires two F-actin bundling proteins. Actin patches require a stable F-actin bundler such as Fim1 to crosslink the branched actin filament network, prevent tropomyosin Cdc8 association, and create boundaries that enhance ADF/cofilin Adf1-mediated severing [27, 162]. On the other hand, a dynamic F-actin bundler is required at the contractile ring to facilitate anti-parallel F-actin contacts while still allowing Cdc8 association and myosin-mediated actin filament sliding and contraction [102]. For these reasons, we assume that the dynamic Ain1 is an ideal actin crosslinker for the contractile ring (Figure 2.10E-G). Though our results suggest that Ain1 is more dynamic on uncoated actin filaments, we showed that wild-type Ain1 is still a dynamic bundler on Cdc8-coated actin filaments and is likely capable of allowing contractile ring ABPs to remain associated with and function optimally at the contractile ring.

Additionally, the binding dynamics of Ain1 and Fim1 on F-actin seem to mediate their

competition with Cdc8. We demonstrated that Fim1, but not Ain1, displaces Cdc8 from F-actin bundles. However, Fim1 competes with Cdc8 specifically at regions where it binds stably (F-actin bundles), and does not compete as strongly with Cdc8 on single filaments [27]. Therefore, the presence of a dynamic bundling protein (Fim1 on single filaments and Ain1 on both single and bundled filaments) may allow Cdc8 to remain associated with F-actin in those circumstances. Future studies will seek to build a fuller picture of how Fim1 and Ain1 differentially affect the activity of other ABPs present at the contractile ring such as myosin-II and cofilin Adf1.

2.4.4 Post-translational modifications and other sorting mechanisms

In vitro, the combined efforts of α-actinin Ain1 and tropomyosin Cdc8 together prevent ~40% of fimbrin Fim1 association with F-actin bundles. It should be noted that though Ain1 and Cdc8 work together to compete with Fim1, our reactions contain low concentrations (50 nM) of Fim1 compared to Ain1 (500 nM or 1 μM) and Cdc8 (2.5 μM). Given the potent F-actin binding and bundling abilities of Fim1 and the high cellular concentration of Fim1, a reasonable assumption is that Cdc8 and Ain1 may only prevent a portion of Fim1 polypeptides from associating with contractile ring F-actin *in vivo*. Therefore, other non-mutually exclusive mechanisms likely contribute to ABP sorting. One possibility is that additional ABPs inhibit Fim1 from associating with the contractile ring. A second possibility is that Fim1 is post-translationally modified, regulating its activity. Budding yeast fimbrin Sac6 is phosphorylated at different stages of the cell cycle, which affects its ability to associate with F-actin [111]. Fission yeast Fim1 might be similarly post-translationally modified [86, 173], and therefore a portion of the cytoplasmic Fim1 pool might be more or less active. A third possibility is that mechanical stresses applied to actin filaments, such as the contractile forces applied by the molecular motor type-II myosin Myo2 during contractile ring assembly and constriction, might differentially alter the F-actin binding and/or activity

of actin patch and contractile ring ABPs [149].

2.4.5 A similar combination of mechanisms could drive ABP sorting to other F-actin networks

We expect that similar fundamental mechanistic principles also promote ABP sorting at other F-actin networks, both in fission yeast and in multicellular organisms. One possibility is that actin assembly factors, such as the Arp2/3 complex (actin patches), formin Cdc12 (contractile rings), and formin For3 (actin cables) might initiate the assembly of actin filaments that have intrinsic differences (such as a specific filament conformation) that facilitate the differential sorting of certain ABPs to actin patches, actin cables, and contractile rings [91, 114]. The initial actin assembly factor-dependent recruitment of one ABP may then subsequently recruit and/or inhibit other ABPs, defining both the subset of ABPs that associate with a particular F-actin network as well as the network's corresponding architecture and dynamics. For example, though fission yeast has a single tropomyosin isoform, Cdc8, it can be either acetylated or unacetylated [163]. While the acetylated form of Cdc8 associates with the contractile ring, the unacetylated form associates with actin cables [32]. Unacetylated Cdc8 preferentially associates with For3-assembled F-actin regardless of where it is assembled [74]. The unacetylated and acetylated forms of Cdc8 may differentially compete or cooperate with other ABPs, resulting in distinct ABP subsets associating with each network. Interestingly, how ABPs influence one another could also depend on the cellular type or context, as tropomyosin and α-actinin-4 exhibit an antagonistic relationship during stress fiber formation in MDCK cells [85]. Future work will involve investigating the potential role of actin assembly factors in regulating ABP sorting and understanding the competitive and cooperation interactions between ABPs in other cell types.

Strain name	Genotype	Reference
KV91	h+, kanMX6::myo2p::gfp-myo2p+, ade6-M210, leu1-32, ura4-D18	[190]
KV343	h?, cdc12-mGFP::KanR	This study
KV459	h+, rlc1-tdTomato-natMX6 ade6-M210 leu1-32 ura4-D18	This study
KV579	h-, ain1-GFP-KanMX6, URA+	[189]
KV588	h+, pAct1 Lifeact-GFP::Leu+; ade6-m216; leu1-32; ura4-D18	[71]
KV707	h-, leu1-32, his3-D1, ura4-D18, ade6-M216, Pnmt41-SpAin1-mGFP::Leu+	This study
KV804	h?, fim1-mCherry-natMX6, ain1-Δ1::kanMX6, Pnmt41-SpAin1-mGFP::Leu+	This study
KV818	h+ kanMX6-Prng2-mEGFP-rng2 ade6-M210 leu1-32 ura4-D18	[94]
KV856	h?, h?, ain1-Δ1:: kanMX6, Pnmt41-SpAin1(R216E)-mGFP::Leu+, fim1-mCherry-natMX6, ade6, leu1-32, ura4-D18	This study
KV861	h?, ain1-GFP-kanMX6, sad1-tdTomato-natMX6, ade6-m21?, leu1-32, ura4-D18	This study
KV878	h+, fim1-mGFP-kanMX6, sad1-tdTomato-natMX6	This study
KV908	h? fim1-1Δ-kanMX6, ain1-GFP-kanMX6, sad1-tdTomato::natMX6	This study
KV963	h?, fim1-1Δ::kanMX6, Pnmt41-SpAin1-mGFP::Leu+	This study
KV968	h? Pnmt41-SpAin1-mGFP::Leu+, ARPC5-mCherry-natMX6	This study

Table 2.1: **Fission yeast strains used in Chapter 2.**

2.5 Materials and Methods

2.5.1 Strain construction and growth

Fission yeast strains were created by genetic crossing on SPA5S plates followed by tetrad dissection on YE5S plates. Strains were screened for auxotrophic (leu, ura) or antibiotic (nat, kan) markers and maintained on YE5S plates. Glycerol stocks were created by pelleting cells and resuspending in 750 μL media and 250 μL of 50% sterile glycerol. Table 2.1 lists the

fission yeast strains used in this study.

2.5.2 Cell imaging and treatment with CK-666

For live cell imaging, cells were grown in YE5S media overnight at 25° C, subcultured into EMM5S media without thiamine, and kept in log phase for 20-22 hours at 25° C. Cells were imaged directly on glass slides. Z-stacks of 10 slices, 0.5 μm apart were acquired with a 100x, 1.4 NA objective on a Zeiss Axiovert 200M equipped with a Yokogawa CSU-10 spinning-disk unit (McBain, Simi Valley, CA) illuminated with a 50-milliwatt 473-nm DPSS laser, and a Cascade 512B EM-CCD camera (Photometrics, Tucson, AZ) controlled by MetaMorph software (Molecular Devices, Sunnyvale, CA). For CK-666 treatments, CK-666 powder stock (Sigma, St. Louis, MO) was diluted to 10 mM in DMSO. Cells were grown as stated above, and incubated with CK-666 or an equivalent volume of DMSO (control) in a rotator at 25° C for 30 min prior to imaging. Cells were then immediately imaged as above.

2.5.3 Contractile ring fluorescence quantification

Contractile ring maturation was divided into three stages by measuring the distance between spindle pole bodies (SPBs, visualized by Sad1-tdTomato) and noting constriction of the contractile ring. Stage 1 cells had SPBs less than 6 μm apart, with no observable ring constriction. Stage 2 cells had SPBs greater than 6 μm apart, with no observable ring constriction. Stage 3 cells had SPBs less than 9 μm apart, with evident ring constriction. Quantification of ABP association with defined contractile rings (stages 2 and 3) is shown in Figure 2.1B-D, and quantification at each distinct ring stage is show in Figure 2.4. The contractile ring region was determined by visually examining the z-stack for the ring site. Normalized contractile ring fluorescence was taken by drawing a region of interest (ROI) around the observed ring and around the whole cell using ImageJ. To obtain a fluorescence value for cells without a visible contractile ring (for example, DMSO-treated Fim1-GFP

cells), mitotic cells were determined by the presence of two spindle pole body markers. These fission yeast cells were measured along their length and a 4-pixel width line was drawn across the exact center of the fission yeast cell (denoted as a yellow dotted-line in Figure 2.1B). The mean fluorescence of the ring divided by the whole cell was then determined. A value of 1.00 indicates no increased fluorescence at the site of the contractile ring, while values >1 indicate increased fluorescence at the ring. Maximum projections were used for images in figures and sum projections were used for quantification.

2.5.4 Tropomyosin Cdc8 antibody staining

Following standard growth and culturing protocols for live cell imaging, fission yeast cells were stained with anti-Cdc8p [35]. Cells were fixed in 16% formaldehyde for 5 min at 20° C. Cells were then washed in cold 1X PBS and resuspended in 140 μL 1.2M sorbitol. 60 μL fresh protoplasting solution (3 mg/ml zymolase 100T in 1.2M sorbitol) was added and cells were incubated for 7 min on a rotator at room temperature. 1 mL of 1% Triton-X was then added to the cells and incubation continued for 2 min. Cells were then pelleted and resuspended in 0.5 mL PBAL (10% BSA, 100 mM lysine monohydrochloride, 1 mM NaN_3, 50 ng/ml ampicillin in PBS) and incubated for 2.5 hr on a rotator at room temperature. Cells were resuspended in 100 μL of anti-Cdc8p 1:10 in PBAL (gift of Sarah Hitchcock-DeGregori) and incubated overnight at 4° C on a rotator. Following incubation with primary antibody, cells were washed 3 times with 0.5 mL PBAL and resuspended in 50 μL Alexa-Flour 555 goat anti-rabbit secondary antibody (Thermo-Fisher Scientific, Carlsbad, CA) (1:100 in PBAL) and incubated for 90 min at room temperature on a shaker in the dark. Cells were then washed 5 times with 0.5 mL PBAL and resuspended in 20-30 μL PBAL for imaging. Cells were stored at 4° C and imaged within 48 hr of staining.

2.5.5 Protein purification

Chicken skeletal muscle actin was purified as described previously. Fimbrin Fim1 and tropomyosin AlaSer-Cdc8 (WT and I76C mutant) were expressed in BL21-Codon Plus (DE3)-RP (Agilent Technologies, Santa Clara, CA). His-tagged Fim1 was purified using Talon Metal Affinity Resin (Clontech, Mountain View, CA). Cdc8 was purified by boiling the cell lysate, performing an ammonium sulfate cut, and running on an anion exchange column. His-tagged wild-type α-actinin Ain1 and mutant Ain1(R216E) were expressed in High Five insect cells using baculovirus expression and purified using Talon Metal Affinity Resin.

The A280 of purified proteins was taken with a Nanodrop 2000c Spectrophotometer (Thermo-Scientific, Waltham, MA). Protein concentration was calculated using extinction coefficients Fim1: 55,140 M^{-1} cm^{-1}, Cdc8 (WT and I76C mutant): 2,980 M^{-1} cm^{-1}, Ain1 and Ain1(R216E): 86477 M^{-1} cm^{-1}. Proteins were labeled with TMR-6-maleimide (Life Technologies, Grand Island, NY) or Cy5-monomaleimide (GE Healthcare, Little Chalfont, UK) dyes following manufacturer's protocols following purification. Proteins were flash-frozen in liquid nitrogen and stored at -80° C.

2.5.6 Low-speed sedimentation assays

To peform low-speed sedimentation assays, 15 μM Mg-ATP actin monomers were spontaneously assembled in 10 mM imidazole, pH 7.0 50 mM KCl, 5 mM $MgCl_2$, 1 mM EGTA, 0.5 mM DTT, 0.2 mM ATP, and 90 μM $CaCl_2$ for 1 hr to generate F-actin. F-actin was then incubated with 500 nM Ain1 and a range of concentrations of Cdc8 (Figure 2.10A,B), or 5 μM Cdc8 and 0.5 μM Fim1-SNAP and/or 5 μM Ain1 (Figure 2.11A,B). This incubation occurred for 20 min at 25° C, followed by a 10,000g spin for 20 min at RT. Supernatant and pellets were separated by 15% SDS-PAGE gel electrophoresis and stained for 30 min with

Coomassie Blue, destained for 16 hr, and analyzed by densitometry with ImageJ.

2.5.7 TIRF microscopy (TIRFM)

Time-lapse TIRFM movies were obtained using an Olympus IX-71 microscope with through-the-objective TIRF illumination, iXon EMCCD camera (Andor Technology), and a cellTIRF 4Line system (Olympus). The actin binding proteins (ABPs) of interest were initially added to a polymerization mix (10 mM imidazole (pH 7.0), 50 mM KCl, 1 mM $MgCl_2$, 1 mM EGTA, 50 mM DTT, 0.2 mM ATP, 50 μM $CaCl_2$, 15 mM glucose, 20 μg/mL catalase, 100 μg/mL glucose oxidase, and 0.5% (400 centipoise) methylcellulose). This ABP/polymerization mix was then added to Mg-ATP-actin (15% Alexa 488-labeled) to induce F-actin assembly in the presence of the ABPs of interest. The mixture was then added to a flow chamber and imaged at room temperature at 5 s intervals (unless otherwise noted).

2.5.8 Quantification of bundling

The percentage of actin filaments bundled was quantified at similar actin filament densities (between 2095 and 2295 μm total filament length) for each experiment. The total actin filament length in the chamber was measured manually by creating ROIs for every actin filament and measuring total actin filament length in FIJI. ROIs for every segment of actin filament present in a bundle were then created and total bundled filament length measured. A 'bundled' segment was identified by looking at the history of the TIRF movie and determining that two actin filaments were associated and had been associated for at least three consecutive frames (at least 15 s) including the frame quantified. The ratio of actin filament present in a bundle vs. total actin filament length was then calculated.

2.5.9 Quantification of fluorescence intensity on actin filaments or bundles

Fluorescence intensity on actin filaments was quantified on movies taken under the same microscope conditions (laser intensity and angle, exposure time) and with the same protein batches. Fluorescence intensity was quantified at the same time point in each compared movie. The actin channel was used to identify single actin filaments or two-filament actin bundles, and ROIs of a 3-pixel segmented line were created along all single filaments or two-filament bundles in the selected frame. The mean fluorescence for each segment was then measured using ImageJ.

2.5.10 Quantifying number of cells with Ain1 in actin patches

To quantify the number of cells containing Ain1-GFP in actin patches, one minute timelapse movies of 1 frame per second were taken, imaging both Ain1-GFP and an actin patch marker (ArpC5-mCherry or Fim1-mCherry). Movie files for independent experiments and replicates were blinded and independently analyzed for number of cells containing Ain1-GFP in actin patches using FIJI. For a single cell to count as positively containing Ain1-GFP in actin patches, three criteria had to be met: 1) at least one distinguishable actin patch containing Ain1-GFP was observed, 2) the observed actin patch(es) contained Ain1-GFP for at least 3 frames and 3) the Ain1-GFP signal trajectory matched the channel expressing either ArpC5-mCherry or Fim1-mCherry. Total number of cells and cells with actin patches containing Ain1-GFP were then calculated to obtain percent of cells containing Ain1-GFP in actin patches.

2.5.11 Quantification of Ain1 spot density

TIRFM images were collected with a cellTIRF 4Line system (Olympus) fitted to an Olympus IX-71 microscope with through-the-objective TIRF illumination and an iXon EMCCD

camera (Andor Technology, Belfast, UK). 1.5 μM Mg-ATP-actin (10% Alexa 488 labeled) was mixed with polymerization TIRF buffer [10 mM imidazole (pH 7.0), 50 mM KCl, 1 mM $MgCl_2$, 1 mM EGTA, 50 mM DTT, 0.2 mM ATP, 50 μM $CaCl_2$, 15 mM glucose, 20 μ/mL catalase, 100 μg/mL glucose oxidase, and 0.5% (400 centipoise) methylcellulose] to induce F-actin assembly, 0.5 μM 0.5% TMR labeled α-actinin, and 2 μ (monomer 1 μM dimer) unlabeled tropomyosin. This mixture was transferred to a flow cell for imaging at room temperature. Once the actin had polymerized and formed bundles, we imaged once in the 488 channel to visualize the labeled actin (1 frame, 488 nm excitation for 50 ms) and then continuously imaged in the 561 channel to visualize the sparsely labeled α-actinin (100 frames, 561 nm excitation for 50 ms, ~110 ms interval).

To measure α-actinin Ain1 spot density, we created kymographs on bundles for each experiment using ImageJ. Ain1 spots were detected in the kymograph as lines at least four pixels wide with a fluorescence value above 1.25 times that of background fluorescence. Spot density was normalized to the length of actin filaments in the bundle. Ain1 spot density was determined using the following formula:

$$\frac{(n/(Lr))}{t} \tag{2.1}$$

Where n is the number of Ain1 spots detected, L is the length of the bundle in μm, r is the actin fluorescence ratio (total amount of fluorescence in the actin bundle divided by the average fluorescence of single actin filaments), and t is the time of measurement in seconds.

CHAPTER 3

ARP2/3 COMPLEX- AND FORMIN-MEDIATED ACTIN NETWORKS TUNE ACTIN-BINDING PROTEIN SORTING IN FISSION YEAST

Preface

The work in this chapter was performed with assistance from Cristian Suarez and Glen Hocky. Cristian Suarez provided assistancd in the development of the project, while Glen Hocky performed the modeling in Figures 3.9 and 3.10. I completed and analyzed the rest of the experimental data and made all of the figures.

3.1 Abstract

F-actin networks are diverse and specialized to carry out specific cellular processes, such as polarization, endocytosis, and cytokinesis. Each F-actin network is tightly regulated by a unique set of actin-binding proteins (ABPs) that initiates and maintains the organization of actin filaments. However, the general mechanistic principles by which specific ABPs sort to particular F-actin networks remain largely unclear. By combining *in vivo* fluorescence microscopy and *in vitro* reconstitution, we discovered that two actin assembly factors, Arp2/3 complex and formin Cdc12, tune the binding of ABPs fimbrin and tropomyosin to specific F-actin networks in fission yeast. Disruption of F-actin networks by small molecule inhibitors or genetic manipulation revealed that fimbrin is preferentially recruited to Arp2/3-complex mediated actin patches, while tropomyosin is preferentially targeted to Cdc12-mediated filaments in the contractile ring. To investigate the role of Arp2/3 complex and Cdc12 in this ABP sorting, we used four-color *in vitro* TIRF microscopy to reconstitute ABP sorting with purified proteins. We discovered that competition between fimbrin and tropomyosin is

critically important for their association with distinct actin networks. Interestingly, either fimbrin or tropomyosin alone binds similarly to Arp2/3 complex- and Cdc12-mediated actin filaments. Conversely, sorting of these ABPs to their preferred actin filaments occurs when Arp2/3 complex- and Cdc12-mediated filaments are assembled together in the presence of both fimbrin and tropomyosin. Under these conditions, fimbrin accumulates ~2-fold more at Arp2/3 complex branch points, while tropomyosin association is enhanced 3.5-fold on filaments assembled by Cdc12. This result is supported by a computational model that uses a system of rate equations to examine the contributions of ABP competition and cooperativity to sorting. According to the model, maximum ABP sorting occurs only when ABPs are allowed to compete for binding to F-actin networks assembled by distinct assembly factors. In summary, these findings reveal for the first time that the F-actin assembly factors Arp2/3 complex and formin Cdc12 facilitate the recruitment of specific ABPs, thereby tuning ABP sorting and subsequently establishing the identity of a given F-actin network.

3.2 Introduction

The self-organization of ordered structures from basic molecular components is a fundamental concept from biological to chemical systems, but central questions remain as to how macromolecular assemblies actually self-organize [82, 115]. The actin cytoskeleton provides an ideal model for the study of cellular self-organization, as cells assemble actin monomers (G-actin) into filamentous polymers (F-actin) with a variety of functionally diverse architectures and dynamics to facilitate essential cellular processes. These distinct F-actin networks are simultaneously built and maintained within a single crowded cytoplasm, and this process is aided by actin-binding proteins (ABPs) that help to define the characteristics of specific F-actin networks by nucleating, severing, bundling, and capping actin filaments [139]. Because the specific identity and function of each specific F-actin network depends on the set of ABPs that decorates it, proper sorting of ABPs is crucial during self-organization. The

cellular functions of many individual ABPs have been studied at length, but we are only recently starting to understand how these ABPs cooperate and compete with one another and how their interactions could mediate global cytoskeletal organization [114, 162, 27, 77].

The molecular mechanisms underlying self-organization of the actin cytoskeleton are optimally studied in fission yeast, where three functionally distinct F-actin network structures are initiated by different assembly factors: endocytic actin patches (Arp2/3 complex), the contractile ring (formin Cdc12), and polarizing actin cables (formin For3). Additionally, each of these networks is associated with a distinct but overlapping set of ABPs. We have recently discovered that competition between ABPs for association with actin filaments is critical for their proper sorting to different F-actin networks in fission yeast [27, 162], but why specific ABPs exhibit preferences for specific F-actin networks *in vivo* is unclear. Work from several groups suggests that actin assembly factors could be sufficient to generate F-actin networks capable of recruiting the proper subset of ABPs [21, 103, 114]. Therefore, in this study we examine the role of actin assembly factors in the initiation of ABP competition. We hypothesize that mechanistically distinct actin assembly factors drive ABP sorting by generating actin filaments with specific characteristics, such as architecture and twist, that recruit different subsets of ABPs to each network. By combining live cell imaging of fluorescent ABPs in fission yeast with multi-color TIRF microscopy of reconstituted Arp2/3 complex- and formin Cdc12-mediated networks, we show that actin assembly factors tune the binding of ABPs fimbrin and tropomyosin to distinct F-actin networks. Specifically, fimbrin preferentially associates with Arp2/3 complex-mediated actin patches *in vivo*, while tropomyosin is targeted to the formin Cdc12-mediated contractile ring. Conversely, we observe that fimbrin and tropomyosin alone bind similarly to both Arp2/3 complex and Cdc12-mediated actin filaments in vitro. Furthermore, neither competition between fimbrin and tropomyosin for binding to a single assembly factor-mediated network nor competition between assembly factors for a single ABP leads to their sorting to distinct actin filaments. However, when Arp2/3

complex- and Cdc12-mediated filaments are assembled in the presence of both fimbrin and tropomyosin, we discovered that remarkably, fimbrin sorts to branched actin filaments mediated by Arp2/3 complex, while tropomyosin sorts to F-actin assembled by Cdc12. This result is supported our computational model, which reveals that the maximum degree of ABP sorting requires competition between ABPs for binding F-actin networks generated by distinct assembly factors. Together, these findings reveal that F-actin assembly factors initiate ABP sorting by recruiting specific ABPs that compete and cooperate with each other to facilitate ABP sorting and establish the identity of each F-actin network.

3.3 Results

3.3.1 Tropomyosin Cdc8 and Fimbrin Fim1 are recruited to different F-actin networks in fission yeast

Tropomyosin and fimbrin are known to compete for binding actin filaments in the fission yeast *Schizosaccharomyces pombe* [27, 162]. Tropomyosin is a dimeric, parallel coiled-coil molecule that cooperatively associates end-to-end to form tropomyosin cables that extend along the sides of α-helical actin filaments. *S. pombe* tropomyosin Cdc8 (hereafter Cdc8) is known to associate with formin-mediated actin filaments to regulate access of other ABPs to these filaments, such as cofilin Adf1 and myosin-I Myo1 [27, 162, 28]. We previously discovered that Cdc8's association with Arp2/3 complex-mediated filaments in actin patches depends on competition with fimbrin Fim1 (hereafter Fim1), an F-actin crosslinking protein [162]. Fim1 association with branched filaments in actin patches prevents Cdc8 from binding to patches, promoting F-actin turnover by allowing cofilin Adf1-mediated severing. Fim1 also actively displaces Cdc8 from bundled filaments *in vitro* [27]. To further investigate the nature of competition between Fim1 and Cdc8 *in vivo*, we utilized time-lapse confocal microscopy to examine the localization of GFP-tagged Cdc8 throughout the cell cycle in

fission yeast cells in both wild-type (WT) and *fim1-1*Δ backgrounds. In each case, GFP-Cdc8 was co-expressed with ARPC5-mCherry to visualize actin patches. As expected, GFP-Cdc8 is diffuse in the cytoplasm of WT background control cells during interphase, but is recruited to the contractile ring upon its assembly during mitosis (Figure 3.1A-B). Only 9% of cellular Cdc8 colocalizes with Arp2/3 complex during interphase in control cells, while this percentage increases ~two-fold during mitosis due to the previously characterized action of Arp2/3 complex-mediated patches at the cell midzone during cell division (Figure 3.1E; [48]). In contrast, GFP-Cdc8 associates with actin patches in the absence of Fim1 (*fim1-1*Δ background) and colocalizes with Arp2/3 complex as we have previously shown [162], but only during interphase (Figure 3.1C-D). Interestingly, we see that upon entry into mitosis, Cdc8 is recruited away from actin patches to the contractile ring, where it remains until the contractile ring is disassembled, when it moves back to the actin patches (Figure 3.1C). A linescan of Cdc8 fluorescence intensity across the length of a *fim1-1*Δ cell indicates that the fluorescence intensity of Cdc8 in the cell tips decreases more than two-fold when the contractile ring is present (Figure 3.1D). Furthermore, the percentage of cellular Cdc8 that colocalizes with Arp2/3 complex in the absence of Fim1 decreases from almost 50% in interphase to 14% when the ring is present (Figure 3.1E). Thus, although Cdc8 is capable of associating with both Arp2/3 complex-mediated branched networks and formin Cdc12-mediated networks, it exhibits a bias toward F-actin in the contractile ring, which we suspect results from its preference for the longer, straight actin filaments assembled by Cdc12.

To determine whether Fim1 exhibits a similar preference for specific F-actin networks, we examined the localization of Fim1-GFP in cells expressing fluorescent myosin-II regulatory light chain Rlc1-tdTomato to mark the contractile ring. In control cells treated with DMSO, Fim1-GFP localizes predominantly to actin patches in cell tips, as expected (Figure 3.1F-G(left)) [189, 121]. However, in cells treated with the Arp2/3 complex inhibitor CK-666, Fim1-GFP is released from actin patches and associates strongly with the contractile ring as

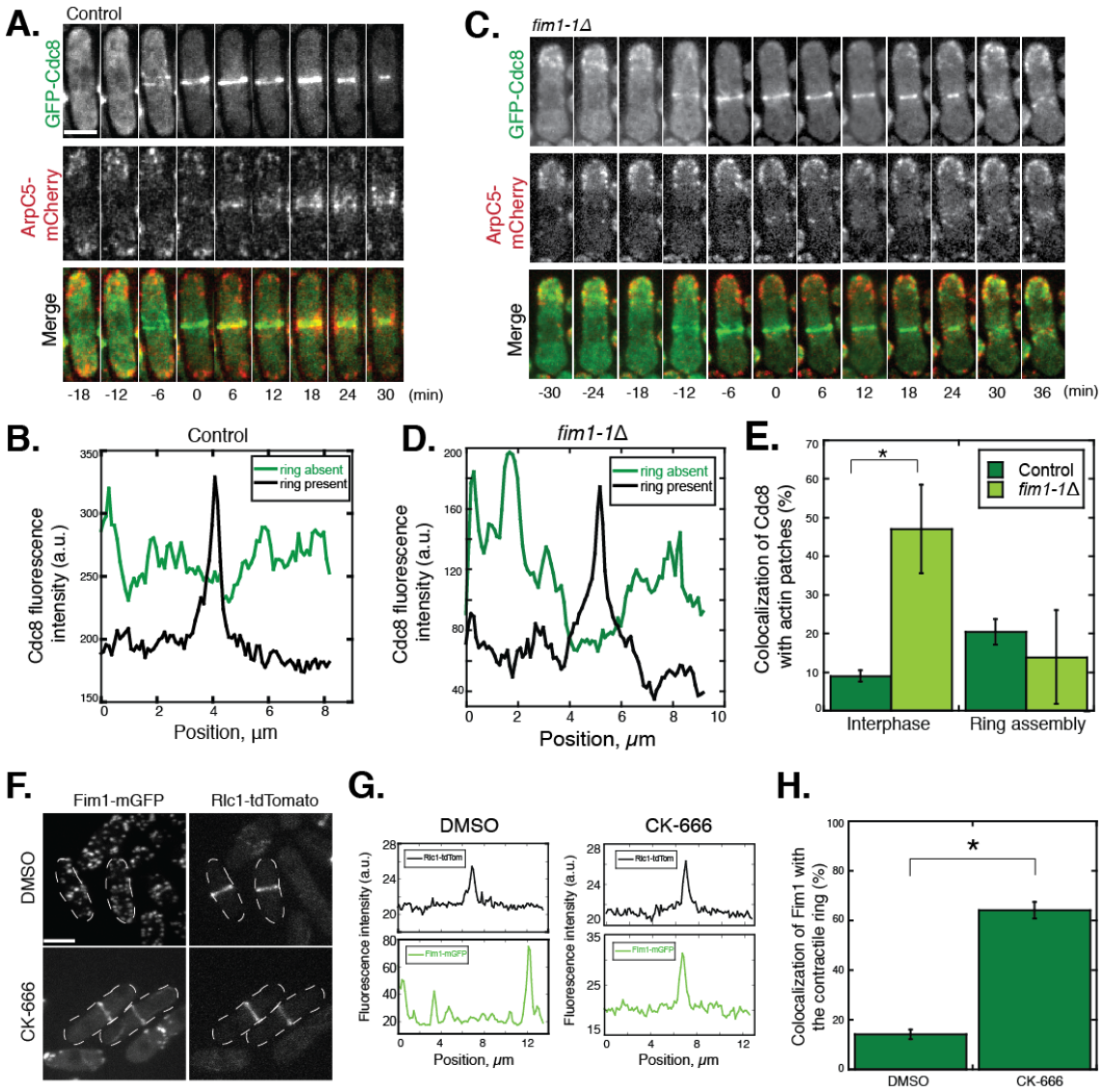

Figure 3.1: **Fimbrin Fim1 and Tropomyosin Cdc8 are recruited to distinct F-actin networks in fission yeast.** **(A)** Time-lapse fluorescence micrographs of control fission yeast cell expressing GFP-Cdc8 and ArpC5-mCherry. Scale bar, 5 μm. Time 0: completion of contractile ring assembly. **(B)** Linescan of GFP-Cdc8 fluorescence intensity in cell from **(A)** during interphase and mitosis. **(C)** Time-lapse fluorescence micrographs of fission yeast cell expressing GFP-Cdc8 and ArpC5-mCherry in a *fim1-1*Δ background. Scale bar, 5 μm. Time 0: completion of contractile ring assembly. **(D)** Linescan of GFP-Cdc8 fluorescence intensity in cell from **(C)** during interphase and mitosis. **(E)** Plot of the percent of colocalization of GFP-Cdc8 with actin patches, marked by ArpC5-mCherry, in the indicated fission yeast strains in the absence (interphase) or presence (ring assembly) of a contractile ring. Error bars=s.e.m. A two tailed t-test for data sets with unequal variance yield p-value *p=0.00311. n$\geq$4 cells from two independent experiments. **(F)** Fluorescent micrographs of fission yeast

Figure 3.1: (continued) cells expressing Fim1-mGFP and Rlc1-tdTomato in a *for3*Δ background following treatment with DMSO (control, top) or Arp2/3 complex inhibitor CK-666 (bottom). Scale bar, 5 μm. **(G)** Linescans of Rlc1-tdTomato (top) and Fim1-mGFP (bottom) fluorescence for single cell from **(F)** under treatment with DMSO (left) or CK-666 (right). **(H)** Plot of the percent colocalization of Fim1-mGFP with the contractile ring, marked by Rlc1-tdTomato, in cells treated with DMSO (left) or CK-666 (right). Error bars=s.e.m. A two tailed t-test for data sets with unequal variance yield p-value *p=0.0058. n$\geq$20 cells from two independent experiments.

seen previously [27], where it colocalizes with Rlc1-tdTomato (Figure 3.1F-G(right)). Indeed, the percent of cellular Fim1 that colocalizes with Rlc1-tdTomato increases ~five-fold upon treatment with CK-666 (Figure 3.1H). Thus, we observe that like Cdc8, Fim1 is capable of associating with both Arp2/3 complex-mediated actin patches and the Cdc12-mediated contractile ring in fission yeast. Unlike Cdc8, Fim1 is preferentially recruited to branched filaments in actin patches under normal cellular conditions, which again suggests that ABPs could recognize the specific F-actin characteristics that are imparted by different assembly factors. However, it is difficult to truly understand the role actin assembly factors play in this "sorting" of Cdc8 and Fim1 to distinct F-actin networks *in vivo*, as we are unable to reach the resolution required to separate the contributions of extrinsic signalling events from the effects of the actin assembly factors. Moreover, the sorting process in fission yeast cells is complicated by the presence of many additional ABPs that influence one another's association with F-actin (see Chapter 2). Thus, we turn to *in vitro* reconstitution to investigate whether actin assembly factors are sufficient to drive ABP sorting.

3.3.2 Direct visualization of tropomyosin Cdc8 and fimbrin Fim1 associating with actin filaments mediated by Arp2/3 complex and Cdc12 in vitro

To elucidate whether ABP sorting to distinct F-actin structures can be recapitulated in vitro, we used TIRF microscopy (TIRFM) to visualize actin filaments assembled by either Arp2/3 complex or formin Cdc12 and analyzed the association of fimbrin Fim1 and tropomyosin Cdc8

with these two types of actin filaments. We previously engineered cysteine mutations within Cdc8 that allowed it to be labeled for visualization with TIRF microscopy. One mutant, Cdc8(D142C), bound F-actin most similarly to WT Cdc8 and caused only mild cytokinesis defects in fission yeast and thus was chosen for further study in TIRF experiments [27]. Based on previous work, we know that saturating concentrations of Fim1 can fully displace Cdc8 from actin filaments, with maximal displacement at 5 μM Fim1 [27, 162]. As a result, we used lower concentrations at which both Fim1 and Cdc8 can occupy the same filament: 250 nM Fim1 and 1.5 μM Cdc8 (dimer).

250 nM Fim1 loads onto actin filaments assembled by Arp2/3 complex by binding along the length of both the Arp2/3 complex mother filament prior to branch formation and the daughter filament as it elongates (Figure 3.2A-B). Similarly, Fim1 binds along the length of actin filaments both nucleated and elongated by formin Cdc12 to a similar extent (Figure 3.2C-E). Additionally, 1.5 μM Cdc8 also binds along the length of Arp2/3 complex mother and daughter filaments, as well as filaments nucleated and elongated by Cdc12 (Figure 3.2F-J). Based on our *in vivo* experiments, it is not surprising that either Fim1 or Cdc8 is capable of binding to actin filaments mediated by Arp2/3 complex and Cdc12 given that they were both shown to occupy Arp2/3 complex-mediated actin patches and the Cdc12-mediated contractile ring under different conditions (Figure 3.1). However, it is undeniable that these ABPs exhibit strong preferences for particular F-actin networks under normal cellular conditions, as Fim1 primarily localizes to actin patches and Cdc8 strictly associates with formin-mediated networks. Therefore, we concluded that a key component necessary for ABP sorting is missing from this experimental setup. Because ABPs are faced with a choice between multiple diverse F-actin networks that are simultaneously present in cells, we hypothesized that sorting events might occur only in the presence of actin filaments mediated by multiple actin assembly factors.

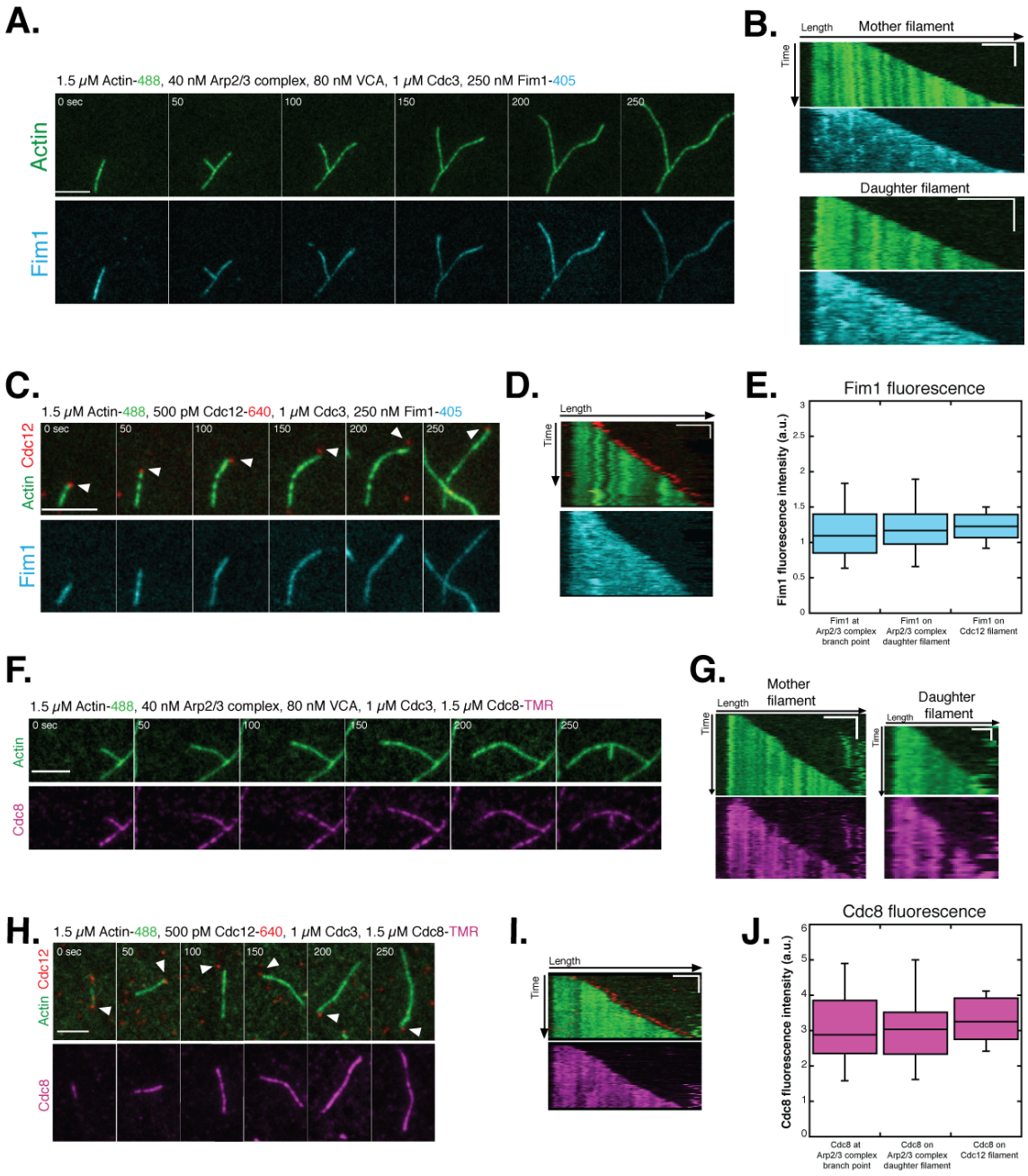

Figure 3.2: **Fim1 and Cdc8 bind similarly to Arp2/3 complex- and Cdc12-mediated actin filaments.** **(A-B)** Two-color TIRFM of 1.5 μM Mg-ATP actin (15% Alexa488-labeled) with 1 μM profilin Cdc3, 250 nM fimbrin Fim1, 40 nM Arp2/3 complex and 80 nM VCA. **(A)** Timelapse of Arp2/3 complex-mediated filament. Scale bar, 5 μm. **(B)** Kymographs of Arp2/3 complex filaments shown in **(A)**. Scale bars, 3 μm. Time bars, 100 s. **(C-D)** Three-color TIRFM of 1.5 μM Mg-ATP actin (15% Alexa488-labeled) with 1 μM profilin Cdc3, 250 nM fimbrin Fim1, and 500 pM formin Cdc12. **(C)** Timelapse of formin Cdc12-mediated filament. White arrowhead tracks Cdc12 at the barbed end. Scale bar, 5 μm. **(D)** Kymograph of filament shown in **(C)**. Scale bar, 2.5 μm. Time bar, 50 s.

Figure 3.2: (continued) **(E)** Plot of Fim1 fluorescence intensity on filament types shown in **(A-D)**. **(F-G)** Two-color TIRFM of 1.5 μM Mg-ATP actin (15% Alexa488-labeled) with 1 μM profilin Cdc3, 1.5 μM tropomyosin Cdc8, 40 nM Arp2/3 complex, and 80 nM VCA. **(F)** Timelapse of Arp2/3 complex-mediated filament. Scale bar, 5 μm. **(G)** Kymographs of Arp2/3 complex filaments shown in **(F)**. For mother filament (left): scale bar, 3 μm. Time bar, 100 s. For daughter filament (right): scale bar, 1 μm. Time bar, 30 s. **(H-I)** Three-color TIRFM of 1.5 μM Mg-ATP actin (15% Alexa488-labeled) with 1 μM profilin Cdc3, 1.5 μM tropomyosin Cdc8, and 500 pM formin Cdc12. **(H)** Timelapse of formin Cdc12-mediated filament. White arrowhead tracks Cdc12 at the barbed end. Scale bar, 5 μm. **(I)** Kymograph of Cdc12 filament shown in **(H)**. Scale bar, 3 μm. Time bar, 100 s. **(J)** Plot of Cdc8 fluorescence intensity on filament types shown in (**F-I**). n = 20 filaments for all measurements. Error bars = s.d.

3.3.3 Actin filaments with distinct architectures are not sufficient to induce ABP sorting in vitro

To reconstitute the presence of multiple F-actin networks simultaneously *in vitro*, we generated F-actin with both Arp2/3 complex and formin Cdc12 in the same TIRFM chamber (Figure 3.3). Addition of 250 nm Fim1 to the chamber resulted in Fim1 coating every actin filament in the reaction, regardless of which assembly factor initiated it (Figure 3.3A-C). While we expected that Fim1 might associate less with formin Cdc12-mediated F-actin in the presence of Arp2/3 complex-mediated actin filaments, we observed no bias of Fim1 toward branched F-actin (Figure 3.3B-C). Similarly, addition of 1.5 μM tropomyosin Cdc8 to the same assay revealed that it too associates with F-actin assembled simultaneously with both Cdc12 and Arp2/3 complex and exhibits no preference for straight, formin-mediated filaments (Figure 3.3D-F). Therefore, using distinct actin assembly factors to assemble F-actin with different architectures is not sufficient to reconstitute the sorting of Fim1 or Cdc8 to a specific type of actin filament. However, in accordance with previous work [162, 27], our *in vivo* data suggest that Fim1 and Cdc8 compete for binding F-actin in fission yeast, so we next investigated whether competition between Fim1 and Cdc8 is sufficient to drive them to distinct F-actin networks.

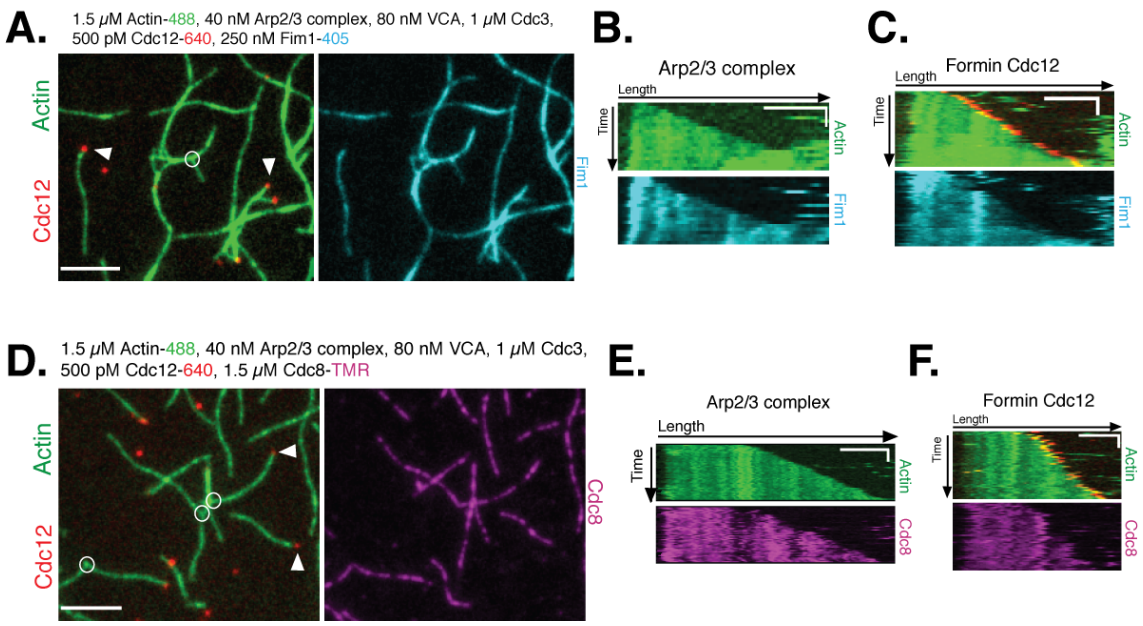

Figure 3.3: **Arp2/3 complex- and formin Cdc12- mediated actin filaments assembled simultaneously are not sufficient to induce ABP sorting.** **(A-C)** Three-color TIRFM of 1.5 μM Mg-ATP actin (15% Alexa488-labeled) with 1 μM profilin Cdc3, 40 nM Arp2/3 complex, 80 nM Wsp1 VCA, 500 pM formin Cdc12-640 and 250 nM fimbrin Fim1-405. **(A)** Still of representative experiment. White arrowheads indicate examples of Cdc12 at the barbed end, while yellow circles indicate branching events. Scale bar, 5 μm. **(B)** Kymograph of Arp2/3 complex mother filament from experiment in **(A)**. Scale bar, 3 μm. Time bar, 30 s. **(C)** Kymograph of Cdc12 filament from experiment in **(A)**. Scale bar, 3 μm. Time bar, 50 s. **(D-F)** Three-color TIRFM of 1.5 μM Mg-ATP actin (15% Alexa488-labeled) with 1 μM profilin Cdc3, 40 nM Arp2/3 complex, 80 nM Wsp1 VCA, 500 pM formin Cdc12-640 and 1.5 μM tropomyosin Cdc8-TMR. **(D)** Still of representative experiment. White arrowheads indicate examples of Cdc12 at the barbed end, while yellow circles indicate branching events. Scale bar, 5 μm. **(E)** Kymograph of Arp2/3 complex mother filament from experiment in **(D)**. Scale bar, 4 μm. Time bar, 50 s. **(F)** Kymograph of Cdc12 filament from experiment in **(D)**. Scale bar, 3 μm. Time bar, 50 s.

3.3.4 Competition between fimbrin Fim1 and tropomyosin Cdc8 drives their mutually exclusive binding at the level of actin filaments, but not actin networks

Because competition between fimbrin Fim1 and tropomyosin Cdc8 is a driving force behind their localization to different F-actin networks (Figure 3.1, [162, 27]), we conducted TIRFM experiments in which Fim1 and Cdc8 compete for binding to actin filaments assembled by either Arp2/3 complex or formin Cdc12 (Figure 3.4). If competition alone is sufficient to induce ABP sorting, we would expect that Fim1's preferential association with Arp2/3 complex-mediated branched filaments might exclude Cdc8 from this network entirely, and vice versa for Cdc8's preferential localization with F-actin generated by formin Cdc12. However, we observed that although they form mutually exclusive, non-overlapping domains, Fim1 and Cdc8 both associate robustly with filaments mediated by both Arp2/3 complex and Cdc12 (Figure 3.4A,C). Not surprisingly, while neither ABP is excluded from either type of F-actin, Cdc8 localizes more strongly to single actin filaments, while Fim1 outcompetes Cdc8 on bundled stretches of F-actin mediated by both assembly factors (Figure 3.4B,D). While Fim1 and Cdc8 compete at the single-filament level, their competition is not sufficient to initiate their localization to distinct F-actin networks.

3.3.5 Competition between ABPs is necessary for their sorting in the presence of F-actin generated by mechanistically distinct assembly factors

Within the cytoplasm, multiple F-actin networks are simultaneously built and dynamically remodeled, necessitating the careful recruitment of only a specific subgroup of ABPs to facilitate actin cytoskeleton self-organization. Additionally, these ABPs are involved in a

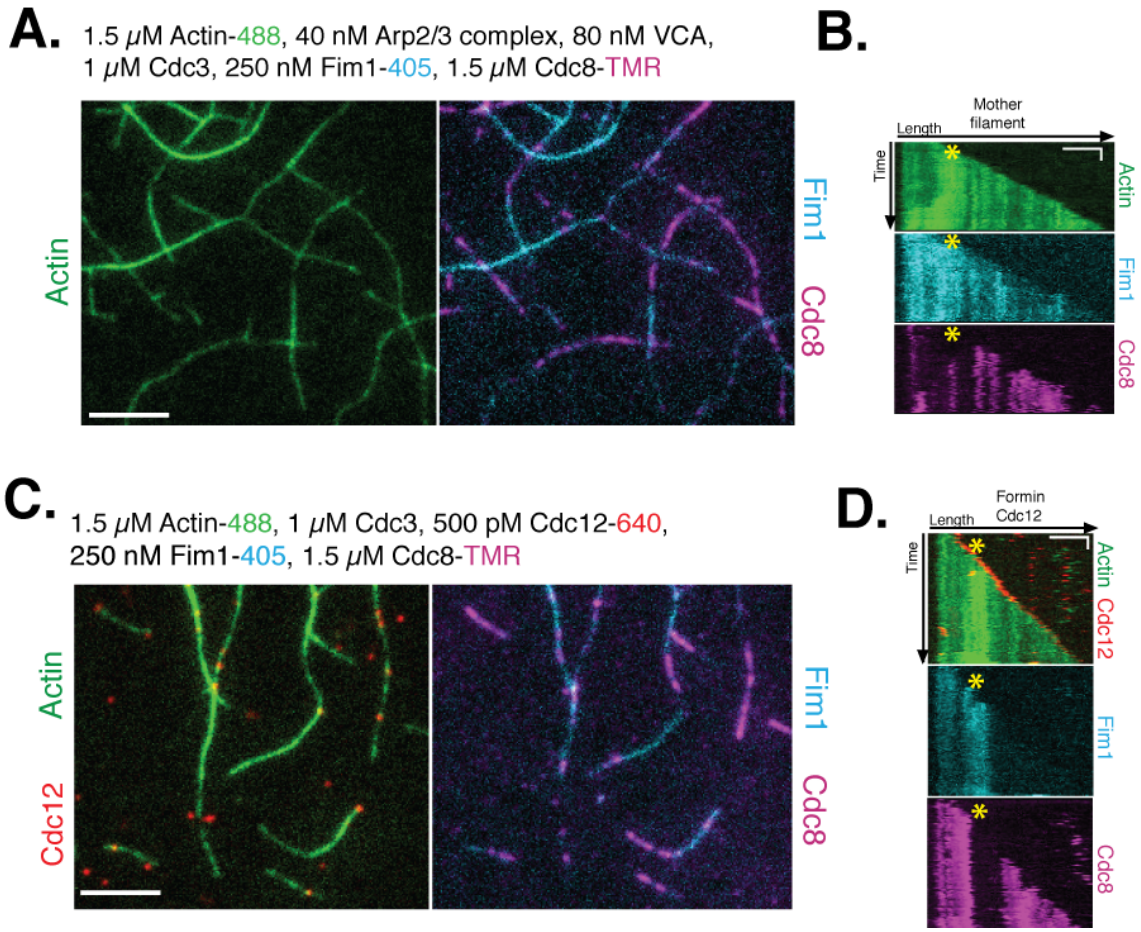

Figure 3.4: **Competition between fimbrin Fim1 and tropomyosin Cdc8 is not sufficient to initiate their sorting to distinct F-actin filaments.** **(A-B)** Three-color TIRFM of 1.5 μM Mg-ATP actin (15% Alexa488-labeled) with 1 μM profilin Cdc3, 40 nM Arp2/3 complex, 80 nM Wsp1 VCA, 250 nM fimbrin Fim1-405, and 1.5 μM tropomyosin Cdc8-TMR. **(A)** Still of representative experiment. Scale bar, 5 μm. **(B)** Kymograph of Arp2/3 complex mother filament from experiment in **(A)**. Asterisk denotes bundled region. Scale bar, 3 μm. Time bar, 50 s. **(C-D)** Four-color TIRFM of 1.5 μM Mg-ATP actin (15% Alexa488-labeled) with 1 μM profilin Cdc3, 500 pM formin Cdc12-640, 250 nM fimbrin Fim1-405, and 1.5 μM tropomyosin Cdc8-TMR. **(C)** Still of representative experiment. Scale bar, 5 μm. **(D)** Kymograph of Cdc12 filament from experiment in **(D)**. Asterisk denotes bundled region. Scale bar, 3 μm. Time bar, 30 s.

Figure 3.4: (continued) of 1.5 μM Mg-ATP actin (15% Alexa488-labeled) with 1 μM profilin Cdc3, 40 nM Arp2/3 complex, 80 nM Wsp1 VCA, 500 pM formin Cdc12-640, 250 nM fimbrin Fim1-405, and 1.5 μM tropomyosin Cdc8-TMR. **(A)** Still of representative TIRFM experiment. Scale bar, 5 μm. Inset (top): Cdc12 filament. Inset (bottom): Arp2/3 complex filament. **(B)** Timelapse images of Arp2/3 complex filament from inset in **(A)**. Scale bar, 5 μm. **(C)** Kymograph of Arp2/3 complex mother filament shown in **(B)**. Scale bar, 3 μm. Time bar, 50 s. **(D)** Plot of normalized Fim1 fluorescence intensity on filaments.

complicated web of competitive and cooperative interactions with one another that facilitates their sorting to distinct F-actin networks (Chapter 2, [27]). Thus, we hypothesized that competition between fimbrin Fim1 and tropomyosin Cdc8 does drive their sorting, but only in the presence of actin filaments assembled by both Arp2/3 complex and formin Cdc12. Using four-color TIRFM, we simultaneously assembled actin with both Arp2/3 complex and Cdc12 and analyzed the association of Fim1 and Cdc8 with these actin filaments (Figure 3.5). Under these conditions, Fim1 associates two-fold more to Arp2/3 complex-mediated actin filaments compared to Cdc12-mediated filaments (Figure 3.5A,D). More specifically, Fim1 preferentially associates with Arp2/3 complex mother filaments, as branched filaments almost always originate from Fim1-coated regions (Figure 3.5A-C). As a consequence of their association with Fim1, mother filaments are often bundled (Figure 3.5B-C), generating filament spacing that promotes cooperative binding of Fim1 and further displacement of Cdc8 (Figure 3.5C). We envision two potential mechanisms that could result in Fim1 localization to the branch site: 1) Arp2/3 complex localizes to F-actin first and recruits Fim1 to the branch site prior to branch formation, or 2) Fim1 coats F-actin and recruits Arp2/3 complex, either directly through a physical interaction or indirectly by modifying the F-actin conformation to promote Arp2/3 complex binding. Ongoing work in our lab aims to fluorescently label purified fission yeast Arp2/3 complex to investigate how it influences Fim1's association with F-actin.

On the other hand, Cdc8 strongly associates with Cdc12-mediated F-actin, just as it does at the contractile ring *in vivo* (Figure 3.5E-F). Specifically, in the presence of Fim1,

Cdc8 localizes 3.5-fold more to formin-mediated F-actin than filaments assembled by Arp2/3 complex (Figure 3.5G). Interestingly, these formin-mediated filaments are less frequently bundled by Fim1, as Cdc8 generally outcompetes Fim1 on single actin filaments (Figure 3.5A, E-H, [27]). In accordance with this idea, Arp2/3 complex daughter filaments initially exhibit a stronger association with Cdc8, we suspect because freshly nucleated, short filaments are less likely to become bundled by Fim1 (Figure 3.5H). However, as these daughter filaments elongate over time, they associate with Fim1, become bundled, and serve as a substrate for additional Arp2/3 complex-mediated branching events (Figure 3.5H, white arrowheads). Since formins are known to affect the twist of actin filaments [116], we hypothesize that Cdc8 has a higher affinity for F-actin with a formin-mediated twist. Cdc8 could then reduce the flexibility of formin-mediated actin filaments by changing the F-actin persistence length [47, 73], thereby decreasing the likelihood of their Fim1-mediated bundling. Future work will seek to generate spatially distinct F-actin networks through the use of micropatterning, where active Arp2/3 complex and Cdc12 are restricted to separate areas of the TIRFM slide to better recapitulate the organization of F-actin networks *in vivo*.

3.4 Model

We have demonstrated that competition between fission yeast ABPs fimbrin Fim1 and tropomyosin Cdc8 is essential for their sorting to distinct F-actin networks mediated by Arp2/3 complex and formin Cdc12. We hypothesize that Fim1 and Cdc8 exhibit slight, experimentally unobservable biases for Arp2/3 complex- and Cdc12-mediated networks, respectively, due to preferences for specific architectures or recognition of slight twists or other conformational changes imparted on F-actin by the assembly factor (Figure 3.7, Step 1). However, ABPs could also be recruited to a specific F-actin network via direct or indirect physical interactions with the assembly factor, as has been suggested to occur in budding yeast with formin Bni1 and tropomyosin Tpm1 [5]. Regardless of the mechanism, this un-

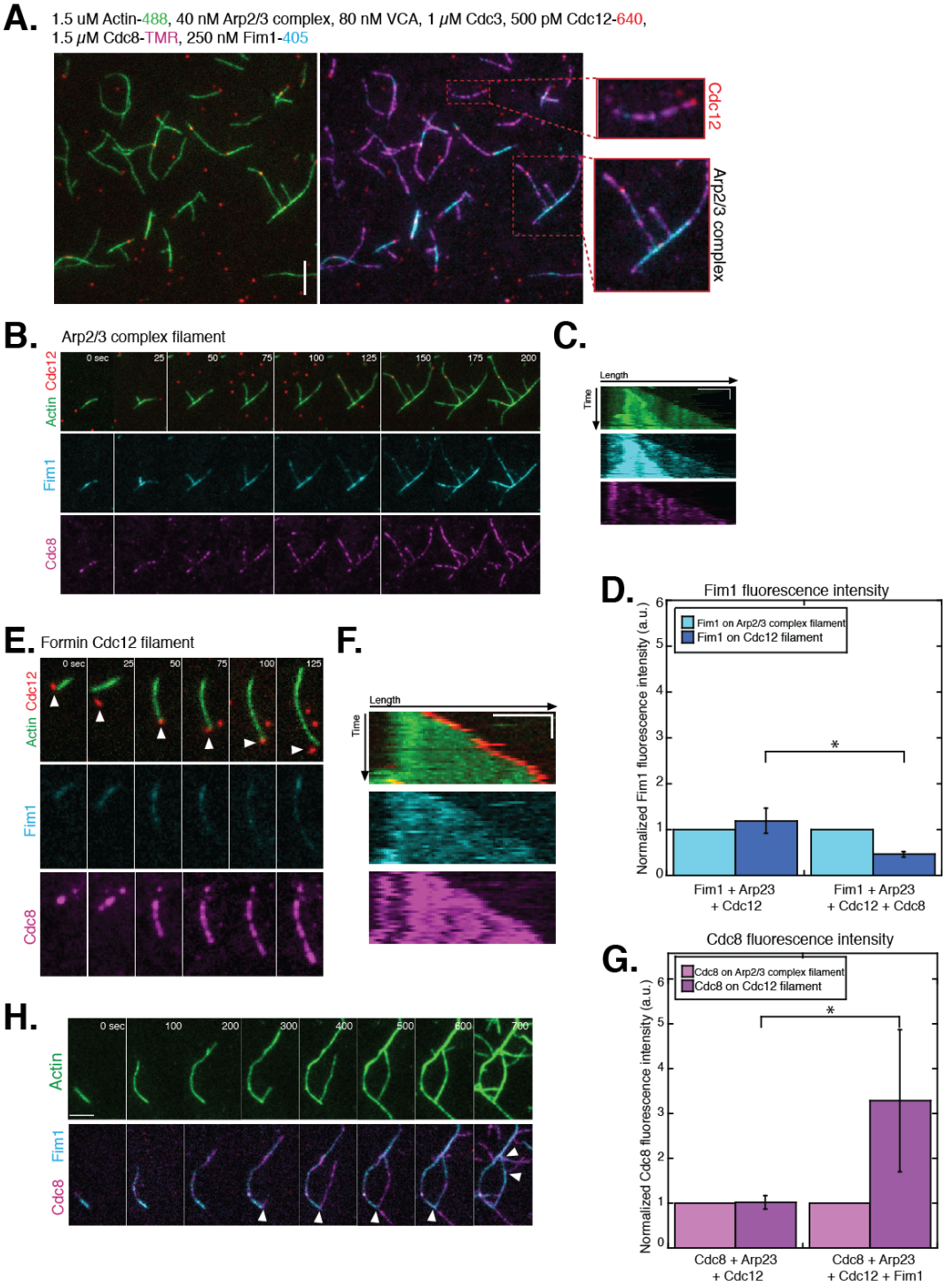

Figure 3.5: **Competition between fimbrin Fim1 and tropomyosin Cdc8 drives their sorting to actin filaments generated by distinct actin assembly factors. (A-H)** Four color TIRFM of 1.5 μM Mg-ATP actin (15% Alexa488-labeled), with 1 μM profilin Cdc3, 40 nM

Figure 3.5: (continued) Arp2/3 complex, 80 nM Wsp1 VCA, 500 pM formin Cdc12-640, 250 nM fimbrin Fim1-405, and 1.5 μM tropomyosin Cdc8-TMR. **(A)** Still of representative TIRFM experiment. Scale bar, 5 μm. Inset (top): Cdc12 filament. Inset (bottom): Arp2/3 complex filament. **(B)** Timelapse images of Arp2/3 complex filament from inset in **(A)**. Scale bar, 5 μm. **(C)** Kymograph of Arp2/3 complex mother filament shown in **(B)**. Scale bar, 3 μm. Time bar, 50 s. **(D)** Plot of normalized Fim1 fluorescence intensity on each type of filament in the absence or presence of Cdc8. Error bars = s.e.m. A two-tailed t-test for data sets with unequal variance yielded p-value *p=0.075. n$\geq$10 measurements for two independent experiments. **(E)** Timelapse images of Cdc12 filament from inset in **(A)**. White arrowhead tracks Cdc12 at the barbed end. Scale bar, 5 μm. **(F)** Kymograph of Cdc12 filament shown in **(E)**. Scale bar, 5 μm. Time bar, 50 s. **(G)** Plot of normalized Cdc8 fluorescence intensity on each type of actin filament in the absence or presence of Fim1. Error bars = s.e.m. A two-tailed t-test for data sets with unequal variance yielded p-value *p=0.385. n$\geq$10 measurements for two independent experiments. **(H)** Timelapse images of Arp2/3 complex daughter filament initially associated with Cdc8 that is later bundled by Fim1 and becomes a mother filament.

observable bias is magnified by the cooperative binding of each ABP (Figure 3.7, Step 2). For example, Cdc8 loads cooperatively onto formin-mediated filaments and prevents Fim1 from associating with them [27], leading to additional binding of Cdc8 and thus initiating a positive feedback loop. Fim1, on the other hand, binds and bundles Arp2/3 complex mother filaments, generating a spacing optimal to recruit additional Fim1 molecules, which leads to more bundling and another positive feedback loop (Figure 3.7, Step 2). Importantly, each of these positive feedback loops of cooperative binding is inhibitory to the other, further amplifying each positive feedback loop in a process we termed "crosstalk inhibition" (Figure 3.7, Step 3). We know from previous work that Fim1-binding to branched F-actin in actin patches inhibits Cdc8's association with these filaments ([162, 27]. Additionally, tropomyosin is known to suppress the branching efficiency of Arp2/3 complex both in this work (Figure 3.8) and in other systems [15, 70]. Thus, we have established what we consider to be the minimal regime necessary and sufficient for ABP sorting to distinct F-actin networks. Future work will aim to understand how the kinetics of actin assembly and the inclusion of additional components, such as more ABPs, will affect ABP sorting.

To quantitatively explore whether each component from our model in Figure 3.7 is re-

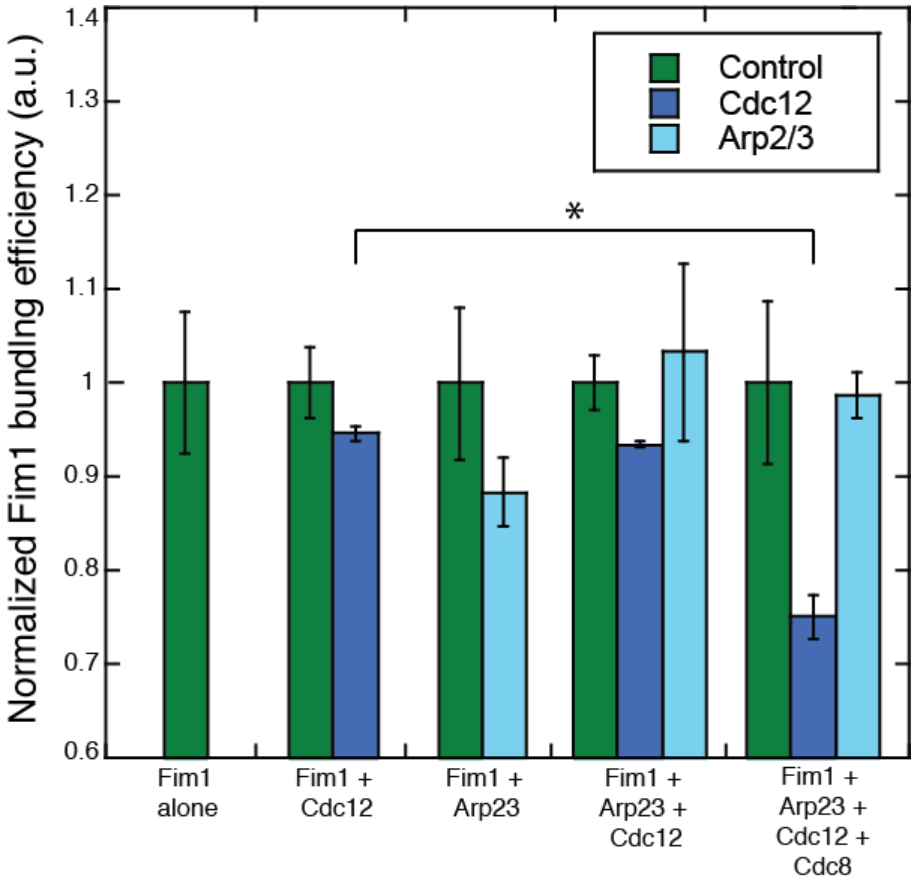

Figure 3.6: **Formin Cdc12-mediated actin filaments are bundled less efficiently by fimbrin Fim1 in the presence of Cdc8.** Plot of the normalized bundling efficiency of Fim1 on control, Cdc12-mediated, or Arp2/3 complex-mediated actin filaments in the presence of the indicated ABPs. Error bars = s.e.m. A two-tailed t-test for data sets with unequal variance yielded p-value *p=0.0061. Measurements are from two independent experiments.

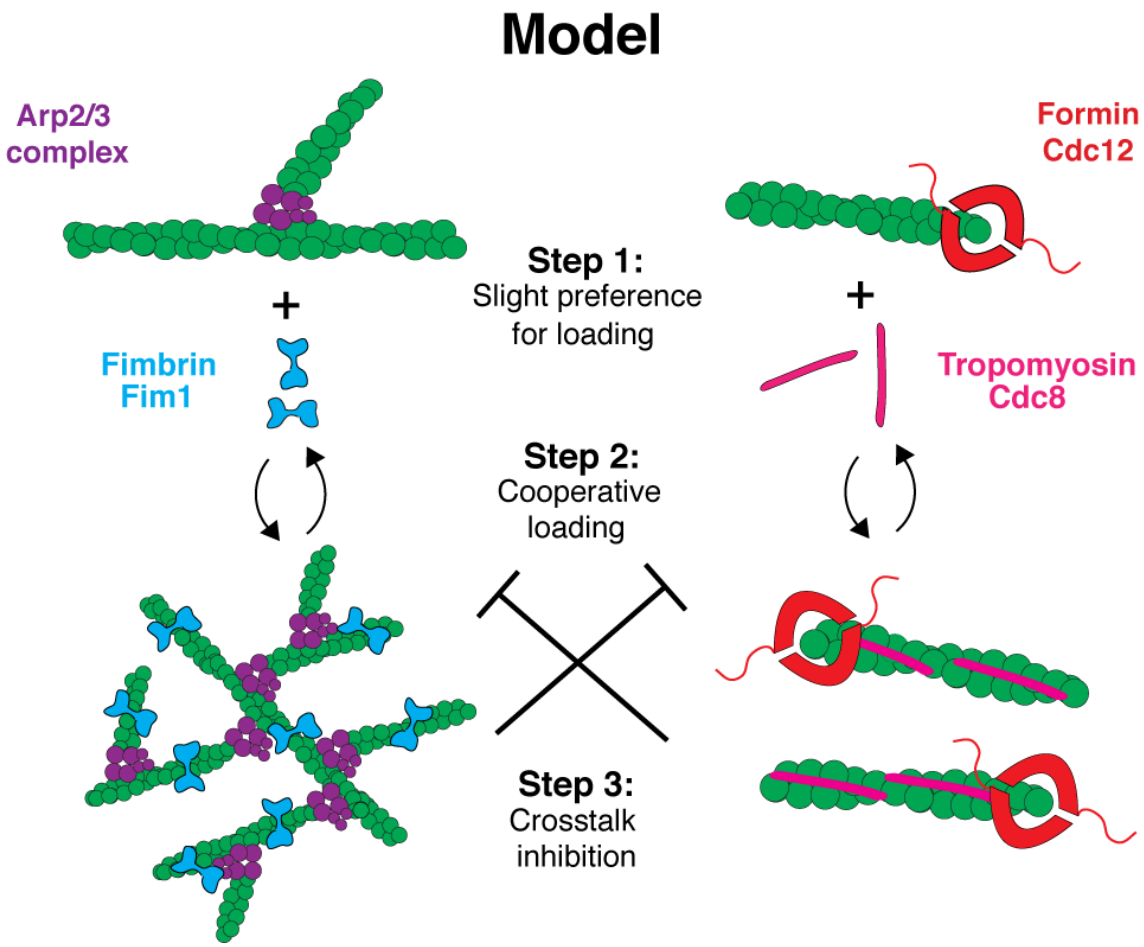

Figure 3.7: **Model.** Our model for ABP sorting includes three steps: 1) a slight, experimentally undetectable preference of Fim1 for Arp2/3 complex filaments and Cdc8 for Cdc12 filaments. 2) This slight bias is magnified by cooperative loading of each ABP onto its respective F-actin network, generating positive feedback loops of ABP association. 3) Crosstalk inhibition, where each ABP association event is inhibitory to the other.

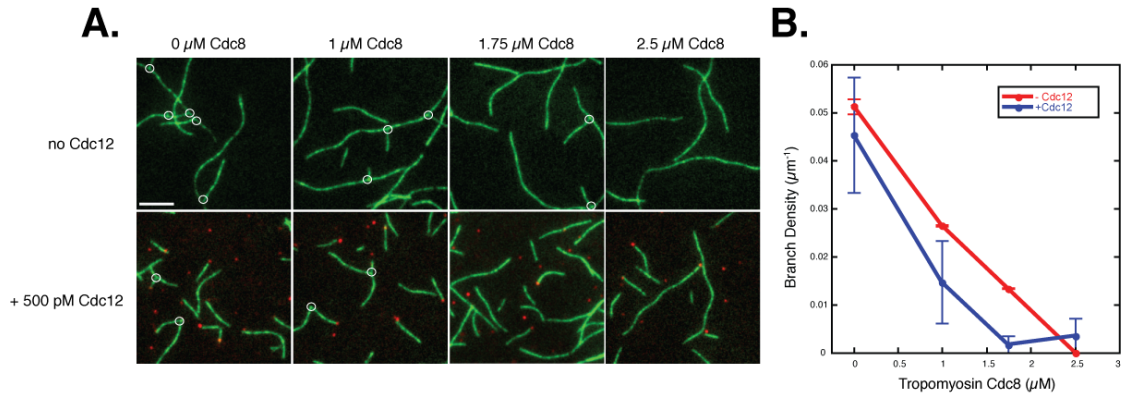

Figure 3.8: **Tropomyosin Cdc8 suppresses the ability of Arp2/3 complex to nucleate F-actin branches *in vitro*. (A)** Fluorescence micrographs of TIRFM experiments containing 1.5 μM Mg-ATP actin (15% Alexa488-labeled) and 1 μM profilin Cdc3 with or without 500 pM formin Cdc12-640 and the indicated concentration of unlabeled tropomyosin Cdc8. White circles indicate branch points. Scale bar, 5 μm **(B)** Plot of the F-actin branch density over a range of Cdc8 concentrations.

quired for ABP sorting, we have developed a simple ordinary differential equation (ODE) model that includes the following components: 1) actively growing F-actin networks nucleated by Arp2/3 complex and formin Cdc12, 2) a pool of fimbrin Fim1 and tropomyosin Cdc8 that binds F-actin with particular rates, 3) the ability to include a slight preference, which means Fim1 binds faster to Arp2/3 complex-mediated networks and Cdc8 binds faster to Cdc12-mediated networks, 4) the ability to include cooperativity, where binding of Cdc8 recruits more Cdc8 and binding of Fim1 recruits more Fim1, and 5) the ability to include inhibition, where binding of Fim1 reduces the rate of Cdc8 binding and vice versa. We can simulate the dynamics of this system, assuming that the base rate of ABP binding to F-actin is proportional to the number of available binding sites. By altering this actin-binding rate to add or remove the effects of a slight preference, cooperativity, or inhibition, we can investigate, for example, specifically how an experimentally undetectable bias for specific F-actin networks might contribute to ABP sorting (Figure 3.9). The results of our simulations suggest that maximal sorting of Fim1 to Arp2/3 complex-mediated F-actin networks and Cdc8 to Cdc12-mediated networks occurs when a slight preference for specific networks,

cooperative binding, and cross-network inhibition are all included in the ODE model (Figure 3.9). While these results are consistent with a role for an inherent bias of Fim1 and Cdc8 for Arp2/3 complex- and Cdc12-mediated actin networks, respectively, additional information will be required to determine the extent to which each of the factors included in the model actually contributes to ABP sorting *in vivo*.

3.5 Discussion

It is clear that ABP sorting is an extremely complex process that likely involves many complementary mechanisms. We showed that ABPs fimbrin Fim1 and tropomyosin Cdc8 exhibit preferences for specific actin filaments, both *in vitro* and in fission yeast cells. Our data suggests that at least two components are absolutely essential for sorting of ABPs to the correct F-actin network: 1) the presence of actin filaments assembled by distinct actin assembly factors (in this case, Arp2/3 complex and formin Cdc12), and 2) competition between ABPs. While our model indicates that Fim1 and Cdc8 could exhibit an experimentally undetectable bias for F-actin mediated by Arp2/3 complex and Cdc12, respectively, this slight bias alone is not sufficient to induce the type of ABP sorting that occurs *in vivo*. In addition to the aforementioned mechanisms, we suspect that several additional non-mutually exclusive factors contribute to ABP sorting.

3.5.1 Factors that drive ABP sorting

3.5.1.1 Diverse F-actin networks

Different actin assembly factors impart actin filaments with inherently distinct characteristics. Most obviously, actin filaments nucleated by Arp2/3 complex and formin have different architectures, with Arp2/3 complex nucleating branched filaments and formin elongating straight filaments. Additionally, formins have been shown to change the twist of F-actin by

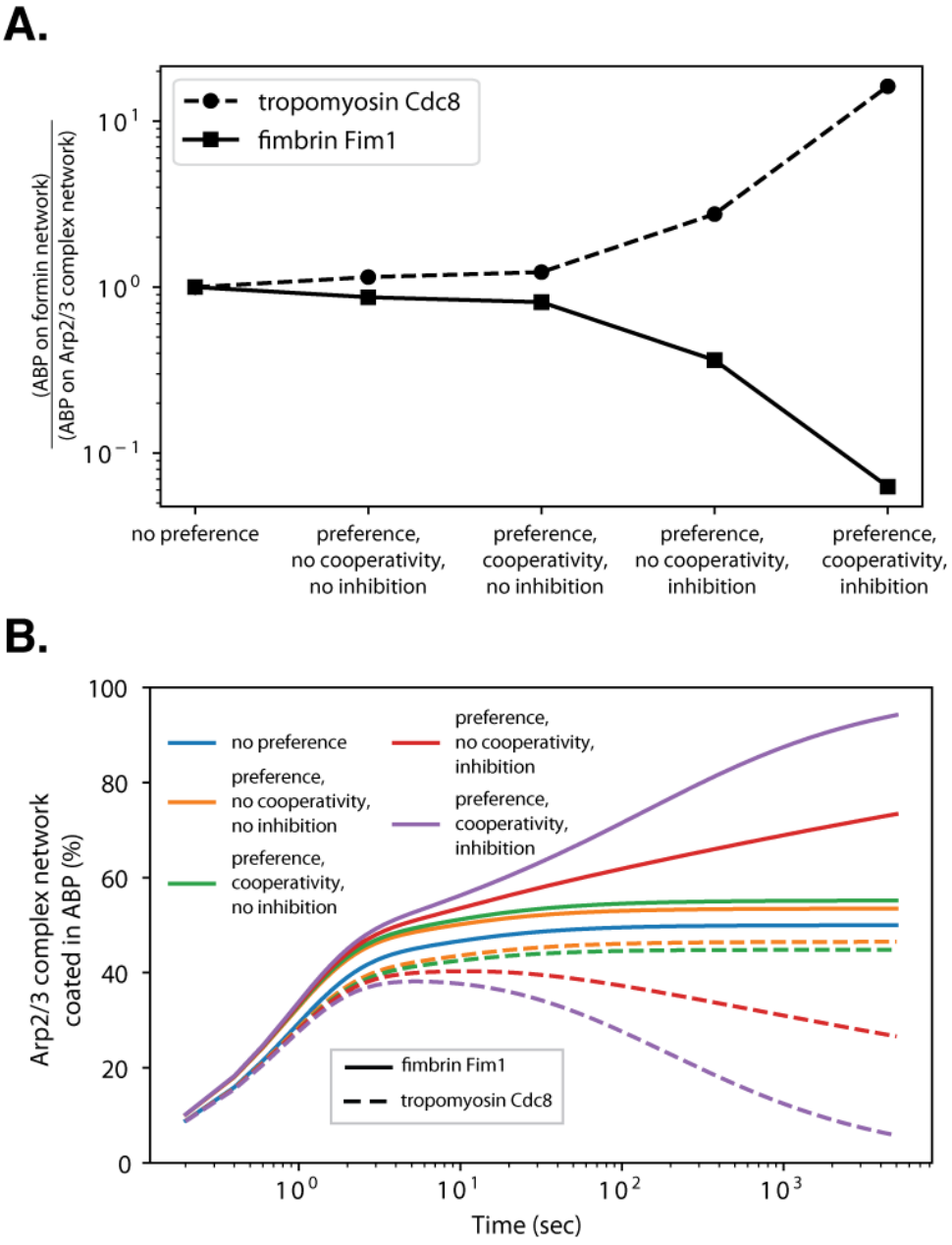

Figure 3.9: **Maximum ABP sorting requires a slight preference, cooperativity, and inhibition. (A)** Output of a simple ordinary differential equations model depicting the ratio of the amount of tropomyosin Cdc8 (dashed line) or fimbrin Fim1 (solid line) on formin networks vs Arp2/3 complex networks for each of the indicated conditions. **(B)** Plot depicting the simulated association of fimbrin Fim1 (solid lines) and tropomyosin Cdc8 (dashed lines) with the Arp2/3 complex-mediated F-actin network over time. The same result for the formin-mediated network would have the solid and dashed lines reversed.

over-rotating actin filaments at the barbed end [132], which could affect the filament's flexibility due to long-range, allosteric interactions [134]. These F-actin architectural features are likely important for recruiting the appropriate subset of ABPs to actin networks, as ABPs could recognize specific F-actin twists or conformations.

ABPs can also alter the actin filament conformation to influence how other ABPs associate with F-actin. It is well-documented that tropomyosin changes the persistence length of F-actin][54, 105]. Thus, it is reasonable to propose that tropomyosin could exert additional changes to the structure of actin filaments, such as curvature, rigidity, or twist, that affect its cooperative binding or competition with other ABPs. Indeed, we have shown that tropomyosin Cdc8 enhances the bundling ability of α-actinin Ain1 in fission yeast (Figure 2.10). Similarly, cofilin creates a twist in F-actin upon binding that promotes the association of additional cofilin molecules and could also restrict the access of its ABP competitors [109]. Understanding how conformational changes in F-actin are induced by assembly factors and ABPs and how these changes affect the recruitment of other ABPs will be crucial steps toward uncovering the mechanisms that govern ABP sorting.

3.5.1.2 The "sink" model and post-translational modifications

Since fimbrin Fim1 preferentially associates with Arp2/3 complex-mediated actin patches over other F-actin networks and ~50% of all fission yeast actin is incorporated into actin patches, actin patches could act as a "sink" that sequesters Fim1 molecules and decreases the concentration of free Fim1 available to associate with formin-mediated actin networks. This hypothesis is supported by our finding that Fim1 associates with the contractile ring after depletion of actin patches, the "sink," using the Arp2/3 complex inhibitor CK-666 (Figure 2.1B). However, the "sink" model alone likely cannot account for Fim1's preferential association with actin patches, as it has been shown that only ~30% of cellular Fim1 localizes to actin patches [159, 191]. Thus, a large portion of cellular Fim1 must be cytoplasmic or

associated with formin-mediated F-actin networks. We postulate that additional mechanisms could drive Fim1's association with actin patches as well as the observed competitive and cooperative interactions amongst Fim1, tropomyosin Cdc8, and α-actinin Ain1.

Post-translational modifications (PTMs) are a common mode of regulating protein-protein interactions across biology, and actin itself is a major substrate for PTMs. Many ABPs are also known to be post-translationally modified. For example, the sole fission yeast isoform of tropomyosin, Cdc8, undergoes acetylation on its N-terminal methionine [163], and its cellular localization is dictated by this acetylation event [74]. Additionally, budding yeast fimbrin Sac6 is phosphorylated in a cell cycle-dependent manner that increases its affinity for F-actin [111]. Thus, one possibility is that post-translational modifications could regulate the cytoplasmic pool of Fim1, affecting its activity and ability to associate with specific F-actin networks. Future experiments should investigate the role of PTMs in regulating the activity and actin-binding dynamics of individual ABPs as well as the the complex set of interactions between ABPs that drives ABP sorting to distinct actin networks.

3.5.1.3 Mechanical stresses

To mediate essential cellular processes that require mechanical forces, actin filaments form higher-order actin networks that can generate and propagate contractile and tensile forces. However, actin filaments themselves also experience mechanical forces that originate from both the interior and exterior of the cell. One common cellular mechanism of force generation is myosin-mediated pulling of F-actin, which mediates muscle contraction and actin-based motility. We suspect that external forces, such as those applied by myosin, could alter the activity of ABPs or their affinity for F-actin. Several ABPs have already been identified as mechanosensors that change their behaviors based on actin filament tension. For example, cofilin's association with F-actin in stress fibers is tension-dependent, with cofilin preferentially binding and severing actin filaments in a relaxed state and associating less with F-actin

under tension [64]. Additionally, mammalian α-actinin ACTN1 contains force-sensitive domains that undergo a conformational change in response to forces on F-actin, revealing additional vinculin-binding sites that mediate regulation of focal adhesions [96]. Thus, future experiments should investigate whether fission yeast ABPs, such as tropomyosin Cdc8 and fimbrin Fim1, are 1) preferentially recruited to actin filaments in either a stressed or relaxed state and 2) more or less active in response to changes in the amount of tension applied to F-actin.

3.6 Materials and Methods

3.6.1 Strain construction and growth

Fission yeast strains were obtained through genetic crosses on SPA5S plates followed by tetrad dissection on YE5S plates. Glycerol stocks were created by resuspending pelleted cells in 600 μL YE5S and 400 μL 50% sterile glycerol. For cell growth, standard growth media (YE5S and EMM5S) were used. Expression of Cdc8 under the nmt1 promoter was regulated by the presence or absence of 10 μg/μL thiamine (Sigma Aldrich, St. Louis, MO). Table 3.1 lists the *S. pombe* strains used in this study.

3.6.2 Live cell microscopy and treatment with CK-666

Prior to imaging, cells were grown in YE5S overnight at 25° C, subcultured into EMM5S media without thiamine, and kept in log phase for 20-22 hr at 25° C. For time-lapse imaging, cells were plated on 25% gelatin EMM5S gelatin pads containing 0.1 mM n-propyl gallate. For visualization of tropomyosin Cdc8 and Arp2/3 complex, z-stacks of 10 slices were acquired at 500 ms exposure with 0.5 μm step size every 2 min for 2 hr. Images were acquired on a Zeiss Axiovert 200M equipped with a Yokogawa CSU-10 spinning disk unit (McBain, Simi Valley, CA) and a 100X, 1.4 NA objective illuminated with 50 milliwatt, 473 and 561

nm DPSS lasers, as well as a Cascade 512B EM-CCD camera (Photometrics, Tucson, AZ) controlled by Metamorph software (Molecular Devices, Sunnyvale, CA).

For CK-666 treatment, CK-666 powder (Sigma Aldrich, St. Louis, MO) was diluted in DMSO to 10 mM. Cells were grown as described above, then incubated at 25° C in a spinning rotator with either CK-666 or DMSO (control) for 30 min prior to imaging. Cells were then imaged directly on a glass slide using z-stacks of 10 slices at 400 ms exposure with 0.5 μm step size.

3.6.3 Protein purification and labeling

Actin was purified from chicken skeletal muscle acetone powder (Spudich and Watt, 1971) and labeled on surface lysines with Alexa488-succinimidyl ester (Life Technologies, Carlsbad, CA) [81].

Fission yeast Arp2/3 complex was purified from *S. pombe* cells using Wsp1(VCA) affinity chromatography as described previously [170, 40, 158]. Fission yeast WASP fragment construct GST-Wsp1(VCA) and formin SNAP-Cdc12p(FH1FH2) were expressed in *Escherichia coli* strain BL21-Codon Plus (DE3-RP) (Agilent Technologies, Santa Clara, CA) as described previously [170, 199]. Briefly, Wsp1(VCA) was purified using Glutathione-Sepharose affinity chromatography (GE Healthcare Life Sciences, Pittsburgh, PA). Cdc12 was purified with Talon Metal Affinity Resin (Clontech, Mountain View, CA) and loaded onto a 1 mL HiTrapTM HP column (GE Healthcare) for anion exchange chromatography. Fission yeast profilin Cdc3 was overexpressed and purified from E. coli using poly-L-proline affinity chromatography as described in [42, 170].

Tropomyosin AlaSer-Cdc8(D142C) and Fimbrin Fim1 were also expressed in BL21-Codon Plus (DE3-RP) cells (Agilent Technologies) as described previously [162, 27]. Cdc8 was purified by boiling the cell lysate, followed by ammonium sulfate precipitation and anion exchange chromatography.

A Nanodrop 2000c Spectrophotometer (Thermo-Scientific, Waltham, MA) was used to obtain A280 measurements of purified proteins. The following extinction coefficients were used to calculate protein concentration: Fim1: 55,140 M^{-1} cm^{-1}, Cdc8: 2980 M^{-1} cm^{-1}, Arp2/3 complex: 250,000 M^{-1} cm^{-1}, Cdc12: 72,350 M^{-1} cm^{-1}, Wsp1 VCA: 49,180, Cdc3: 20,065 M^{-1} cm^{-1}. Proteins were labeled with TMR-6-maleimide (Life Technologies, Grand Island, NY), CF^{TM}405M (Sigma Aldrich), or SNAP-Surface® Alexa Fluor®647 (New England Biolabs, Ipswich, MA) dyes according to the manufacturer's protocols immediately following purification, then flash-frozen in liquid nitrogen and stored at -80° C. Cdc8 was reduced with 100 μM DTT before and during labeling.

3.6.4 Glass preparation for TIRF microscopy

Microscope slides (#1.5, Fisher Scientific) and coverslips were washed for 7 min in acetone, isopropanol, and water, followed by sonication in isopropanol for 30 min. Washed glass was then cleaned using either plasma cleaning or piranha solution. For plasma cleaning, washed glass was placed in a Harrick PDC-32G plasma cleaner (Harrick plasma, Ithaca, NY) for 2 min. For piranha solution, washed glass was incubated with piranha solution (66.6% H2SO4, 33.3% H_2O_2) for 2 hr, then washed with diH_2O and dried with air. Immediately following plasma or piranha cleaning, glass was passivated by incubation in 1 mg/mL PEG-Si (5000 MW) in 95% ethanol for 18 hr [185]. After glass was rinsed with ethanol and water, flow chambers were prepared as described previously [200].

3.6.5 TIRF microscopy (TIRFM)

TIRFM movies were collected using an Olympus IX-71 microscope with through-the-objective TIRF illumination and an iXon EMCCD camera (Andor Technology, Belfast, UK) equipped with a cellTIRF 4Line system (Olympus). 15% Alexa 488-labeled Mg-ATP-Actin was mixed with ABPs and polymerization buffer (10 mM imidazole (pH 7.0), 50 mM KCL, 1 mM

$MgCl_2$, 1 mM EGTA, 50 mM DTT, 0.2 mM ATP, 50 μM $CaCl_2$, 15 mM glucose, 20 μg/mL catalase, 100 μg/mL glucose oxidase, and 0.5% 400 centipoise methylcellulose) to induce F-actin assembly [185, 27]. This mixture was flowed into a chamber on ultraclean glass and imaged at 5 s intervals at room temperature.

3.6.6 Measurement of ABP fluorescence intensity

The fluorescence intensity of a "formin Cdc12 filament" was measured once a formin Cdc12 dimer was associated with an actin filament, either nucleated by the formin or pre-existing, long enough to elongate at least 4 μm of F-actin. Then, the mean fluorescence of the ABPs was measured on that 4 μm. The fluorescence intensity of an "Arp2/3 complex filament" was measured at the branch point once an Arp2/3 complex-mediated F-actin branch was visible via TIRFM. The mean fluorescence of the ABPs was measured on a region 4 μm long total, bisected by the branch point (2 μm on each side of the branch point). In cases where Cdc12 associates with the exposed barbed end of an Arp2/3 complex-mediated filament, the filaments were not analyzed. Control filaments are classified as those that are not generated by Arp2/3 complex or Cdc12, although we cannot eliminate the possibility that control filaments could associate with unlabeled Arp2/3 complex molecule, as the efficiency of branch production by Arp2/3 complex is inherently low and thus some Arp2/3 complex molecules are bound to F-actin but do not nucleate branched filaments.

3.6.7 Arp2/3 complex branch density analysis

Branch density was measured by counting the number of branching events visualized by TIRFM and dividing by the total amount of actin filament for each condition. This analysis was performed at time points exhibiting 150-300 μm of total actin filament. Branch density analysis was performed using unlabeled Cdc8.

3.6.8 Bundling efficiency

Bundling efficiency was quantified as described previously [27]. Briefly, the percentage of actin filaments incorporated into bundles was quantified at similar F-actin densities. ROIs were generated for every actin filament to measure the total amount of F-actin assembled by each assembly factor (Arp2/3 complex, formin Cdc12, or control). The percentage of total filament length incorporated into bundles for each type of filament was then calculated.

3.6.9 Modeling

We wanted to have a quantitative model representing our hypothesis in Figure 3.7. We want this model to be able to represent the following features:

1. There is a growing Arp2/3-nucleated actin network and a growing formin-nucleated actin network.

2. A pool of tropomyosin Cdc8 and fimbrin Fim1 which can bind to free sites in the two actin networks. These bind with particular rates to an open actin binding site in the absence of the other protein. This pool of proteins is in excess, so we don't have to represent it explicitly, but it is not in a particularly high concentration, which means the networks can also compete for the proteins.

3. Include/not include a slight preference ("pref"), which means Cdc8 binds faster to formin nucleated actin networks and fimbrin binds faster to Arp2/3 nucleated networks.

4. Include/not include cooperativity ("coop"): binding of Cdc8 enhances Cdc8 binding, and binding of Fim1 enhances Fim1 binding.

5. Include/not include inhibition ("inhib"): binding of Cdc8 reduces the rate of Fim1 binding, and binding of Fim1 reduces the rate of Cdc8 binding.

There are many possible models that would satisfy these conditions, so we chose to utilize a simple ordinary differential equation model that includes all these features to illustrate how

an experimentally-undetectable preference of Cdc8 for formin networks and Fim1 for Arp2/3 networks can be magnified to produce the sorting shown in Figure 3.9A, but only when all five network components (actin, Arp2/3, formin, Cdc8, and Fim1) are present.

We represent this system as an ordinary differential equation, which means that the dynamics can be expressed in the following simple way:

$$\frac{d\vec{v}}{dt} = f(v) \tag{3.1}$$

Here, $\vec{v}(t)$ is the state of the system at time t, and f is a function which expresses the rate of change of each entry in $\vec{v}$. After expressing our system in this way, we simulate the dynamics using the SciPy ODE solver scipy.integrate.ode.

For our system, $\vec{v}$ will be the following:

$$\vec{v} = \begin{cases} \text{unbound actin subunits in Arp2/3 complex network} - v_0 \\ \text{Cdc8 on Arp2/3 complex network} - v_1 \\ \text{Fim1 on Arp2/3 complex network} - v_2 \\ \text{unbound actin subunits in formin network} - v_3 \\ \text{Cdc8 on formin network} - v_4 \\ \text{Fim1 on formin network} - v_5 \end{cases}$$

The goal is to develop the function f which has the properties 1-5 above.

3.6.9.1 Change in unbound actin

Cdc8 and Fim1 each "take up" a certain amount of space on an actin filament. Fim1, a crosslinker, binds every 13 subunits in an F-actin bundle. Cdc8 spans eight actin subunits but binds as a coiled-coil along F-actin, so two Cdc8 molecules are near each subunit. For

the purpose of having a very simple model, we set the number of subunits coated by each protein to be the same ($l_{Cdc8} = l_{Fim1} = 10$). If they are not the same, then the on-rate of the protein to a site has to be adjusted to create roughly-equal affinity crosslinkers. The change in number of unbound subunits in a filament will be equal to the number of subunits added to the network, minus the number covered by incoming proteins.

$$f(v_0) = k_{grow}^{Arp2/3} - f(v_1)l_{Cdc8} - f(v_2)l_{Fim1} \tag{3.2}$$

$$f(v_3) = k_{grow}^{formin} - f(v_4)l_{Cdc8} - f(v_5)l_{Fim1} \tag{3.3}$$

3.6.9.2 Default binding kinetics

Without any cooperativity or inhibition, we assume that the binding of proteins to F-actin is proportional to available binding sites. Hence we have four rates (which we will modify in the next section):

$$f(v_1) = k_{on}^{Cdc8 \to Arp2/3}(\frac{v_0}{l_{Cdc8}}) \tag{3.4}$$

$$f(v_2) = k_{on}^{Cdc8 \to Arp2/3}(\frac{v_0}{l_{Fim1}}) \tag{3.5}$$

$$f(v_4) = k_{on}^{Cdc8 \to formin}(\frac{v_2}{l_{Cdc8}}) \tag{3.6}$$

$$f(v_5) = k_{on}^{Cdc8 \to formin}(\frac{v_2}{l_{Fim1}}) \tag{3.7}$$

3.6.9.3 Cooperativity and inhibition factors

We wish to invent the simplest possible factors that could represent cooperativity and inhibition. To do this, we assert that the simplest possible form of cooperativity/inhibition we can assume is that the rates increase/decrease linearly in proportion to the fraction of a

network coated by the same/other actin binding protein. We will write this for $f(v_1)$ and $f(v_2)$ and the other two follow by analogy.

The fraction of the Arp2/3 complex network coated in Cdc8 and by Fim1 are:

$$p^{Cdc8}_{Arp2/3} = \frac{v_1}{v_1 + v_2 + \frac{v_0}{l_{Cdc8}}}, p^{Fim1}_{Arp2/3} = \frac{v_2}{v_1 + v_2 + \frac{v_0}{l_{Cdc8}}} \tag{3.8}$$

If cooperativity is turned on, then we include a multiplicative factor:

$$C^{Cdc8}_{Arp2/3} = 1 + p^{Cdc8}_{Arp2/3}, C^{Fim1}_{Arp2/3} = 1 + p^{Fim1}_{Arp2/3} \tag{3.9}$$

If inhibition is turned on, then we include a multiplicative factor:

$$I^{Cdc8}_{Arp2/3} = 1 - p^{Fim1}_{Arp2/3}, I^{Fim1}_{Arp2/3} = 1 - p^{Cdc8}_{Arp2/3} \tag{3.10}$$

If both are turned on, then we would multiply by both, e.g.

$$f^{coop,inhib}(v_1) = k^{Cdc8 \to Arp2/3}_{on}(\frac{v_0}{l_{Cdc8}})C^{Cdc8}_{Arp2/3}I^{Cdc8}_{Arp2/3} \tag{3.11}$$

For this example, the rate of addition of Cdc8 to the Arp2/3 complex network is proportional to the number of available sites in the network, times a factor which grows proportional to the amount of Cdc8 in the network, times a factor that decreases proportional to the amount of Fim1 in the network.

3.6.9.4 Network effect

While the above hypothesis seems sufficient, it is not enough to produce a collective sorting, because there is no cross-talk between the formin and Arp2/3 complex networks. To produce this collective sorting, we must have some way of saying, e.g. that if the rate of Cdc8 on the

formin network increases, it must also be decreasing to the Arp2/3 complex network. This can be done with network coupling factors like, e.g. $N^{Cdc8}_{Arp2/3} = 1 - p^{Cdc8}_{formin}$, but it adds more complexity to the model. Instead we decided to "renormalize" the cooperativity and inhibition factors. So, if we call

$$A^{Cdc8}_{Arp2/3} = \begin{cases} C^{Cdc8}_{Arp2/3}, coop \\ I^{Cdc8}_{Arp2/3}, inhib \\ C^{Cdc8}_{Arp2/3} I^{Cdc8}_{Arp2/3}, coop + inhib \end{cases}$$

Then we set

$$\breve{A}^{Cdc8}_{Arp2/3} = \frac{A^{Cdc8}_{Arp2/3}}{A^{Cdc8}_{Arp2/3} + A^{Fim1}_{formin}} \tag{3.12}$$

which adds a coupling between the two networks.

As a result, we have the following as our final four rates of change:

$$f(v_1) = k^{Cdc8 \to Arp2/3}_{on}(\frac{v_0}{l_{Cdc8}})\breve{A}^{Cdc8}_{Arp2/3} \tag{3.13}$$

$$f(v_2) = k^{Fim1 \to Arp2/3}_{on}(\frac{v_0}{l_{Fim1}})\breve{A}^{Fim1}_{Arp2/3} \tag{3.14}$$

$$f(v_4) = k^{Cdc8 \to formin}_{on}(\frac{v_3}{l_{Cdc8}})\breve{A}^{Cdc8}_{formin} \tag{3.15}$$

$$f(v_5) = k^{Fim1 \to formin}_{on}(\frac{v_3}{l_{Fim1}})\breve{A}^{Fim1}_{formin} \tag{3.16}$$

Since $\breve{A}^{Cdc8}_{Arp2/3} + \breve{A}^{Cdc8}_{formin} = 1$, this formulation means that when the number of available sites in each network are equal, we get two equations like:

$\frac{d[boundCdc8]}{dt} = f(v_1) + f(v_4) = (k^{Cdc8 \to Arp2/3}_{on} + k^{Cdc8 \to formin}_{on})$[available sites]

which is intuitively appealing.

Lastly, these renormalized $\breve{A}$ parameters can only have values between 0 and 1. Hence the k_{on} then represents a maximum rate to unbound sites.

In this model, when the system is mostly sorted, the result is that the $\breve{A}$ value of adding e.g. Cdc8 to a Cdc8-coated formin network is close to 1, while the $\breve{A}$ value for adding Fim1 is close to zero.

3.6.9.5 Initial conditions and simulation parameters

As initial conditions, we take the initial number of actin subunits in Arp2/3 complex and formin networks to be 500 each. Based on experimental observations, we see the Arp2/3 complex network growing about twice as fast as the formin network, and to represent this, we set $k_{grow}^{Arp2/3} = 100$ subunits/sec and $k_{grow}^{formin} = 50$ subunits/sec. We take the ODE timestep to be 0.2 seconds and simulate up to time 5000 seconds. We set all k_{on} values to 1/sec/binding-site for the no preference-case. For the "pref" case, we set $k_{on}^{Cdc8 \to formin} = k_{on}^{Fim1 \to Arp2/3}$ = 1.15 /sec/binding-site.

We then perform simulations for all possible models derived from the above cases. The result for the Arp2/3 complex network is shown in Figure 3.9B (Fim1, solid lines; Cdc8, dashed lines), with the result for the formin network having the solid and dashed lines reversed.

To summarize the amount of sorting produced by this model, we take the ratio of the ABP on one network versus the other at the final time point and show the result in Figure 3.9A.

Strain name	**Genotype**	**Reference**
KV368	h+, ARPC5-mCherry-natMX6, leu1::nmt41gfp-cdc8:ura4, ade6-M216 leu1-32	[162]
KV369	h+, ARPC5-mCherry-natMX6, leu1::nmt41gfp-cdc8:ura4, fim1-1Δ::kanMX6	[162]

Table 3.1: **Fission yeast strains used in Chapter 3.**

CHAPTER 4

FORMIN CDC12'S SPECIFIC ACTIN ASSEMBLY PROPERTIES ARE TAILORED FOR CYTOKINESIS IN FISSION YEAST

Preface

The work in the following chapter was performed with assistance from Erin Neidt, Tamara Bidone, and Vilmos Zsolnay. Erin Neidt generated the original formin chimera strains, while Tamara Bidone and Vilmos Zsolnay performed the modeling in Figures 4.6, 4.7, and 4.8. I performed the experiments and analysis in Figures 4.1, 4.2, 4.3, 4.4, and 4.5 and created the figures.

4.1 Abstract

Formins associate processively with actin filament barbed ends to elongate straight filaments, mediating essential cellular processes such as cell migration, cell polarity, and cytokinesis. Most cells express multiple formin isoforms, including two in budding yeast, three in fission yeast, at least 15 in mammals and more than 20 in plants. Despite their structural similarities and conserved general mechanisms, different formin isoforms are required for distinct cellular processes and stimulate actin filament assembly by significantly different rates. Thus, we hypothesize that the particular actin assembly properties of each formin tailor it for a specific cellular role. To test this possibility, we engineered chimera formin strains in which the FH1FH2 actin assembly domains of full length fission yeast formin Cdc12 were replaced with the FH1FH2 domains from functionally and evolutionarily diverse formins with different actin assembly properties: For3 (fission yeast), Bni1 (budding yeast), CYK-1 (worm), mDia1 (mouse) and mDia2 (mouse). Live-cell imaging indicates that chimera formin strains are viable, but exhibit cytokinesis defects ranging from mild to severe. Furthermore, chimera

formin strains experience delays in different steps of contractile ring assembly. Our findings suggest that cells containing formin chimeras whose nucleation efficiencies are most similar to Cdc12 are generally less defective in cytokinesis than cells containing chimeras that are poor nucleators. Thus, diverse FH1FH2 domains can support life in fission yeast. We also tested these findings using a computational model to selectively isolate actin assembly properties of formins and found that variations in nucleation efficiency critically impact both the probability and timing of contractile ring formation. Together, our experimental and computational results indicate that cytokinesis is robust, but is ideally mediated by formins with properly tailored actin assembly parameters.

4.2 Introduction

Formins (formin homology proteins) are a group of large, highly conserved proteins that associate processively with the barbed end of actin filaments (F-actin) to modulate their elongation, nucleation, capping, and bundling throughout various fundamental cellular processes, including polarity, motility, division, and adhesion [34, 17]. Formins are identified by two highly conserved formin homology (FH) domains that nucleate and processively elongate unbranched F-actin. The FH2 domain is a tethered, head-to-tail dimer that nucleates F-actin and processively encircles the growing barbed end, while the unstructured FH1 domain binds profilin-actin via its multiple proline-rich regions and delivers it to the FH2-bound barbed end to facilitate elongation [34, 137]. The conserved FH1FH2 domains are flanked by less well-conserved regulatory and localization regions, including the FH3 domain. Most organisms express several formin isoforms, from two in budding yeast, three in fission yeast, and seven in nematode worms, to 15 in mammals and more than 20 in plants [66, 147, 153]. Although the specific cellular functions of each formin have yet to be determined, it is apparent that despite having well-conserved structural properties and general actin-assembly mechanisms, distinct formin isoforms are required for different cellular processes in many cell

types. Many formins have been extensively studied and found to have significantly different actin assembly properties, such as *in vitro* F-actin nucleation, elongation, and dissociation rates [56]. We previously determined that the biochemical and actin assembly properties of all three formin isoforms expressed in fission yeast (For3, Cdc12, and Fus1) vary widely, indicating that a formin's specific properties might tailor it for its cellular role [154]. However, the extent to which each specific actin assembly property contributes to F-actin assembly and dynamics *in vivo* is unclear.

The role of cytokinesis formin Cdc12 in fission yeast cell division is well established, making it an ideal candidate for understanding how a formin's actin assembly characteristics might influence its cellular role. Fission yeast contractile ring assembly is accomplished via a mechanism known as Search-Capture-Pull-Release (SCPR), which depends on the assembly of several conserved cytokinesis proteins, including formin Cdc12 and type II myosin Myo2, into ~65 "pre-ring" cytokinesis nodes that are cortically distributed around the cell middle [97, 178, 192]. After an initial search phase, filaments nucleated and assembled by Cdc12 on one node are captured by Myo2 on another node. Myo2 subsequently exerts a pulling force on F-actin, bringing the two nodes closer together. After many rounds of capture and pull by Myo2 in addition to release of these node-node contacts by the severing protein cofilin, actin filaments from pre-ring nodes coalesce into a continuous contractile ring [178, 192]. While formins are required for cytokinesis in other organisms, it is unclear whether cell division in other organisms occurs via a similar SCPR mechanism. Interestingly, while the C. elegans formin CYK-1 is required for cell division in the early embryo, its *in vitro* actin assembly properties differ significantly from Cdc12's [126].

To examine whether a formin is tailored for a particular cellular role by its actin assembly properties, we engineered formin chimera fission yeast strains in which the FH1FH2 actin assembly domains of the cytokinesis formin Cdc12 are replaced with the FH1FH2 domains of functionally and evolutionarily diverse formins from different organisms (formin "chimeras").

These formin chimera strains are viable, but experience a range of cytokinesis defects, including delays in contractile ring assembly and abnormal cell morphologies. Formin chimera strains containing FH1FH2 domains with measured nucleation efficiencies closest to that of Cdc12 are generally less defective at cell division than those containing chimeras that are poor nucleators. We directly tested the effect of formin actin assembly properties on contractile ring assembly by extending a previously validated computational model, based on the SCPR mechanism, to incorporate formin nucleation efficiency [178, 14, 94]. The model shows that proper ring assembly is more dependent on a formin's nucleation efficiency than its F-actin elongation rate, supporting our experimental observations. Cytokinesis in fission yeast is robust, but is ideally mediated by a formin with actin assembly parameters that are optimized for its specific cellular role.

4.3 Results

4.3.1 Fission yeast formin Cdc12 chimeras localize to the contractile ring and produce viable cells that complete cell division

To determine whether the specific actin assembly parameters of formin Cdc12 tailor it for cytokinesis in fission yeast, we engineered chimera formin strains in which the FH1FH2 actin assembly domains of full length Cdc12 were replaced with the FH1FH2 domains from functionally and evolutionarily diverse formins with significantly different actin assembly properties: For3 (fission yeast), Bni1 (budding yeast), mDia1 (mouse), mDia2 (mouse), and CYK-1 (worm) (Figure 4.1A). Because Cdc12's N- and C-terminal regulatory regions are primarily responsible for its regulation and localization, we expect these properties to be maintained in formin chimera strains. However, these formin chimeras should exhibit a wide range of actin assembly properties. One copy of each formin chimera was integrated into the *ura4* locus under control of the endogenous *cdc12* promoter and tagged at the C-terminus

with GFP. Endogenous *cdc12* was deleted by replacement with a kanR cassette [20]. For observation of the contractile ring, the myosin-II regulatory light chain Rlc1 was tagged with tdTomato. Control strains include endogenous *cdc12* tagged C-terminally with GFP ($Cdc12^{endo}$) and full length Cdc12-GFP integrated into the *ura4* locus with endogenous *cdc12* deleted ($Cdc12^{ura}$).

With the exception of fission yeast Fus1, all of the formin chimera strains produce viable cells (Figure 4.1B), indicating that cytokinesis is generally robust. Like control Cdc12 strains, the formin chimeras co-localize with Rlc1-tdTomato in the contractile ring or contractile ring-like material at the cell midzone (Figure 4.1B), which suggests that they are properly recruited to the division site during cell division. It is possible that cells exclusively expressing Fus1 chimeras fail to grow because Fus1's actin assembly domains are specifically regulated to elongate F-actin only during mating. Fus1's specific actin assembly properties could also contribute to the strain's inviability, although this is less likely, since Fus1's actin assembly parameters are more similar to Cdc12's than several other viable formin chimeras (Table 4.1). Fus1(FH1FH2) nucleates actin filaments as efficiently as Cdc12, but elongates barbed ends half as fast and dissociates from them an order of magnitude faster than Cdc12. Unlike Cdc12, Fus1 is also capable of bundling actin filaments [154].

Formin	**Nucleation efficiency**	**Elongation rate**	**Dissociation rate**
Fission yeast Cdc12	1 (1 filament per 2.5 dimers)	1 (10-12 subunits $sec^{-1}\mu M^{-1}$)	1 (4.7-6.0 x $10^{-5} sec^{-1}$)
Fission yeast For3	0.015	0.90	0.77
Mouse Dia1	1.0	3.9	20
Mouse Dia2	0.25	1.0	2.2
Worm CYK-1	0.03	5.0-6.0	55
Budding yeast Bni1	0.10	2.0	2.8
Fission yeast Fus1	1.0	0.50	14

Table 4.1: ***In vitro* actin assembly properties of formins used to generate formin chimeras.** The actin assembly properties of all formins are normalized relative to Cdc12.

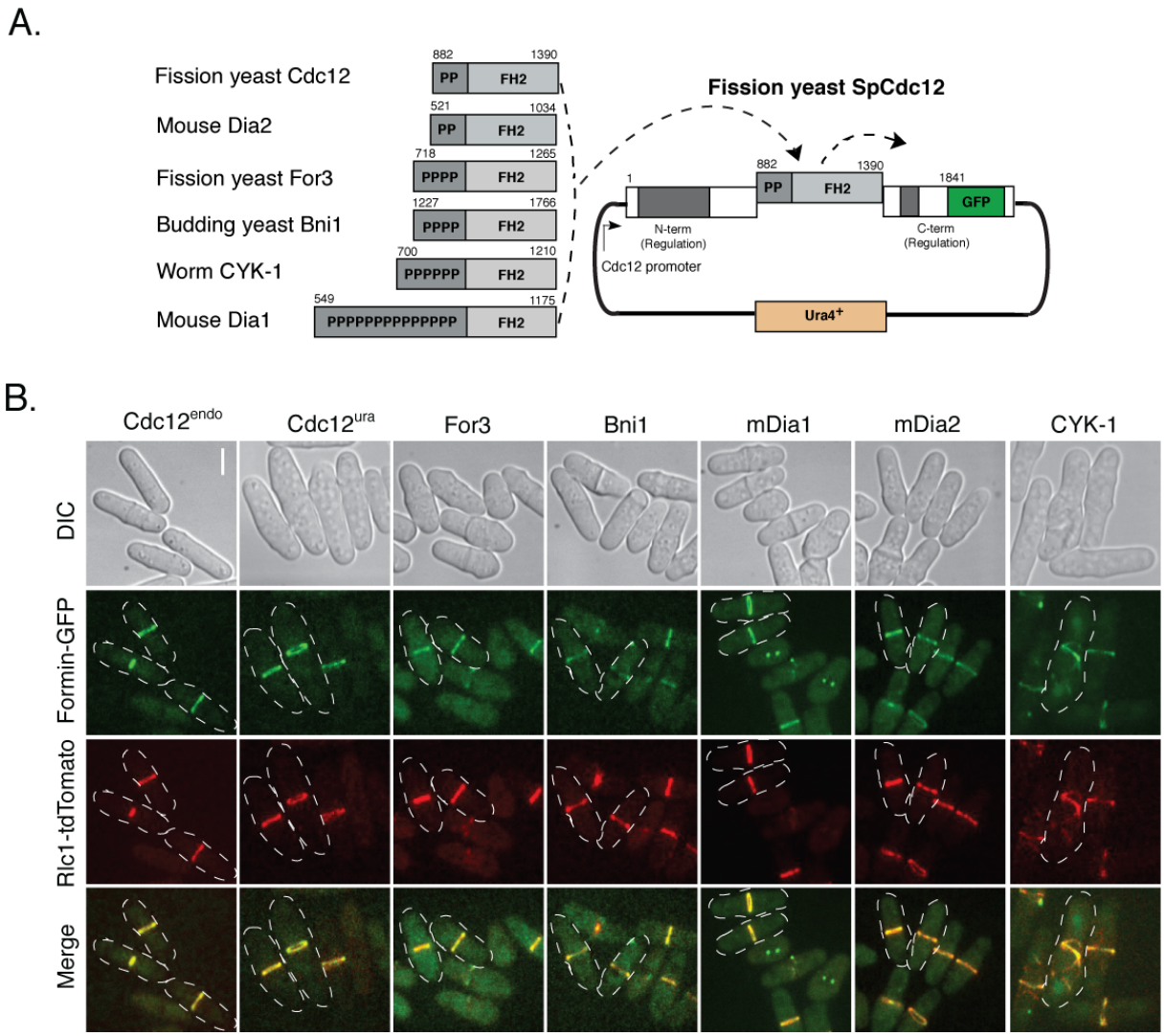

Figure 4.1: **Formin Cdc12 chimeras localize to the division site.** Fission yeast formin Cdc12 chimeras localize to the contractile ring and produce viable cells that divide. **(A)** Schematic of fission yeast formin Cdc12 chimeras, in which the FH1FH2 actin assembly domains were replaced by FH1FH2 domains from formins with diverse actin assembly properties. **(B)** Fluorescent micrographs of formin chimera fission yeast cells showing morphology (DIC), the formin chimera (Formin-GFP), the contractile ring (Rlc1-tdTomato), and the merge. Scale bar, 5 μm.

That formin chimera strains produce viable cells is even more striking when the diverse *in vitro* actin assembly parameters of each formin are considered (Table 4.1). Fission yeast For3 is a 70-fold less potent nucleator than Cdc12, but elongates filament barbed ends and dissociates from them at approximately the same rates as Cdc12 [154]. In contrast, nematode worm CYK-1 is significantly different from Cdc12 in all properties, nucleating filaments ~30-fold less efficiently, elongating filaments ~five-fold faster, and dissociating from barbed ends 55-fold faster [126]. Budding yeast Bni1 elongates F-actin only twice as fast as Cdc12 and dissociates from barbed ends only three times faster, but is a 10-fold less potent nucleator [118]. Conversely, mouse mDia1 nucleates filaments with the same efficiency as Cdc12, elongates barbed ends four-fold faster and dissociates from them 20-fold faster [148]. Mouse mDia2 is generally more similar to Cdc12 than the other formins, nucleating filaments only four-fold less well, elongating filaments only 1.5-fold faster, and dissociating only two-fold faster [62, 89]. If formin's specific actin assembly parameters are important for its role in cytokinesis, we hypothesize that mDia1 and mDia2 chimeras will compromise cytokinesis the least, as their actin assembly properties are most similar to Cdc12.

4.3.2 Formin Cdc12 chimera fission yeast strains display a range of cytokinesis and morphology defects

Although formin chimera fission yeast strains are viable, it was evident from initial imaging that some formin chimera strains appear more similar to control strains than others (Figure 4.1B). First, we quantified the total amount of formin-GFP fluorescence to determine the expression levels of formin chimeras relative to the $Cdc12^{endo}$ control (Figure 4.2A). The expression levels of formin chimeras were not statistically different from $Cdc12^{endo}$, which confirms that any potential effects on cytokinesis are not due to differences in formin chimera expression between strains. Additionally, a 24-hour cell growth assay showed that the overall rates of formin chimera strain growth as measured by optical density are similar to that of

control strains (Figure 4.2B). To visualize the actin cytoskeleton of formin chimera strains, we stained fixed cells with BoDipy-phallicidin, which revealed no obvious differences in actin cytoskeleton architecture between formin chimera and control strains (Figure 4.2C). Therefore, we quantified general cytokinesis defects. Staining methanol-fixed cells with DAPI and Calcofluor allowed for quantification of nuclei count and abnormal septa, respectively (Figure 4.3A-C). First, while only 15-20% of $Cdc12^{endo}$ and $Cdc12^{ura}$ cells have two nuclei, 28% of For3, 30% of Bni1, 28% of mDia1, 30% of mDia2, and 36% of CYK-1 cells have two or more nuclei (Figure 4.3A-B). The presence of more than two nuclei in higher percentage of formin chimera cells suggests a defect in the completion of cytokinesis. Second, whereas no $Cdc12^{endo}$ or $Cdc12^{ura}$ cells have abnormal septa, 34% of For3, 52% of Bni1, 25% of mDia1, 28% of mDia2, and 86% of CYK-1 cells contain abnormal septa (Figure 4.3A,C). In addition, the spindle pole body (SPB) marker Sad1-tdTomato revealed the percentage of formin chimera cells in mitosis (containing two SPBs). While only 14% of control strains had two SPBs, 39% of For3, 32% of Bni1, 32% of mDia1, 28% of mDia2, and 42% of CYK-1 cells were in mitosis (Figure 4.3E).

In addition to cytokinesis defects, some formin chimera cells exhibit abnormal bulging, indicating morphology defects (Figure 4.3A,F). We quantified this phenotype by measuring the cell width at three positions: two μm from each tip (m1 and m3) and the cell middle (m2) (Figure 4.3F). The average standard deviation of these measurements is significantly larger for formin chimera cells than control cells. Compared to $Cdc12^{endo}$, the normalized standard deviation is 0.95 for $Cdc12^{ura}$, 2.0 for For3, 2.0 for Bni1, 2.3 for mDia1, 2.2 for mDia2, and 4.8 for CYK-1. Additionally, CYK-1 chimera cells also exhibited abnormal cell lengths, presumably because the cells fail to divide properly (Figure 4.3D). The average length of $Cdc12^{endo}$ cells is 12.8 μm, while CYK-1 cells grow to an average length of 21.6 μm (Figure 4.3D). Together, these data indicate that mDia1 and mDia2 formin chimeras are generally less defective in cytokinesis than For3, Bni1, and CYK-1 chimeras.

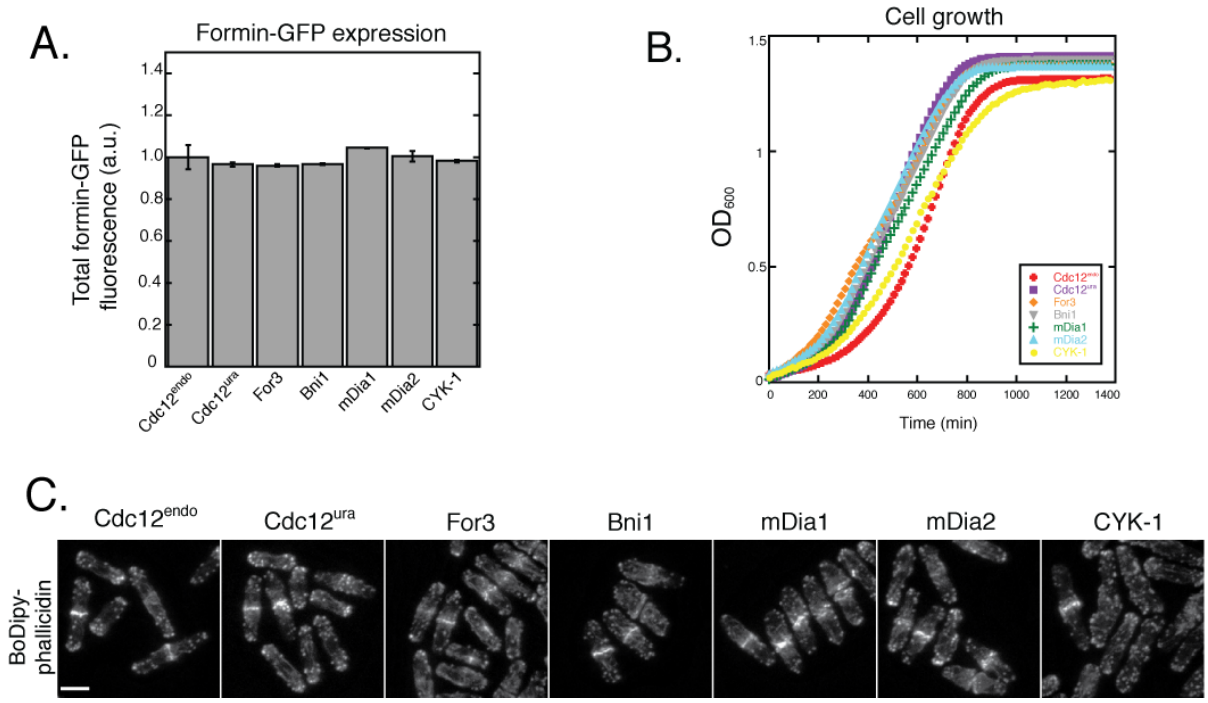

Figure 4.2: **Formin chimera expression levels and resulting cell growth rates and F-actin organization are similar to controls.** **(A)** Plot of formin-GFP expression levels normalized to $Cdc12^{endo}$. Error bars represent the standard error of two independent experiments. Two-tailed t-tests for data sets with unequal variance comparing each strain to $Cdc12^{endo}$ yielded p-values $p>0.20$ for all strains. **(B)** Growth curve of formin chimera strains. **(C)** Micrographs of fixed formin chimera cells stained with BoDipy-phallicidin to label actin filaments. Scale bar, 5 μm.

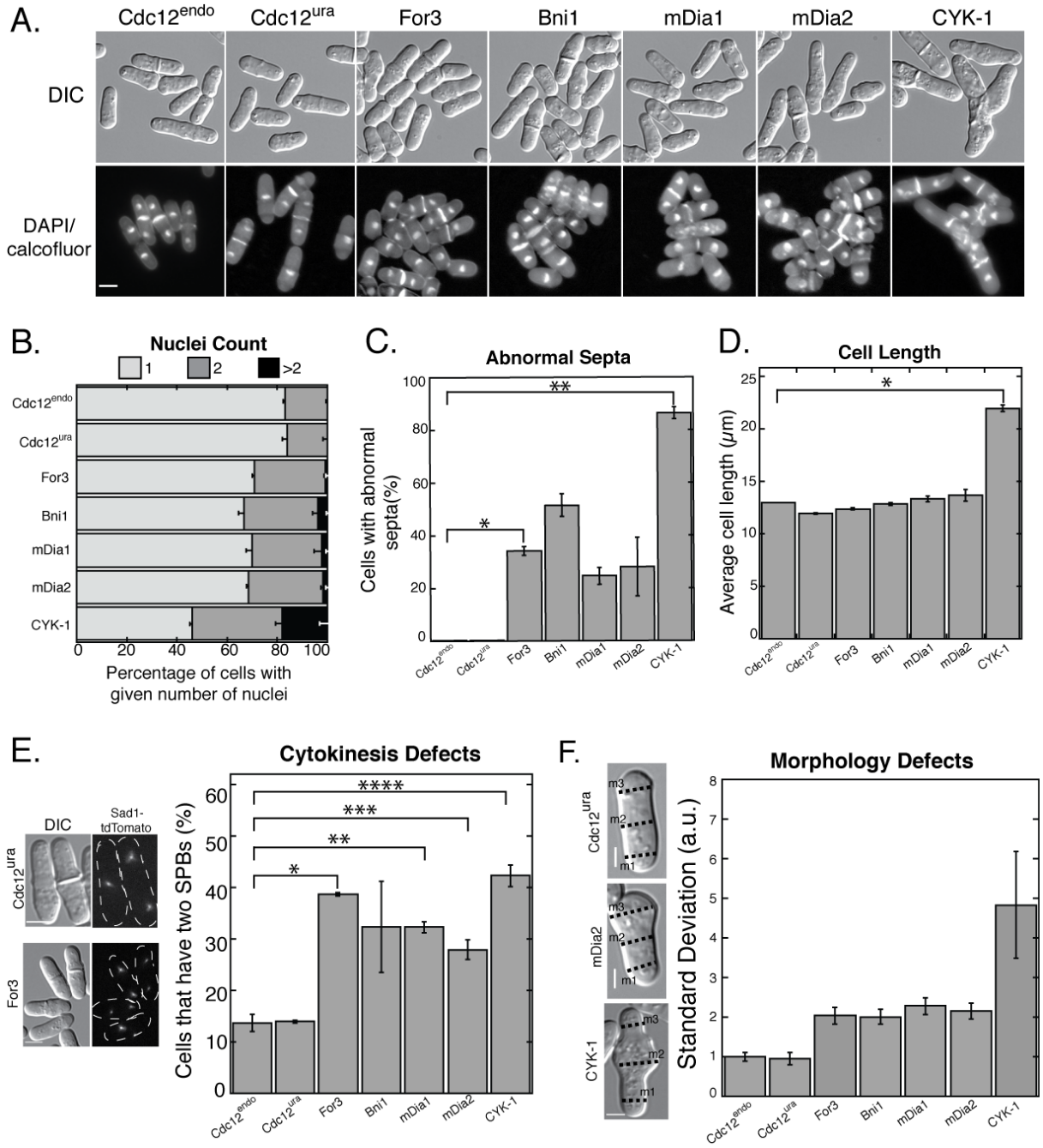

Figure 4.3: **Formin chimera fission yeast cells exhibit a range of cytokinesis and morphology defects(A)** Fluorescence micrographs of the indicated formin chimera strains; DIC (morphology) and methanol fixed cells stained with DAPI (nuclei) and Calcofluor (septa). Scale bar, 5 μm. **(B-D)** Quantification of general cytokinesis defects. Error bars indicate standard error of two replicates of at least 50 (polarity defects) to 500 (abnormal septa) cells. **(B)** Percent of cells with one, two or >two nuclei. **(C)** Percent of cells with abnormal septa (misplaced, misoriented, or abnormally broad). Error bars=s.e.m. Two tailed t-tests for data sets with unequal variance yielded p-values *p=0.030, **p=0.017.

Figure 4.3: (continued) **(D)** Plot of average cell lengths. Error bars=s.e.m. A two tailed t-test for data sets with unequal variance yielded p-values *p=0.023. **(E)** Plot of cytokinesis defects, as indicated by the number of spindle pole bodies. Scale bar, 5 μm. Error bars=s.e.m. Two tailed t-tests for data sets with unequal variance yielded p-values *p=0.045, **p=0.011, ***p=0.030, ****p=0.0079. **(F)** Plot of morphology defects, determined by calculating the standard deviation of three cell width measurements. Scale bar, 3 μm.

4.3.3 Formin chimera fission yeast cells progress through cytokinesis at different rates

Because formin chimera cells exhibit varying degrees of general cytokinesis defects, we aimed to understand which steps of cytokinesis are specifically compromised in each strain. Although fission yeast cells can assemble contractile rings through both "precursor cytokinesis nodes" and "spot" pathways, we focused on cells assembling rings from cytokinesis nodes, which follow well-defined events (Figure 4.4A): (1) formation of a broad band of precursor nodes, (2) contractile ring assembly, (3) initiation of constriction, (4) completion of constriction, and (5) cell separation [178, 190]. We imaged dividing cells expressing the contractile ring marker Rlc1-tdTomato by time-lapse fluorescence microscopy of a single plane to compare the extent to which specific steps in cytokinesis are impaired for each formin chimera strain (Figure 4.4B).

To compare the entire cytokinesis time course, we analyzed cells that completed cytokinesis from node appearance to cell separation within our imaging window of three hours (Figure 4.4B-C). In wild-type fission yeast, spindle pole bodies separate around 10 minutes after Rlc1 appears in nodes. However, we noticed that separation of spindle pole bodies and initiation of ring assembly are uncoupled in some formin chimera strains, where Rlc1 fluorescence appears in nodes up to an hour before spindle pole body separation (Figure 4.4B, bottom panel). Therefore, the initial appearance of a broad band of cytokinetic precursor nodes, as indicated by Rlc1-tdTomato, represents time zero in our experiments. 100% of $Cdc12^{endo}$ and $Cdc12^{ura}$ control cells complete cytokinesis with remarkably little variability

in ~90 minutes after the appearance of pre-ring nodes. In contrast, each formin chimera strain has a distinct profile of cytokinesis progression, some with significant delays (Figure 4.4C). mDia1 and mDia2 strains progress through cytokinesis with only a slight delay as compared to control cells, with 100% of cells completing cell division within two hours of node appearance. In contrast, For3, Bni1, and CYK-1 strains display significant delays, finishing cell division 100-200 minutes after node appearance.

Because fission yeast cytokinesis occurs via a pathway of distinct steps, we quantified the time elapsed between specific well-defined events in order to understand which step(s) causes delays in formin chimera strain cytokinesis: ring assembly (Figure 4.4D), ring maturation (Figure 4.4E), ring constriction (Figure 4.4F), or cell separation (Figure 4.4G). For ring assembly, we quantified how long it took for each cell to assemble a fully formed contractile ring after the initial appearance of node fluorescence at the midzone (Figure 4.4D). Interestingly, two populations of ring assembly profiles emerged from this analysis. Similar to control strains, 100% of mDia1 and mDia2 cells assembled contractile rings within 25 minutes of broad brand appearance. In contrast, For3, Bni1, and CYK-1 exhibited a large lag in ring assembly, with 100% of cells finally forming contractile rings between 70-100 minutes after node appearance (Figure 4.4D). After the contractile ring was assembled, we quantified the ring maturation time, or the time elapsed prior to the onset of cell constriction (Figure 4.4E). Remarkably, the time course of ring maturation was similar for all formin chimeras, with most cells finishing ring maturation within 20 minutes of ring formation. Only For3 and Bni1 cells exhibited a brief lag but were still more similar to control strains than during ring assembly. Similarly, we examined the time elapsed during ring constriction and cell separation and found that all formin chimera cells behave similarly to control strains. Therefore, defects in the specific step of ring assembly are primarily responsible for the long delays in the overall time course of cytokinesis (Figure 4.4C). Following the SCPR model of fission yeast cytokinesis, formins with low nucleation efficiency will produce few actin filaments,

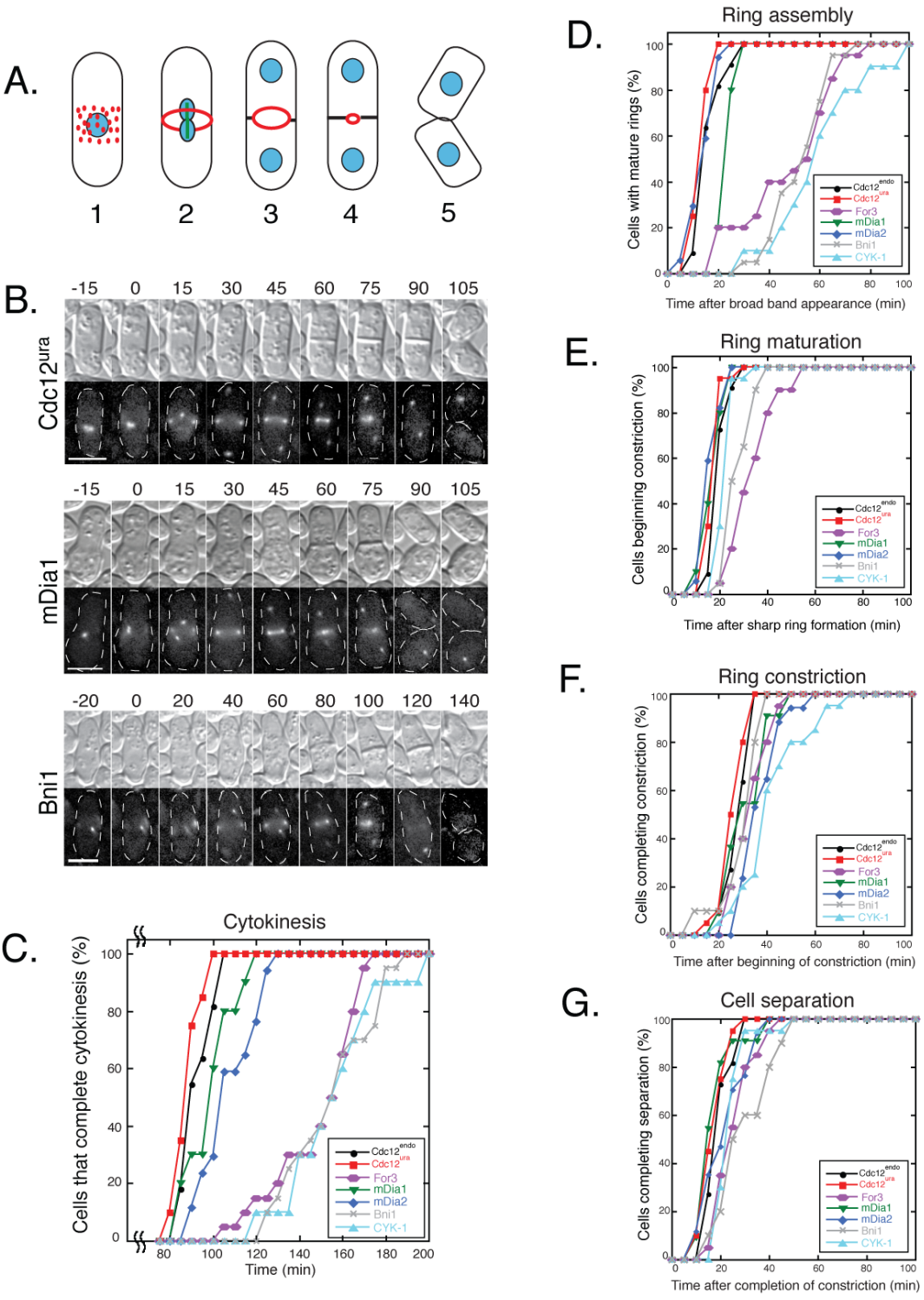

Figure 4.4: **Formin chimeras with poor nucleation efficiency exhibit delays in ring assembly.**

Figure 4.4: (continued) **(A)** Schematic of fission yeast cytokinesis: (1) node assembly (2) ring assembly (3) Ring maturation (4) Ring constriction (5) Cell separation. **(B)** Time-lapse micrographs of the morphology (DIC) and contractile ring (Rlc1-tdTomato) of representative formin chimera cells. Time is indicated in minutes. Scale bars, 5 μm. **(C)** Time required for at least 20 cells to complete cytokinesis for each strain. **(D-G)** Time required for at least 20 cells to complete the given cytokinesis step for each strain. **(D)** Frequency of cells that assemble a sharp ring over time. **(E)** Frequency of cells that complete ring maturation. **(F)** Frequency of cells that complete ring constriction. **(G)** Frequency of cells that complete cell separation.

leading to difficulty with node coalescence and overall ring assembly.

4.3.4 Formin chimera strains assemble contractile rings through different pathways

Previous work has indicated that fission yeast cells that are unable to assemble pre-ring nodes can still accomplish cytokinesis via a mechanism known as the "leading cable" model [24, 7], where a few leading actin cables originating from a single spot on the cortex wrap around the circumference of the cell to form the contractile ring. We noticed that some formin chimera strains expressing Rlc1-tdTomato exhibit a spot of Rlc1 at the midzone long before spindle pole body separation (time zero) (Figure 4.5A). This early Rlc1-tdTomato fluorescence suggests that these cells might be progressing through cytokinesis via a different pathway, so we quantified the number of cells from each formin chimera strain that form contractile rings through the traditional SCPR pathway, or "nodes," and through this alternate "spot" pathway (Figure 4.5B). Not surprisingly, mDia1 and mDia2 chimera cells, like control strains, all form contractile rings by first forming pre-ring cytokinesis nodes. At least 50% of For3, Bni1, and CYK-1 cells, however, exhibit this Rlc1 "spot" and form a contractile ring prior to SPB separation, supporting the idea that they must use an alternate pathway for ring assembly since the poor nucleation efficiency of their contractile ring formins precludes ring assembly via SCPR.

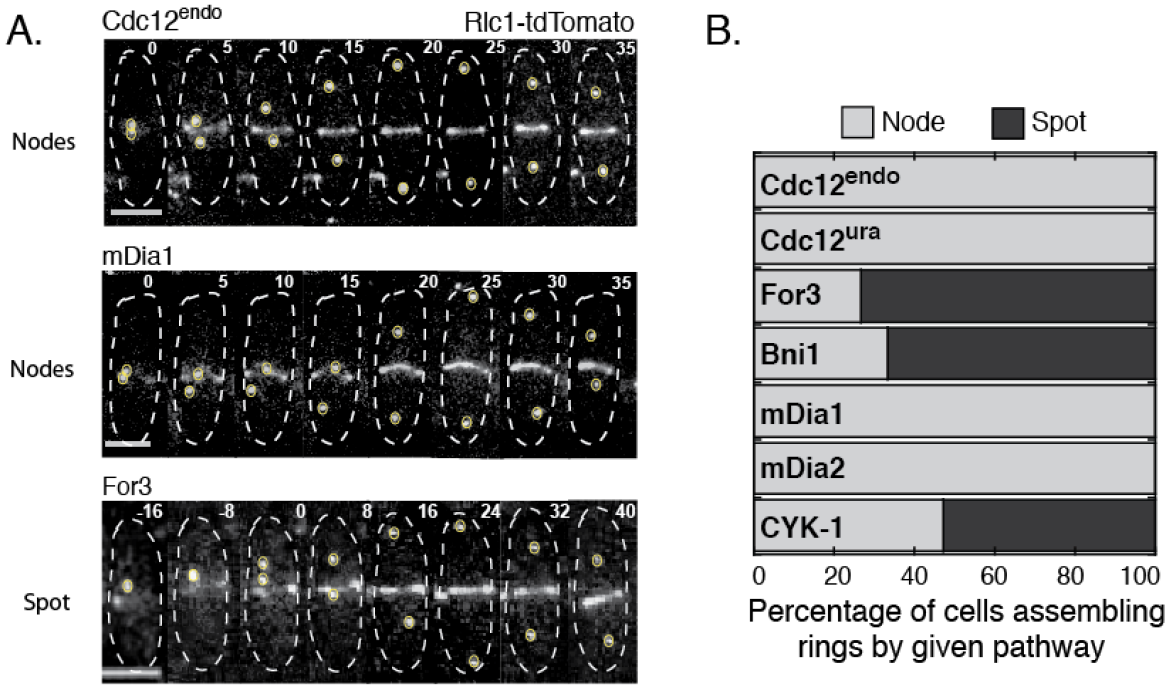

Figure 4.5: **Formin chimeras utilize different mechanisms to assemble contractile rings.** **(A)** Confocal time-lapse images of the indicated formin chimera strains showing assembly of the contractile ring (Rlc1-tdTomato). Time zero: spindle pole body (SPB) separation. Scale bar, 5 μm. **(B)** Percentage of cells that build contractile rings through pre-ring node or spot pathways.

4.3.5 Computational model based on Search, Capture, Pull, and Release shows that specific actin assembly properties of formin are tailored for proper cytokinetic ring assembly

In order to understand mechanistically how formin nucleation efficiency and polymerization rate could account for abnormal ring assembly in cells expressing formin chimeras, we extended a computational 3D model that was previously validated [14]. Different from previous SCPR models [178, 94, 14], the current implementation incorporates a varying number of filaments, N, which represents the degree of formin nucleation efficiency. First, we systematically varied N from 130 (corresponding to two filaments per node) to 30 (corresponding to about one filament every two nodes), mimicking changes in formin nucleation efficiency. Second, we simulated changes in formin polymerization activity by varying the actin polymerization rate in the range of 0.04-0.2 μm/s. Third, we introduced force-sensitive inhibition of formin when the tension at the filament barbed end exceeded 1 pN due to recent experimental reports identifying the inhibition of formin-dependent actin polymerization in response to tension [199]. This model allowed us to examine the individual and collective contributions of the formin nucleation efficiency and polymerization rate on the probability of ring assembly, with and without formin inhibition. Last, we examined how the timing of ring assembly varied across the different conditions and quantified other dynamic and structural parameters in the parameter space given by N and v_{pol} such as node velocity and distribution.

Simulations reproduced ring assembly at the value of formin nucleation efficiency and actin polymerization rate mimicking Cdc12 ($N = 130$ and $v_{\mathrm{pol}} = 0.1$ μm/s, respectively). Keeping $N = 130$ and varying v_{pol}, the model predicted clumping of nodes that elongate short filaments radially at low v_{pol}, and assembly of nodes into few clumps at the center of the simulation domain that elongate long actin cables along the domain's long axis at high

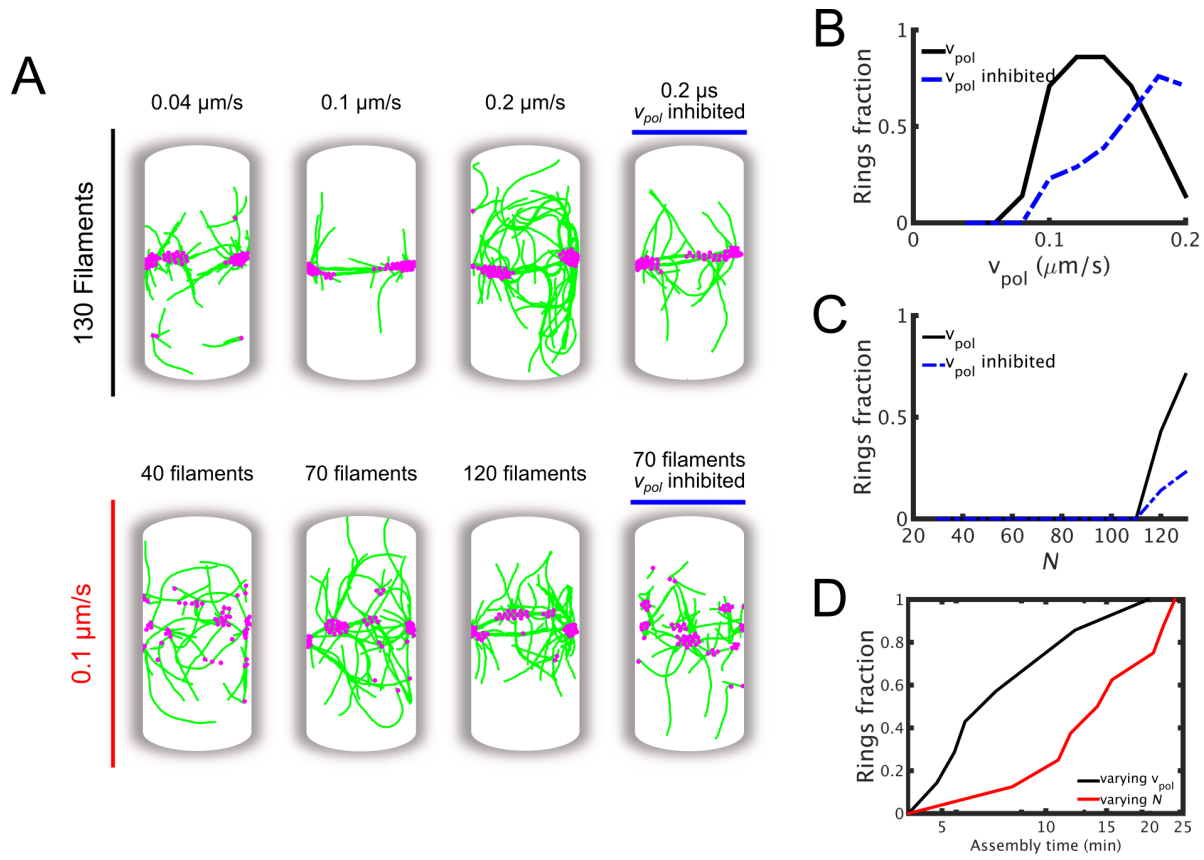

Figure 4.6: **Formin nucleation efficiency and polymerization rate are critical for proper ring assembly.** **(A)** Snapshots taken in different conditions of v_{pol} and N. Upper line: snapshots at 20 min of ring assembly simulations by keeping N=130 and varying v_{pol}. Lower line: snapshots between 15-20 min of simulations by keeping $v_{\mathrm{pol}} = 0.1$ μm/s and varying N. **(B)** Probabilities of ring assembly at N=130 and varying v_{pol}. Data are averages from 3-5 independent runs for cases without and with inhibition of formin activity due to tension. **(C)** Probabilities of ring assembly at $v_{\mathrm{pol}} = 0.1$ μm/s and varying N. Data are averages from 3 independent runs, for cases without and with inhibition of formin activity. **(D)** Cumulative probabilities of ring assembly times, computed from cases with fixed N=130 and varying v_{pol} in the range 0.08-012 μm/s (black curve) or fixed $v_{\mathrm{pol}} = 0.1$ μm/s and varying N in the range 90-130 (red curve).

v_{pol} (see first row of Figure 4.6A). Keeping $v_{\mathrm{pol}} = 0.1$ μm/s and varying N, our simulations showed: for N ~40, many small clumps of nodes that were far apart along the domain's long axis; for increasing N, a decrease in the number of node clumps. By incorporating force-dependent inhibition of actin polymerization, ring assembly was rescued at high values of v_{pol} (Figure 4.6A).

We then computed the probabilities of ring assembly when varying either v_{pol} or N. With $N = 130$ and varying v_{pol}, the fraction of assembled rings was spread out around 0.1 μm/s (Figure 4.6B). In contrast, variations in N resulted in highly impaired ring assembly, with a narrow distribution of assembled rings around $N = 130$ (Figure 4.6C). With force-independent inhibition of actin polymerization, for $N = 130$ and varying v_{pol}, the fraction of assembled rings shifted toward higher v_{pol} with respect to corresponding uninhibited cases (Figure 4.6B). For $v_{\mathrm{pol}} = 0.1$ m/s and varying N, the probability of ring assembly decreased from about ~80% at $N = 130$ in uninhibited cased to ~20% in the force inhibited simulations (Figure 4.6C). Rings could only be detected at N close to the nominal value of 130 filaments in both uninhibited and inhibited cases. This result supports the experimental observation that formin chimeras with nucleation efficiencies different from Cdc12 critically impact ring assembly (Figures 4.3-4.4). Incorporating force-dependent inhibition of actin polymerization and varying N while keeping $v_{\mathrm{pol}} = 0.1$ μm/s did not rescue ring assembly (Figure 4.6A). Probabilities of ring formation by simultaneously varying v_{pol} and N are reported in Figure 4.7A-B. When varying nucleation efficiency N, the time of ring formation was longer than when varying v_{pol} (Figure 4.6D). Consistent with the result that more rings form for $N = 130$, the degree of node coalescence from an initial broad band, which was computed from the dispersion in node positions along the longitudinal domain axis, depend on N but not on v_{pol} (Figure 4.7C-D). Times of ring assembly were in the range of 5-25 minutes at $v_{\mathrm{pol}} > 0.1$ μm/s and $N > 100$ (Figure 4.8A-B). The average node velocity did not vary significantly with v_{pol} and was around 30 nm/s at N ~130, consistent with previous results (Figure

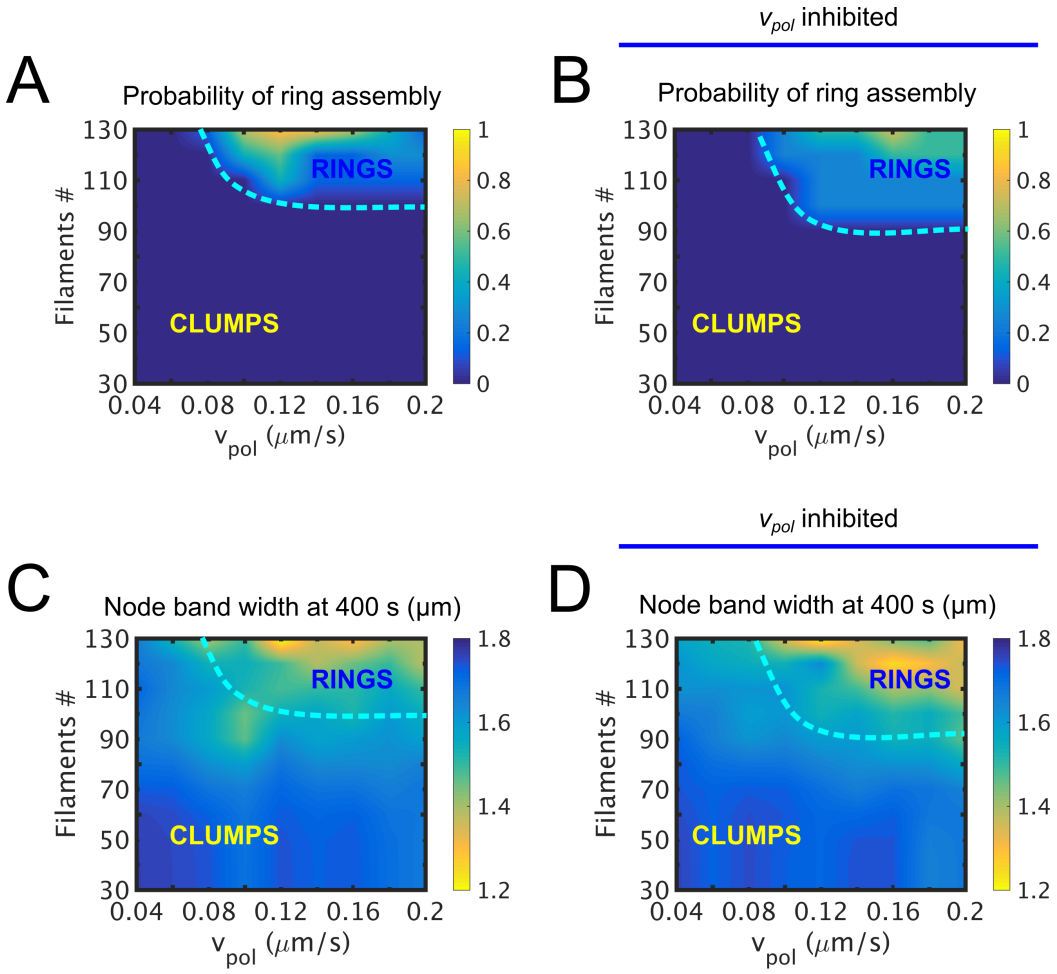

Figure 4.7: **Mechanosensitive inhibition of actin polymerization shift the ring assembly probability distribution towards higher values of polymerization rate.** **(A)** Probabilities of ring assembly varying N and v_{pol}, without inhibition of actin polymerization. Results are averages from 3-5 independent runs. **(B)** Probabilities of ring assembly varying N and v_{pol}, with mechanosensitive inhibition of actin polymerization. Results are averages from there independent runs. **(C)** Node band width varying N and v_{pol}, without inhibition of actin polymerization. Results are computed as twice the standard deviation of nodes positions along the domain longitudinal axis, as averages from 3-5 independent runs. **(D)** Node band width varying N and v_{pol}, with inhibition of actin polymerization. Results are computed as twice the standard deviation of nodes positions along the domain longitudinal axis, as averages from three independent runs.

4.8C-D) [178, 14].

When we incorporated force-dependent inhibition of v_{pol}, keeping $N = 130$ and varying v_{pol}, the spread of the nodes decreased ~20% with increasing v_{pol} (Figure 4.7D). Times of ring assembly increased with v_{pol}, spanning a range of 10-30 nm/s (Figure 4.8D). The effect that we detect in these simulations with respect to rescuing ring formation in cases of high v_{pol} is consistent with previous experimental and computational findings showing that inhibition of formin-mediated actin polymerization results in more efficient ring formation [199]. In particular, the probability of ring assembly was generally increased for cases with $N > 100$ by inhibition of filament elongation compared to uninhibited cases. This signifies that mechanosensitive formin activity rescues ring assembly not only when v_{pol} is high, but also when nucleation efficiency is mildly decreased from the nominal value.

4.4 Discussion

4.4.1 Cytokinesis is remarkably robust, but best mediated by a formin that is tailored for this specific process

Formins associate processively with the growing barbed end of actin filaments to polymerize straight F-actin and facilitate diverse cellular processes. While different formins elongate actin filaments by the same general mechanisms, distinct formins are required for distinct cellular roles and exhibit a wide range of biochemical properties. We previously determined that the actin assembly properties of all three fission yeast formin isoforms vary widely, indicating that a formin's specific properties might be tuned for a particular cellular role [154]. Here, we investigated whether fission yeast formin Cdc12 is tailored for cytokinesis by engineering formin chimera fission yeast strains in which the FH1FH2 actin assembly domains of Cdc12 were replaced with the FH1FH2 domains from a group of evolutionary and functionally distinct formins: For3 (fission yeast), Bni1 (budding yeast), mDia1 (mouse),

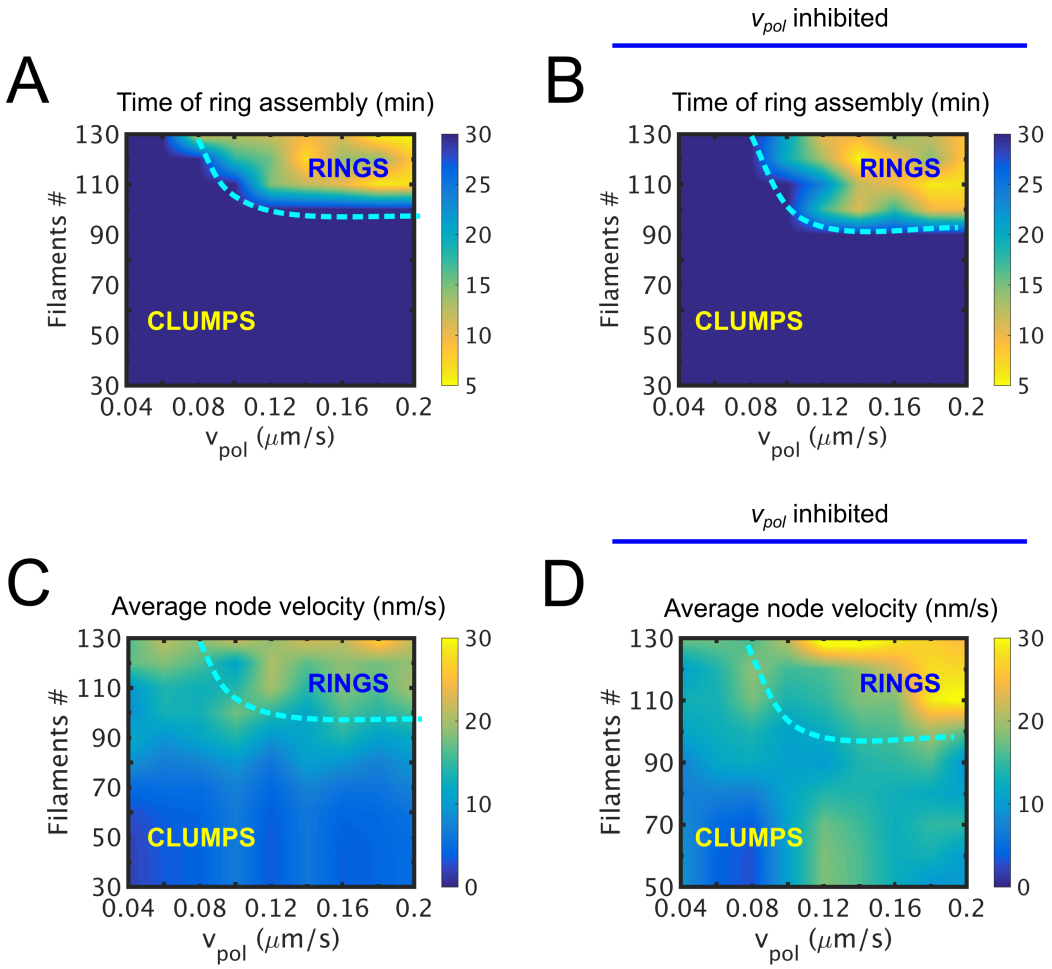

Figure 4.8: **Mechanosensitive inhibition of actin polymerization accelerates ring assembly at high polymerization rates.** **(A)** Times of ring assembly varying N and v_{pol}, without inhibition of actin polymerization. Results are averages from 3-5 independent runs. **(B)** Times of ring assembly varying N and v_{pol}, with mechanosensitive inhibition of actin polymerization. Results are averages from 3 independent runs. **(C)** Average node velocity varying N and v_{pol}, without inhibition of actin polymerization. Data are computed between 90-100 s of simulations as averages from 3-5 independent runs. **(D)** Average node velocity varying N and v_{pol}, with inhibition of actin polymerization. Data are computed between 90-100 s of simulations as averages from three independent runs.

mDia2 (mouse), and CYK-1 (worm) (Figure 4.1A). These formin "chimeras" retain Cdc12's localization and regulation, but demonstrate a wide range of actin assembly properties (Table 4.1).

We found that cells expressing formin chimeras are viable, but exhibit a range of cytokinesis and morphological defects, despite proper localization of formin chimeras to the division site. Many formin chimera cells contain more than two nuclei and multiple septa, which is indicative of impaired cytokinesis. Interestingly, we see that mDia1 and mDia2 formin chimeras are generally less defective in cytokinesis than For3, Bni1, and CYK-1 formin chimeras (Figure 4.3). An analysis of their *in vitro* actin assembly properties reveals that while For3, Bni1, and CYK-1 elongate actin as fast or faster than Cdc12, their nucleation efficiencies are 1.5%, 10%, and 3% as efficient as Cdc12, respectively. To investigate which specific step of cytokinesis is defective in formin chimera strains, we utilized time-lapse fluorescence microscopy to image the entire time course of cytokinesis in dividing cells. Again, For3, Bni1, and CYK-1 formin chimeras exhibit long delays in the completion of cytokinesis compared to control strains (Figure 4.4). Control strains complete ring assembly in ~25 minutes, while For3, Bni1, and CYK-1 chimeras take three- to four-fold longer to assemble mature contractile rings (Figure 4.4D). Interestingly, formin chimera strains that exhibit slow ring assembly complete subsequent steps of cytokinesis (ring maturation, ring constriction, and cell separation) at similar rates as control strains (Figure 4.4E-G). mDia1 and mDia2 chimeras, on the other hand, complete all steps of cytokinesis at similar rates as control strains. Together, these data indicate that fission yeast cytokinesis is extremely robust, but formins with low nucleation efficiency are unable to build a mature contractile ring as effectively as Cdc12.

Fission yeast cells use the Search-Capture-Pull-Release (SCPR) model of contractile ring assembly, which relies upon ~65 pre-ring cytokinesis nodes that contain formin Cdc12 and myosin, as well as other regulatory and scaffolding proteins [178, 192]. Node-bound Cdc12

elongates actin filaments that are captured and pulled by myosin on nearby nodes, bringing nodes closer together to assemble a continuous F-actin ring. These F-actin connections between nodes are severed by cofilin, and process starts again until the ring is fully formed [178, 192]. It follows, then, that Cdc12's efficient nucleation of F-actin (one filament for every 2.5 Cdc12 dimers) is paramount in its role as the sole cytokinesis formin in fission yeast because the initial step of contractile ring assembly requires efficient formation of actin filaments. It has been shown that each pre-ring cytokinesis node contains only two to four Cdc12 dimers, which explains why the formin chimeras that are poor nucleators exhibit a long lag in ring assembly. For3, Bni1, and CYK-1 produce fewer actin filaments per formin dimer, resulting in impaired node coalescence and slower contractile ring formation.

While a formin's elongation rate is also likely to be tailored for its cellular role, recent evidence reveals that formin elongation rates can be modulated by external forces. We showed that Cdc12 acts as a mechanosensor whose elongation is inhibited by myosin pulling of Cdc12-bound filaments [199]. Conversely, application of force to budding yeast Bni1 increases its F-actin elongation rate in the presence of profilin [33]. Similarly, mouse mDia1 exhibits a ~two-fold increase in its elongation rate of actin filaments in response to pulling forces [76]. Actin filaments, especially in contractile networks, often experience mechanical forces that could modify elongation by mechanosensitive formins to facilitate assembly of particular F-actin networks. Thus, formin chimera elongation rates might affect fission yeast cytokinesis less than their nucleation efficiencies.

Interestingly, it has also been shown that some formins associate with cofactors that stimulate actin nucleation. For example, budding yeast nucleation promoting factor Bud6 interacts with formin Bni1 to enhance nucleation by recruiting actin monomers [57]. Additionally, formin mDia1 synergizes with adenomatous polyposis coli (APC) to stimulate F-actin nucleation in mammalian cells [18, 130]. Any such interactions that could increase nucleation rates of formin chimeras that are poor nucleators would be absent in fission yeast,

which could contribute to the long contractile ring assembly delays seen in Bni1 and CYK-1 chimera strains. However, we also see severe cytokinesis defects in cells expressing For3 formin chimeras even though For3 is a fission yeast formin that could potentially still interact with important accessory proteins. It is likely that For3's poor nucleation efficiency is also tailored for its role in fission yeast, as it builds polarizing actin cables that are formed through multiple rounds of asynchronous nucleation and elongation to push old actin filaments into the cell interior. It is also possible that For3 bypasses F-actin nucleation by associating with and elongating existing filaments nucleated by Arp2/3 complex in actin patches. Future work should investigate the regulation of fission yeast formins to determine whether they require cofactors to modulate F-actin nucleation.

Manipulation of Cdc12's nucleation efficiency *in vivo* via point mutations would allow for direct analysis of the contribution of nucleation to fission yeast cytokinesis. However, disruption of FH2 domains often leads to a nonfunctional formin protein due to the importance of FH2 domains in formin dimerization and barbed-end binding. Instead, we directly tested the effects of actin assembly properties of formin on cytokinetic ring assembly using a computational model that was previously developed and validated for reproducing fission yeast ring formation in 3D based on the Search, Capture, Pull, and Release mechanism [178, 94, 14]. The model allowed us to independently control formin nucleation efficiency and polymerization rate and to characterize their relative effects on ring assembly. Different from the previous SCPR models [178, 94, 14], varying the number of actin filaments N, which represents the degree of formin nucleation efficiency, and changing the rate of filament elongation, which corresponds to the velocity of actin polymerization v_{pol}, allows us to directly identify regimes of actomyosin reorganization that are comparable to experiments using formin chimeras. Time and probability of ring assembly from the simulations, as well as other dynamics and morphological features, including the velocity and spatial distribution of nodes, vary in the parameter space given by N and v_{pol}. Variations in formin nucleation

efficiency critically impact both probabilities and times of ring formation.

In contrast, changes in polymerization rate have a smaller effect on both the morphology and dynamics of ring assembly. In addition, the model shows that while mechanosensitive inhibition of actin polymerization rescues cytokinetic ring assembly with formins that exhibit fast elongation of filaments, it is inefficient with poor nucleators. The experimental observation that formin chimeras with nucleation efficiencies that diverge from Cdc12 critically impact ring assembly (Figures 4.3, 4.4) is entirely supported by our computational model. In addition, our modeling results are fully consistent with our experimental observations that formin chimeras with low nucleation efficiencies show severe cytokinetic defects as opposed to formins that are slow polymerizers. The significance of the computational model hinges on the fact that it allows us to not only isolate and control formin actin assembly properties and how they impact contractile ring formation, but it also provides a valid tool to interpret the experimental data within a rigorous conceptual framework.

4.5 Materials and Methods

4.5.1 Formin chimera strain construction

cdc12 N-terminal sequence was amplified by PCR (iProof, Bio-Rad Laboratories) from wild-type *S. pombe* genomic DNA and cloned into pBluescript II KS (-) (Stratagene) using restriction enzymes XhoI and BamHI. Overlap PCR was used to link formin (FH1FH2) sequences from For3, Fus1, Bni1, mDia1, mDia2, and CYK-1 to *cdc12* C-terminal sequences, followed by homologous recombination using the In-Fusion Advantage PCR Cloning Kit (Clontech, Mountain View, CA) into pBluescript already containing *cdc12* N-terminus, resulting in the *cdc12* chimera fragment *cdc12*(N)::formin(FH1FH2)::*cdc12*(C). PCR amplifications of the *cdc12* promoter (1-700 bp upstream of the translation start site) from the wild-type *S. pombe* genome and monomeric GFP (mGFP) from the pSGP-572 vector were cloned into the *S.*

pombe integration vector pJK210 [83] with restriction enzyme SacI. *Cdc12* chimeras were also cloned into pJK210 by In-Fusion downstream of the *cdc12* promoter and confirmed by sequencing.

Chimera formin constructs were integrated into the *ura4* locus under control of the *cdc12* promoter and tagged C-terminally with GFP to create pJK210-Pcdc12-cdc12(N-term)-formin(FH1FH2)-cdc12(C-term)-GFP::ura+ (Zimmermann 2017). Endogenous *cdc12* was deleted through Kan cassette gene replacement [20], while markers for contractile rings (rlc1-tdTomato-natMX6) and spindle pole bodies (sad1-tdTomato-natMX6) were introduced to formin chimera strains through mating. Table 4.2 lists the fission yeast strains used in this study.

4.5.2 Cell imaging and growth

Differential interference contrast (DIC) and epifluorescence images were collected on an IX-81 microscope (Olympus, Tokyo, Japan) fitted with an Orca-ER camera (Hamamatsu, Bridgewater, NJ) and a 60X, 1.4 NA Plan Apo objective. Confocal images were acquired on a Zeiss Axiovert 200M microscope (Zeiss) equipped with a Yokogawa CSU-10 spinning-disk unit (McBain, Simi Valley, CA) fitted with a Cascade 512B EM-CCD camera (Photometrics, Tuscon, AZ) controlled by MetaMorph software (Molecular Devices, Sunnyvale, CA) and illuminated with 50 milliwatt 473- and 561-nm DPSS lasers.

For live cell DIC and epifluorescence imaging, cells were grown overnight in YE5S media at 25° C, subcultured into EMM5S minimal media without thiamine, and kept in log phase for 20-22 hr. They were then imaged directly on glass slides using Z-stacks of 10 slices with a 0.5 μm step size.

4.5.3 Cell growth assay

Each strain was grown for 24-36 hr in YE5S and then seeded in triplicate in a 96-well plate at initial OD_{600} readings of 0.03 and 0.06. OD_{600} readings were measured every 10 min for 24 hr in a Tecan Inifinite M200Pro (Tecan Systems, Inc., San Jose, CA) plate reader at 30° C with an orbital shaking amplitude of 4 mm.

4.5.4 BoDipy-phallicidin staining

Upon receipt, BoDipy-phallicidin stocks were prepared by resuspending 300 units BoDipy-phallicidin (Thermo Fisher Scientific, Waltham, MA) in 1.5 mL methanol. This solution was divided into 25 μL aliquots, vacuum dried, and stored at -20° C. Immediately prior to use, one dry BoDipy-phallicidin aliquot was resuspended in 10 μL PEM buffer (0.1 M NA PIPES pH 6.8, 1 mM EGTA, 1 mM $MgCl_2$).

Cells were grown in YE5S for 36 hr. 1 mL cells for each strain growing at 25° C and OD_{600} ~0.4 were fixed with 333 μL 16% paraformaldehyde for 5 min. The fixed cells were washed 3 times at RT with PEM with 30 s spins at 7000 rpm in between. Cells were permeabilized in 1 mL PEM buffer with 1% Triton X-100 (Sigma-Aldrich, St. Louis, MO) at RT for 1 min. Cells were then washed three times as before and resuspended in 10 μL PEM and stained by adding 1 μL BoDipy-phallicidin solution for 30 min in the dark at room temperature. After staining, cells were washed once with PEM and spun for 30 s at 7000 rpm to obtain a pellet. The supernatant was removed, leaving a small amount of liquid. 4 μL of cells were imaged directly on glass slide as described above on an IX-81 microscope (Olympus).

4.5.5 DAPI/Calcofluor staining

Cells were grown in YE5S for 36 hr, and DIC images were acquired directly on glass before fixation. DAPI/Calcofluor staining was conducted as described previously [27]. Briefly, cells

were grown in YE5S at 25° C for 36 hr and then fixed with 100% cold methanol. For staining, cells were incubated in 300 μL 50 mM sodium citrate with 4 μL Calcofluor White Stain (Fluka Analytical, Sigma-Aldrich, St. Louis, MO) for 5 min at 37° C. They were then washed with 1 mL 50 mM sodium citrate and resuspended in 15 μL sodium citrate and 4 μL DAPI stock (1 mg/mL in H_20, Life Technologies, Carlsbad, CA) and kept on ice until imaging. 2.5 μL of stained cells were placed on glass slide and imaged as described above on an IX-81 microscope (Olympus) with an Orca-ER camera (Hamamatsu) and 60X, 1.4 NA Plan-Apo objective.

4.5.6 Quantification of DIC and DAPI/Calcofluor images

DAPI/Calcofluor stained cells were scored for number of nuclei and appearance of septa, where abnormal septa were those that were misplaced or misshapen. DIC images were used for quantification of cell length, cytokinesis defects, and morphology defects. Cell length was measured along the long axis of each cell. For cytokinesis defects, strains containing spindle pole body marker Sad1-tdTomato were quantified for number of spindle pole bodies. For morphology defects, DIC images of each strain were quantified for three cell width measurements: 2 μm from each cell tip (m1 and m3) and in the cell midzone (m2). The standard deviation of these cell width measurements was then calculated for each cell.

4.5.7 Quantification of formin chimera expression

Z-stacks of strains expressing formin chimeras tagged with GFP and Rlc1-tdTomato were imaged on glass slides as described above and sum slice projections were compiled. To measure formin chimera expression, ROIs were created of both contractile rings and the corresponding whole cell. The mean fluorescence of the formin-GFP was measured in the contractile ring and divided by the mean formin-GFP of the whole cell to control for background fluorescence. The average of this ratio was calculated for two replicates for each strain and

normalized to the control.

4.5.8 Time of cell division

For time-lapse images, cells expressing Rlc1-tdTomato and Sad1-tdTomato were imaged at a single Z-plane once a min for 3 hr on gelatin pads on the epifluorescence microscope as described for DAPI/Calcofluor staining. Time was quantified by first appearance of Rlc1-tdTomato at the cell midzone.

4.5.9 Modeling

In order to isolate actin assembly properties of formin and test their effect on fission yeast cytokinetic ring assembly, we extended a previously characterized 3D model based on the SCPR mechanism [14]. The model implements a Brownian Dynamics algorithm within a domain that mimics the shape, dimensions and other physical properties of fission yeast cells, such as cytoplasmic drag and membrane friction. By integrating the *Langevin* equation of motion over time [135, 125], the model reproduces the time evolution of actin filament elongation and severing together with nodes containing myosin and formin. The particles representing the various elements in the simulation domain are in implicit solvent and the stochastic Search-Capture-Pull-Release mechanism is incorporated, as in [14]. According to this mechanism, transient connections between nodes are established when myosin motors associated with one node capture and exert force on actin filaments growing from another node. These connections allow filaments and nodes to coalesce and bundle into a medial ring.

Our computational domain is a cylinder of radius 1.74 μm and length 13 μm, reproducing the dimensions of a fission yeast cell. Nodes are represented as explicit point particles and actin filaments as a series of beads and springs [4]. Nodes are initially distributed according to a Gaussian distribution with the mean centered along the long axis with a standard

deviation of 0.9 μm. Nodes elongate zero, one, or two actin filaments, corresponding to the addition of actin monomers to the barbed ends of the filaments by an attached formin [90]. The number of filaments per node represents the different actin nucleation efficiencies in the simulated conditions and is a varying parameter of the model. Nodes also exert 4 pN tension on actin filaments separated by less than 0.1 μm from the node, representing the power-stroke of myosin heads. Node motion is constrained by a membrane drag ζ= 0.400 pN s/μm, mimicking the cell membrane.

Filaments are represented as semiflexible polymers of beads and springs with persistence length 10 μm [73, 175]. The filaments crosslink one another when closer than 0.1 μm apart by establishing a weak harmonic potential interaction between adjacent beads, which mimics the effect of crosslinking proteins. This harmonic potential has an equilibrium length of 0.03 μm and stiffness of 1 pN/μm to mimic the structural properties of crosslinking protein Ain1 [95]. The effective bead drag is ζ = 0.108 pN s/μm, accounting for cytoplasmic viscosity.

The positions of both filament beads and nodes, $\boldsymbol{r}_i$, are updated at each time step of the simulation following the *Langevin* equation of motion [135, 125] with inertia neglected:

$$\boldsymbol{F}_i = \zeta[\frac{dr_i}{dt}] \tag{4.1}$$

Where $\boldsymbol{F}_i$ is the total force acting on the particle and ζ is the drag coefficient. The force $\boldsymbol{F}_i$ acting on each particle is the 3D vector sum of a deterministic and stochastic force. In the case of filament beads, the deterministic force is the sum of crosslinking, bending, extension, myosin capturing, and myosin pulling interactions. For the nodes, the deterministic force comes from filament elongation and node capturing and pulling. For both filament and node beads, the stochastic force follows the fluctuation dissipation theorem:

$$[\boldsymbol{F}_i^{thermal}\boldsymbol{F}_i^{thermal}]\alpha,\beta = 2(\frac{k_B T\zeta}{dt})\hat{I}\alpha,\beta \tag{4.2}$$

Where $\hat{I}\alpha,\beta$ is the second-order unit tensor [135].

Properties of ring assembly from the simulations are computed as follows. Ring assembly is detected from the model by evaluating positions of the actin filament beads in both the longitudinal and circumferential directions, at the domain middle, between 270-2000 seconds of simulations (see Supplementary Information). The node band width is computed as 2σ of the node's position along the longitudinal domain axis (two times the standard deviation). Node velocity is computed as the average velocity of node particles within 10 s, between 40-100 s of simulations.

Strain name	Genotype	Reference
KV343	h?, cdc12-mGFP::KanR	This study
KV405	h-, cdc12Δ::KanR, cdc12(Nterm)-cdc12(FH1FH2)-cdc12(Cterm)-GFP::ura4+	This study
KV407	h-, cdc12Δ::KanR, cdc12(Nterm)-for3(FH1FH2)-cdc12(Cterm)-GFP::ura4+	This study
KV408	h-, cdc12Δ::KanR, cdc12(Nterm)-bni1(FH1FH2)-cdc12(Cterm)-GFP::ura4+	This study
KV437	h-, cdc12Δ::KanR, cdc12(Nterm)-mdia1(FH1FH2)-cdc12(Cterm)-GFP::ura4+	This study
KV445	h-, cdc12Δ::KanR, cdc12(Nterm)-mdia2(FH1FH2)-cdc12(Cterm)-GFP::ura4+	This study
KV451	h-, cdc12Δ::KanR, cdc12(Nterm)-cyk-1(FH1FH2)-cdc12(Cterm)-GFP::ura4+	This study
KV489	h?, rlc1-tdTomato::natMX6; FY527 cdc12-mGFP::KanR	This study
KV552	h?, sad1-mCherry-NatMX6, cdc12Δ::KanR, cdc12(Nterm)-cyk-1(FH1FH2)-cdc12(Cterm)-GFP::ura4+	This study
KV778	h? rlc1-tdTomato-natMX6, cdc12Δ::KanR, cdc12(Nterm)-cdc12(FH1FH2)-cdc12(Cterm)-GFP::ura4+	This study
KV779	h? rlc1-tdTomato-natMX6, cdc12Δ::KanR, cdc12(Nterm)-bni1(FH1FH2)-cdc12(Cterm)-GFP::ura4+	This study
KV790	h? rlc1-tdTomato-natMX6, cdc12Δ::KanR, cdc12(Nterm)-for3(FH1FH2)-cdc12(Cterm)-GFP::ura4+	This study
KV791	h? rlc1-tdTomato-natMX6, cdc12Δ::KanR, cdc12(Nterm)-mDia1(FH1FH2)-cdc12(Cterm)-GFP::ura4+	This study
KV793	h? rlc1-tdTomato-natMX6, cdc12Δ::KanR, cdc12(Nterm)-mDia2(FH1FH2)-cdc12(Cterm)-GFP::ura4+	This study
KV794	h? rlc1-tdTomato-natMX6, cdc12Δ::KanR, cdc12(Nterm)-CYK1(FH1FH2)-cdc12(Cterm)-GFP::ura4+	This study
KV942	h?, cdc12Δ::KanR, cdc12(Nterm)-bni1(FH1FH2)-cdc12(Cterm)-GFP::ura4+, sad1-tdTomato-natMX6	This study
KV944	h? cdc12Δ::KanR, cdc12(Nterm)-mdia1(FH1FH2)-cdc12(Cterm)-GFP::ura4+, sad1-tdTomato-natMX6	This study
KV948	h? cdc12-mGFP::KanR, sad1-tdTomato-natMX6	This study
KV949	h? cdc12Δ::KanR, cdc12(Nterm)-cdc12(FH1FH2)-cdc12(Cterm)-GFP::ura4+, sad1-tdTomato-natMX68	This study
KV950	h? cdc12Δ::KanR, cdc12(Nterm)-for3(FH1FH2)-cdc12(Cterm)-GFP::ura4+, sad1-tdTomato-natMX6	This study
KV951	h- cdc12Δ::KanR, cdc12(Nterm)-mdia2(FH1FH2)-cdc12(Cterm)-GFP::ura4+, sad1-tdTomato-natMX6	This study

Table 4.2: **Fission yeast strains used in Chapter 4.**

CHAPTER 5

DISCUSSION AND FUTURE DIRECTIONS

5.1 Competitive and cooperative interactions between actin-binding proteins influence their association with F-actin

In accordance with previous work from our lab [27], we have shown that a complex web of competitive and cooperative interactions between ABPs mediates their association with F-actin. In particular, we demonstrated that two fission yeast crosslinking proteins, fimbrin Fim1 and α-actinin Ain1, compete for binding F-actin both *in vivo* and *in vitro*, with Fim1 generally outcompeting Ain1 (Figure 2.1). Fim1 and Ain1 are thought to associate with a similar site on F-actin, which suggests that their competition could occur through a passive mechanism, where Fim1 binds F-actin first to inhibit Ain1's association. Fim1's ability to outcompete Ain1 could also arise from its longer residence time on two-filament F-actin bundles (residence time of 43.4 sec vs. 0.3 sec for Ain1). We investigated whether an ABP's residence time on F-actin could influence its ability to compete by taking advantage of a previously characterized, less dynamic Ain1 mutant [102], Ain(R216E) (residence time of 1.5 sec). Ain1 and Ain1(R216E) compete with Fim1 to a similar degree on two-filament actin bundles *in vitro* (Figure 2.7), but overexpressed Ain1(R216E) is capable of associating with actin patches *in vivo*, while overexpressed Ain1 is not (Figure 2.8). Ain1's short residence time on F-actin bundles could tailor it for its role as the primary contractile ring crosslinking protein in fission yeast cells, as a more dynamic crosslinker is optimal to allow F-actin sliding during ring contraction.

Interestingly, we also discovered that the competitive interaction between Fim1 and Ain1 is altered in the presence of tropomyosin Cdc8, which competes with Fim1 (Figure 2.7; [27]) but cooperates with Ain1 (Figure 2.10). In fact, we demonstrated that Cdc8 significantly enhances the bundling ability of Ain1 (Figures 2.10, 2.12). We suspected that Cdc8 could

increase Ain1-mediated bundling by changing the kinetics of Ain1 binding to F-actin. Indeed, we analyzed the single molecule dynamics of Ain1 on F-actin and observed three-fold more Ain1 binding events on F-actin coated with Cdc8 than on uncoated actin filaments (Figure 2.10E-G). It is well-documented that tropomyosins also exert a change in the persistence length of F-actin that could mediate a conformational change to make F-actin more amenable to Ain1-binding [47, 73]. The stability of bundles could also be increased by Cdc8's change in the persistence length of F-actin.

Finally, we showed that although Fim1 outcompetes both Ain1 and Cdc8 head-to-head, the combination of Ain1 and Cdc8 is capable of inhibiting Fim1's association with F-actin (Figures 2.11, 2.12), which could help explain why little Fim1 localizes to the contractile ring in fission yeast cells. We speculate that competition with Ain1 inhibits Fim1's cooperative binding on F-actin, thus preventing the formation of long stretches of Fim1 that are optimal for displacing Cdc8 [27]. However, several other non-mutually exclusive mechanisms likely contribute to the sorting of Fim1, Ain1, and Cdc8 to the proper F-actin network, including post-translational modifications, mechanical stresses, and diverse actin conformations, all of which are discussed further in sections 2.4 and 3.5. Future work should aim to understand how competitive and cooperative interactions drive ABP sorting to distinct F-actin networks in other cell types.

5.2 Actin assembly factors are also required for ABP sorting in fission yeast

Competition and cooperation between ABPs helps elucidate why proteins such as fimbrin Fim1 and α-actinin Ain1 localize to different actin networks in fission yeast, but are not sufficient to explain why Fim1 is specifically recruited to actin patches, while Cdc8 preferentially associates with the contractile ring. Our longstanding hypothesis is that actin assembly factors generate F-actin with distinct characteristics that are recognized by specific

"upstream" ABPs. These "upstream" ABPs then dictate how "downstream" ABPs access F-actin, thereby initiating a cascade of ABP recruitment that facilitates F-actin network organization and optimizes each network for its cellular role. Thus, we extended our study of the mechanisms that govern ABP sorting by investigating how actin assembly factors might influence the recruitment of the proper subset of ABPs to specific F-actin networks.

We discovered that ABPs fimbrin Fim1 and tropomyosin Cdc8 are recruited to distinct F-actin networks in fission yeast, even though both Fim1 and Cdc8 are capable of associating with both actin patches and the contractile ring. Fim1 preferentially localizes to actin patches, while Cdc8 is targeted to the contractile ring during cytokinesis (Figure 3.1), a process we call ABP "sorting". To understand which components are necessary and sufficient for ABP sorting, we sought to reconstitute this process *in vitro* using purified proteins. Multi-color TIRFM allows us to assemble F-actin with both Arp2/3 complex and formin Cdc12 and analyze how labeled ABPs interact with actin filaments with distinct architectures. Interestingly, we detect no inherent bias of Fim1 or Cdc8 alone for specific actin filaments, as they both associate with Arp2/3 complex- and Cdc12-mediated F-actin *in vitro*. However, when Fim1 and Cdc8 are allowed to compete for binding to F-actin assembled by both Arp2/3 complex and Cdc12, we observe a two-fold increase in the amount of Fim1 on Arp2/3 complex mother filaments and a 3.5-fold increase in the amount of Cdc8 on Cdc12-mediated filaments. Thus, we can reconstitute ABP sorting with just two competing proteins and actin filaments generated by two distinct assembly factors. We suspect that effective sorting of ABPs to diverse F-actin networks requires an initial, inherent bias of specific ABPs for specific F-actin networks, cooperative ABP binding, and competition between ABPs that inhibits their association with the wrong F-actin network. This hypothesis is supported by our ordinary differential equations model, which shows that maximal ABP sorting occurs when all three of these factors are present.

While this work identifies the minimal regime necessary for ABP sorting, the mechanism

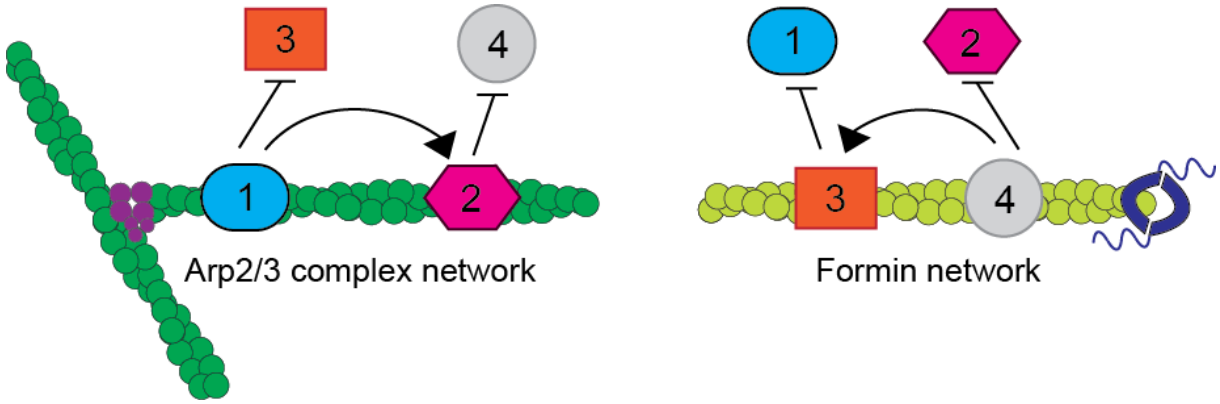

Figure 5.1: **Model of intrinsic mechanisms that guide ABP sorting.** ABP1 (blue) preferentially associates with Arp2/3 complex-mediated actin filaments and recruits ABP1 (pink) but inhibits ABP3 (orange). ABP2 inhibits ABP4 (gray). On the other hand, ABP4 associates with formin-mediated F-actin and inhibits ABP2 but recruits ABP3, which inhibits ABP1.

by which actin assembly factors initiate this sorting is still unclear. We hypothesize that ABPs have preferences for specific F-actin characteristics imparted by different assembly factors, such as architecture and twist. Understanding how particular F-actin attributes impact ABP sorting will require biophysical techniques beyond those discussed throughout this dissertation. For example, optical tweezers could be used to apply a known twist to actin filaments and investigate whether the association of ABPs is affected by changes in the F-actin conformation.

5.3 Formin Cdc12 is tailored for fission yeast cytokinesis

Despite their sequence homology, well-conserved structural properties, and generally similar mechanism of actin assembly, different formin isoforms are utilized to carry out distinct cellular functions. Most organisms express many formin isoforms, and we have previously shown that the biochemical and actin assembly properties of all three fission yeast formins (For3, Fus1, and Cdc12) vary widely [154]. Thus, we hypothesized that a formin's specific actin assembly properties could tailor it for a particular cellular role. To test this idea,

we engineered formin "chimera" fission yeast strains in which the FH1FH2 actin assembly domains of cytokinesis formin Cdc12 were replaced with the FH1FH2 domains from a range of evolutionarily and functionally diverse formins. We discovered that although formin chimeras produce viable cells that divide, formin chimera fission yeast cells exhibit a range of cytokinesis and morphology defects (Figure 4.3). Interestingly, the formin chimeras with nucleation efficiencies most similar to Cdc12 are less defective at cytokinesis than those that are poor nucleators (Figure 4.4). We also tested the effects of formin actin assembly properties on contractile ring assembly directly using a computational model (Figure 4.6). The model reveals that proper contractile ring assembly in fission yeast is more dependent on formin's nucleation efficiency than its F-actin elongation rate, which supports our experimental observations. Thus, cytokinesis in fission yeast is robust, but ideally mediated by a formin with actin assembly properties that are tailored for its specific cellular function.

Future work should investigate how other formins could be optimized for their cellular roles. For example, For3's poor nucleation efficiency could be tailored for generating short actin cables through multiple rounds of asynchronous nucleation and elongation. In fact, it is unclear whether For3 nucleates F-actin in vivo at all, as it could bypass nucleation by elongating existing Arp2/3 complex-mediated filaments in actin patches at cell tips. Additionally, the FH2 domain of *Drosophila* formin Cappuccino contains a long lasso region that decreases its F-actin nucleation and elongation rates [196]. It is possible that this lasso region makes Cappuccino a less potent assembly factor to optimize it for its physiological role of building an actin meshwork in oocytes.

To truly understand how Cdc12 might be tailored to carry out fission yeast cytokinesis, we must first understand how it is regulated and targeted to the cell middle. While many formins are inherently autoinhibited and activated by association with Rho family GTPases, no Rho GTPase regulation has been demonstrated for Cdc12, as mutating the conserved DID and DAD domains responsible for autoinhibition does not alter Cdc12's activity [195]. However,

as the sole cytokinesis formin in fission yeast, Cdc12 must be regulated to generate F-actin specifically during cell division. It is possible that the previously discussed competition for actin monomers or modulation of profilin levels (Section 1.3.1) could limit Cdc12's activity during interphase, but the area of Cdc12 regulation awaits further study.

5.4 Future directions

5.4.1 Fission yeast actin

All of the fission yeast actin-binding proteins (ABPs) used in our *in vitro* reconstitution assays are purified directly from fission yeast or recombinantly expressed and purified from bacteria or insect cells. However, the purified actin used in our *in vitro* assays is purified as has been described from chicken skeletal muscle [165], as attempts at fission yeast actin purification have historically resulted in low yield due to protein degradation [63]. Recently, it has become increasingly apparent that despite their sequence identity, different mammalian actin isoforms exhibit distinct subcellular localizations and functional interactions with myosin [120]. Additionally, budding yeast ABPs have a species-specific preference for actin that results in poor association with actins purified from organisms other than budding yeast. Thus, it follows that fission yeast ABPs could interact differently with fission yeast actin compared to chicken skeletal muscle actin.

To address this potential discrepancy, we are currently involved in a collaboration that aims to purify a stable form of fission yeast actin purified from insect cells for use in future *in vitro* studies of actin dynamics and ABP sorting. Our strategy for avoiding actin degradation involves a single point mutation (Y371H) that improves actin stability throughout purification, and we have introduced this mutation into fission yeast actin *in vivo* to ensure that it does not disrupt normal cell growth and F-actin assembly (Figure 5.2). We observe that fission yeast cells expressing Y371H mutant actin grow and divide at similar rates as

wild-type cells, and the F-actin organization appears to be unaffected by the point mutation. In the future, it will be important to verify that the principles of ABP sorting highlighted in this dissertation hold true when tested using purified fission yeast actin.

5.5 Using mathematical models to understand cytoskeletal self-organization

Computational models have been used in this dissertation to explore parameter space that is impossible to accomplish experimentally (Section 4.3.5) and to provide quantitative support of our theoretical model (Section 3.6.9). In the future, mathematical models will certainly be critical in determining the degree to which each factor involved in ABP sorting (competition between ABPs, conformation of F-actin, post-translational modifications, mechanical stresses on F-actin) drives ABP localization to diverse F-actin networks. It seems likely that we will eventually understand the distinct parameters and F-actin binding kinetics for each ABP, making it possible to completely recapitulate ABP sorting *in silico*. Combined with single molecule biochemistry and live cell imaging, mathematical modeling will be a powerful tool for both describing and predicting the behavior of this complex system of ABP interactions.

5.6 How do the principles of actin cytoskeleton self-organization apply to other organisms?

We are only beginning to scratch the surface in elucidating the principles that govern ABP sorting in fission yeast. Even so, understanding how multiple distinct F-actin networks are simultaneously built and maintained in a single cell is relatively easy in fission yeast, as actin assembly factors impart F-actin with a specific identity that is maintained throughout the filament's lifetime. On the other hand, the actin cytoskeleton in higher eukaryotes is

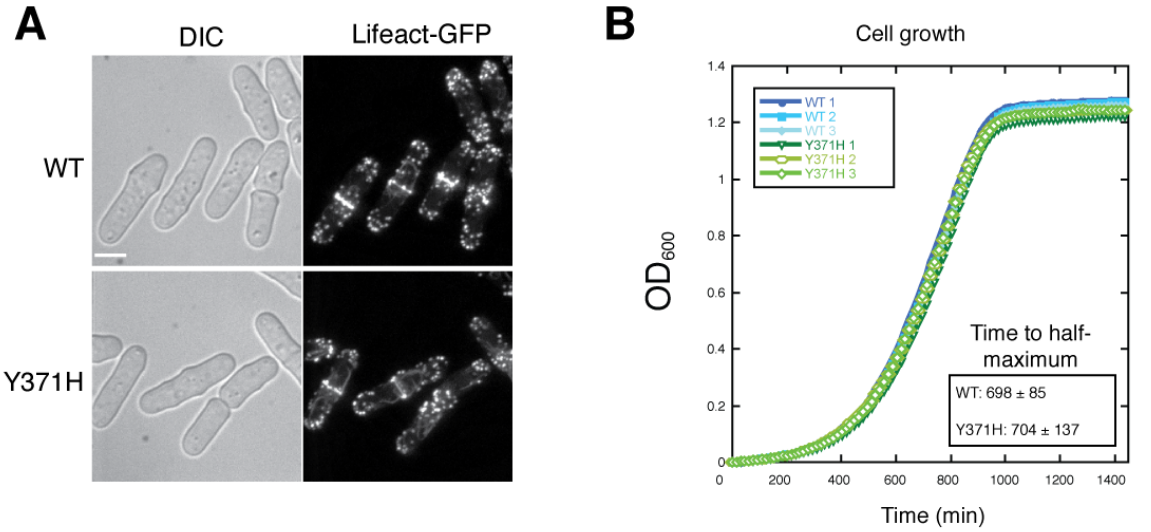

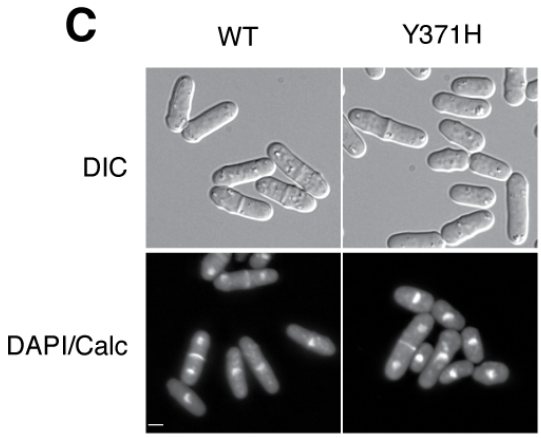

D

	WT	Y371H
Cells with one nucleus (%)	77.3 ± 1.7	78.6 ± 1.8*
Cells with two nuclei (%)	22.7 ± 1.7	20.8 ± 1.9**
Cells with >two nuclei (%)	0	.60 ± .06***
Cells with normal septa (%)	100	100
Cells with abnormal septa (%)	0	0

Figure 5.2: **Growth characteristics of fission yeast cells containing actin mutant Y371H are similar to wild-type cells.** **(A)** Fluorescence micrographs of wild-type (WT) and actin mutant Y371H fission yeast cells showing morphology (DIC) and organization of actin networks (Lifeact-GFP). Scale bar, 5 μm. **(B)** Growth curve of WT and Y371H actin mutant strains. Three replicates of each strain are shown. Average time to half-maximum OD_{600} of each strain was calculated from 15 replicates each. For the average time to half-maximums, a two-tailed t-test for data sets with unequal variance yielded a p-value of 0.87. **(C)** Fluorescence micrographs of WT and Y371H actin mutant cells including DIC (morphology) and methanol fixed cells stained with DAPI (nuclei) and Calcofluor (septa). Scale bar, 5 μm. **(D)** Table of quantification of cells shown in **(C)**. Percentage of cells with one, two, or greater than two nuclei as well as the percentage of cells exhibiting normal and abnormal (misplaced, unusually broad, or misshapen) septa are shown. Two replicates were analyzed, n$>$ 300 for each replicate. To compare WT and Y371H, two-tailed t-tests for data sets with unequal variance were conducted, yielding p-values of: *p-value=0.66, **p-value=0.53, ***p-value=0.061.

infinitely more complex, as they express multiple isoforms of actin and hundreds of ABPs and build ~20 different types of actin networks. Additionally, the delineation between these diverse networks is often much less obvious. For example, the convergent elongation model of filopodia formation posits that filopodia are generated from a reorganization of the dendritic network nucleated by Arp2/3 complex in the lamellipodia. This lamellipodia-to-filopodia transition is driven by barbed end elongation factors such as formins and/or Ena/VASP that cluster dendritic barbed ends, resulting in their convergence, bundling by fascin, and eventual elongation. Thus, F-actin networks in higher eukaryotes can be intertwined both in identity and in space, complicating our understanding of how different ABPs could be targeted to these contiguous F-actin networks. Nonetheless, it is becoming clear that the principles of ABP sorting described above for fission yeast hold true in other organisms. Recently, it was shown that tropomyosin and α-actinin compete for binding F-actin in stress fibers in MDCK cells, and tropomyosin shields F-actin from cofilin-mediated severing as it does in fission yeast [85].

Not surprisingly, the complexity of the actin cytoskeleton in higher eukaryotes also heightens the complexity of actin cytoskeleton self-organization beyond that discussed for fission yeast throughout this dissertation. Recently, the topic of actin in the nucleus has been revitalized. A variety of functions have been uncovered for nuclear actin, and it is now widely accepted that transport of actin in and out of the nucleus is highly regulated [84]. Actin affects protein expression by regulating the activity of RNA polymerase and specific transcription factors and has also been implicated to have a role in chromatin organization and movement [84]. Thus, an obvious question is how disruption of cytoplasmic actin might affect the activity, concentration, or import of nuclear actin. For example, when we underexpress or overexpress cytoplasmic actin (Section 1.3.1), could the resulting phenotype be influenced by a change in nuclear actin? We have recently learned to think more globally about the effects of genetic perturbations, as the changes in fission yeast actin patch dynamics upon

deletion of crosslinker fimbrin Fim1 are not solely consequence of the absence of Fim1, but rather are at least partially explained by the mislocalization of tropomyosin Cdc8 to actin patches in the absence of its competitor. There is obviously still much to be learned about the role of actin in the nucleus, and future studies involving disruption of the cytoplasmic actin pool should certainly consider how the resulting changes might be affected by nuclear actin.

As more complex organisms build more numerous and diverse F-actin networks, they naturally also utilize more numerous and diverse actin assembly factors. In addition to formins and Arp2/3 complex, higher eukaryotes express multiple WH2 domain-containing nucleators, including Ena/VASP. These distinct F-actin nucleation and elongation factors generate actin networks with different architectures and dynamics and stimulate actin assembly by different rates, characteristics which almost certainly contribute to ABP sorting in these organisms. Indeed, an interesting question is how differences in the rates of F-actin network assembly might control competition for G-actin and/or ABP sorting. Are F-actin networks that assemble faster and utilize more G-actin more likely to dictate how ABPs sort by recruiting the most "upstream" gatekeeper ABPs that initiate the cascade of "downstream" ABP localization? Future work should aim to understand if the dynamics of F-actin network assembly contribute to ABP sorting.

Finally, the complex actin networks in higher eukaryotes are also regulated by complicated signaling cascades that activate specific assembly factors at the correct time and place. Phosphoinositides such as PIP2 have recently been shown to modulate the activity of many key actin regulatory factors. PIP2 could potentially be involved in multiple pathways for generating F-actin, as it stimulates the activity of WASP family activators of Arp2/3 complex, dissociates capping proteins such as gelsolin and CapZ from F-actin barbed ends, and inhibits cofilin-mediated severing [194]. Additionally, several F-actin crosslinking proteins, including α-actinin and filamin, are regulated by PIP2, as well as some membrane attach-

ment proteins [194]. To consider the role of extrinsic factors such as PIP2 signalling in actin cytoskeleton self-organization and ABP sorting, the next step should include supported lipid bilayers as a foundation for our reconstitution experiments [169] to serve as a proxy for the plasma membrane. One interesting consequence of the reconstitution of signalling pathways using lipid bilayers is the clustering of multivalent proteins through a process known as a "phase separation." While the functional ramifications of phase separated protein clusters are not yet well understood, it is clear that clustering of multivalent membrane proteins is important for regulating many signalling pathways. More specifically, it was recently discovered that increasing the density of WASP proteins via phase separation generates a non-linear increase in F-actin assembly [38]. Thus, future studies of F-actin organization in higher eukaryotes must expand to incorporate extrinsic factors that likely play important roles in actin cytoskeleton regulation.

References

[1] Barbara Addario, Linda Sandblad, Karina Persson, and Lars Backman. Characterisation of schizosaccharomyces pombe α-actinin. 4:e1858.

[2] Rashmi Ahuja, Roser Pinyol, Nicole Reichenbach, Laura Custer, John Klingensmith, Michael M. Kessels, and Britta Qualmann. Cordon-bleu is an actin nucleation factor and controls neuronal morphology. 131(2):337–350.

[3] Arthur S. Alberts. Identification of a carboxyl-terminal diaphanous-related formin homology protein autoregulatory domain. 276(4):2824–2830.

[4] Jonathan B. Alberts. Biophysically realistic filament bending dynamics in agent-based biological simulation. 4(3):e4748.

[5] Salvatore L. Alioto, Mikael V. Garabedian, Danielle R. Bellavance, and Bruce L. Goode. Tropomyosin and profilin cooperate to promote formin-mediated actin nucleation and drive yeast actin cable assembly. 26(23):3230–3237.

[6] R. Arai, K. Nakano, and I. Mabuchi. Subcellular localization and possible function of actin, tropomyosin and actin-related protein 3 (arp3) in the fission yeast schizosaccharomyces pombe. 76(4):288–295.

[7] Ritsuko Arai and Issei Mabuchi. F-actin ring formation and the role of f-actin cables in the fission yeast schizosaccharomyces pombe. 115:887–898.

[8] D. Axelrod, N. L. Thompson, and T. P. Burghardt. Total internal inflection fluorescent microscopy. 129:19–28.

[9] M. K. Balasubramanian, D. McCollum, L. Chang, K. C. Wong, N. I. Naqvi, X. He, S. Sazer, and K. L. Gould. Isolation and characterization of new fission yeast cytokinesis mutants. 149(3):1265–1275.

[10] Mohan K. Balasubramanian, Erfei Bi, and Michael Glotzer. Comparative analysis of cytokinesis in budding yeast, fission yeast and animal cells. 14(18):R806–818.

[11] James R. Bartles. Parallel actin bundles and their multiple actin-bundling proteins. 12(1):72–78.

[12] Francesca Bartolini, James B. Moseley, Jan Schmoranzer, Lynne Cassimeris, Bruce L. Goode, and Gregg G. Gundersen. The formin mDia2 stabilizes microtubules independently of its actin nucleation activity. 181(3):523–536.

[13] Julien Berro, Vladimir Sirotkin, and Thomas D. Pollard. Mathematical modeling of endocytic actin patch kinetics in fission yeast: disassembly requires release of actin filament fragments. 21(16):2905–2915.

[14] Tamara C. Bidone, Haosu Tang, and Dimitrios Vavylonis. Dynamic network morphology and tension buildup in a 3d model of cytokinetic ring assembly. 107(11):2618–2628.

[15] L. Blanchoin, T. D. Pollard, and S. E. Hitchcock-DeGregori. Inhibition of the arp2/3 complex-nucleated actin polymerization and branch formation by tropomyosin. 11(16):1300–1304.

[16] Jeffrey P. Bombardier, Julian A. Eskin, Richa Jaiswal, Ivan R. Corrêa, Ming-Qun Xu, Bruce L. Goode, and Jeff Gelles. Single-molecule visualization of a formin-capping protein 'decision complex' at the actin filament barbed end. 6.

[17] Dennis Breitsprecher and Bruce L. Goode. Formins at a glance. 126(1):1–7.

[18] Dennis Breitsprecher, Richa Jaiswal, Jeffrey P. Bombardier, Christopher J. Gould, Jeff Gelles, and Bruce L. Goode. Rocket launcher mechanism of collaborative actin assembly defined by single-molecule imaging. 336(6085):1164–1168.

[19] Thomas A. Burke, Jenna R. Christensen, Elisabeth Barone, Cristian Suarez, Vladimir Sirotkin, and David R. Kovar. Homeostatic actin cytoskeleton networks are regulated by assembly factor competition for monomers. 24(5):579–585.

[20] J. Bähler, J. Q. Wu, M. S. Longtine, N. G. Shah, A. McKenzie, A. B. Steever, A. Wach, P. Philippsen, and J. R. Pringle. Heterologous modules for efficient and versatile PCR-based gene targeting in schizosaccharomyces pombe. 14(10):943–951.

[21] L. A. Cameron, M. J. Footer, A. van Oudenaarden, and J. A. Theriot. Motility of ActA protein-coated microspheres driven by actin polymerization. 96(9):4908–4913.

[22] M. F. Carlier and D. Pantaloni. Direct evidence for ADP-inorganic phosphate-f-actin as the major intermediate in ATP-actin polymerization. rate of dissociation of inorganic phosphate from actin filaments. 25(24):7789–7792.

[23] Dimitra Chalkia, Nikolas Nikolaidis, Wojciech Makalowski, Jan Klein, and Masatoshi Nei. Origins and evolution of the formin multigene family that is involved in the formation of actin filaments. 25(12):2717–2733.

[24] F. Chang, D. Drubin, and P. Nurse. cdc12p, a protein required for cytokinesis in fission yeast, is a component of the cell division ring and interacts with profilin. 137(1):169–182.

[25] F. Chang, A. Woollard, and P. Nurse. Isolation and characterization of fission yeast mutants defective in the assembly and placement of the contractile actin ring. 109 (Pt 1):131–142.

[26] Qian Chen and Thomas D. Pollard. Actin filament severing by cofilin dismantles actin patches and produces mother filaments for new patches. 23(13):1154–1162.

[27] Jenna R. Christensen, Glen M. Hocky, Kaitlin E. Homa, Alisha N. Morganthaler, Sarah E. Hitchcock-DeGregori, Gregory A. Voth, and David R. Kovar. Competition between tropomyosin, fimbrin, and ADF/cofilin drives their sorting to distinct actin filament networks. 6.

[28] Joseph E. Clayton, Matthew R. Sammons, Benjamin C. Stark, Alex R. Hodges, and Matthew Lord. Differential regulation of unconventional fission yeast myosins via the actin track. 20(16):1423–1431.

[29] Valerie C. Coffman, Aaron H. Nile, I.-Ju Lee, Huayang Liu, and Jian-Qiu Wu. Roles of formin nodes and myosin motor activity in mid1p-dependent contractile-ring assembly during fission yeast cytokinesis. 20(24):5195–5210.

[30] Valerie C. Coffman, Jennifer A. Sees, David R. Kovar, and Jian-Qiu Wu. The formins cdc12 and for3 cooperate during contractile ring assembly in cytokinesis. 203(1):101–114.

[31] John A. Cooper, E. Loren Buhle, Simon B. Walker, Tian Y. Tsong, and Thomas D. Pollard. Kinetic evidence for a monomer activation step in actin polymerization. 22(9):2193–2202.

[32] A. T. Coulton, D. A. East, A. Galinska-Rakoczy, W. Lehman, and D. P. Mulvihill. The recruitment of acetylated and unacetylated tropomyosin to distinct actin polymers permits the discrete regulation of specific myosins in fission yeast. 123(19):3235–3243.

[33] N. Courtemanche, J. Y. Lee, T. D. Pollard, and E. C. Greene. Tension modulates actin filament polymerization mediated by formin and profilin. 110(24):9752–9757.

[34] Naomi Courtemanche. Mechanisms of formin-mediated actin assembly and dynamics.

[35] S. Cranz-Mileva, B. MacTaggart, J. Russell, and S. E. Hitchcock-DeGregori. Evolutionarily conserved sites in yeast tropomyosin function in cell polarity, transport and contractile ring formation. 4(8):1040–1051.

[36] Mark J. Dayel and R. Dyche Mullins. Activation of arp2/3 complex: addition of the first subunit of the new filament by a WASP protein triggers rapid ATP hydrolysis on arp2. 2(4):E91.

[37] Vera DesMarais, Ilia Ichetovkin, John Condeelis, and Sarah E. Hitchcock-DeGregori. Spatial regulation of actin dynamics: a tropomyosin-free, actin-rich compartment at the leading edge. 115:4649–4660.

[38] Jonathon A. Ditlev, Paul J. Michalski, Greg Huber, Gonzalo M. Rivera, William A. Mohler, Leslie M. Loew, and Bruce J. Mayer. Stoichiometry of nck-dependent actin polymerization in living cells. 197(5):643–658.

[39] Marc Edwards, Adam Zwolak, Dorothy A. Schafer, David Sept, Roberto Dominguez, and John A. Cooper. Capping protein regulators fine-tune actin assembly dynamics. 15(10):677–689.

[40] C. Egile, T. P. Loisel, V. Laurent, R. Li, D. Pantaloni, P. J. Sansonetti, and M. F. Carlier. Activation of the CDC42 effector n-WASP by the shigella flexneri IcsA protein promotes actin nucleation by arp2/3 complex and bacterial actin-based motility. 146(6):1319–1332.

[41] W. Austin Elam, Hyeran Kang, and Enrique M. De la Cruz. Biophysics of actin filament severing by cofilin. 587(8):1215–1219.

[42] Obidimma C. Ezezika, Noah S. Younger, Jia Lu, Donald A. Kaiser, Zachary A. Corbin, Bradley J. Nolen, David R. Kovar, and Thomas D. Pollard. Incompatibility with formin cdc12p prevents human profilin from substituting for fission yeast profilin. 284(4):2088–2097.

[43] B. Feierbach and F. Chang. Roles of the fission yeast formin for3p in cell polarity, actin cable formation and symmetric cell division. 11(21):1656–1665.

[44] Yunfeng Feng, Hai Ngu, Shannon K. Alford, Michael Ward, Frank Yin, and Gregory D. Longmore. α-actinin1 and 4 tyrosine phosphorylation is critical for stress fiber establishment, maintenance and focal adhesion maturation. 319(8):1124–1135.

[45] Kenneth N. Fish. Total internal reflection fluorescence (TIRF) microscopy. 0 12:Unit12.18.

[46] Carl Frieden and Dean W. Goddette. Polymerization of actin and actin-like systems: evaluation of the time course of polymerization in relation to the mechanism. 22(25):5836–5843.

[47] Satoru Fujime and Shin'ichi Ishiwata. Dynamic study of f-actin by quasielastic scattering of laser light. 62(1):251–265.

[48] Yannick Gachet and Jeremy S. Hyams. Endocytosis in fission yeast is spatially associated with the actin cytoskeleton during polarised cell growth and cytokinesis. 118:4231–4242.

[49] Vitold E. Galkin, Albina Orlova, Olga Cherepanova, Marie-Christine Lebart, and Edward H. Egelman. High-resolution cryo-EM structure of the f-actin-fimbrin/plastin ABD2 complex. 105(5):1494–1498.

[50] Vitold E. Galkin, Albina Orlova, Anita Salmazo, Kristina Djinovic-Carugo, and Edward H. Egelman. Opening of tandem calponin homology domains regulates their affinity for f-actin. 17(5):614–616.

[51] Meghal Gandhi, Benjamin A. Smith, Miia Bovellan, Ville Paavilainen, Karen Daugherty-Clarke, Jeff Gelles, Pekka Lappalainen, and Bruce L. Goode. GMF is a cofilin homolog that binds arp2/3 complex to stimulate filament debranching and inhibit actin nucleation. 20(9):861–867.

[52] Lina Gao and Anthony Bretscher. Analysis of unregulated formin activity reveals how yeast can balance f-actin assembly between different microfilament-based organizations. 19(4):1474–1484.

[53] M.A. Geeves. 4.13 thin filament regulation. In *Comprehensive Biophysics*, pages 251–267. Elsevier.

[54] F. Gittes. Flexural rigidity of microtubules and actin filaments measured from thermal fluctuations in shape. 120(4):923–934.

[55] Erin D. Goley, Stacia E. Rodenbusch, Adam C. Martin, and Matthew D. Welch. Critical conformational changes in the arp2/3 complex are induced by nucleotide and nucleation promoting factor. 16(2):269–279.

[56] Bruce L. Goode and Michael J. Eck. Mechanism and function of formins in the control of actin assembly. 76(1):593–627.

[57] Brian R. Graziano, Amy Grace DuPage, Alphee Michelot, Dennis Breitsprecher, James B. Moseley, Isabelle Sagot, Laurent Blanchoin, and Bruce L. Goode. Mechanism and cellular function of bud6 as an actin nucleation-promoting factor. 22(21):4016–4028.

[58] Peter W. Gunning, Umesh Ghoshdastider, Shane Whitaker, David Popp, and Robert C. Robinson. The evolution of compositionally and functionally distinct actin filaments. 128(11):2009–2019.

[59] Pinar S. Gurel, Mu A, Bingqian Guo, Rui Shu, Dale F. Mierke, and Henry N. Higgs. Assembly and turnover of short actin filaments by the formin INF2 and profilin. 290(37):22494–22506.

[60] A. Hall. Rho GTPases and the actin cytoskeleton. 279(5350):509–514.

[61] J. Hanson and J. Lowy. THE STRUCTURE OF ACTIN FILAMENTS AND THE ORIGIN OF THE AXIAL PERIODICITY IN THE i-SUBSTANCE OF VERTEBRATE STRIATED MUSCLE. 160:449–460.

[62] Elizabeth S. Harris, Isabelle Rouiller, Dorit Hanein, and Henry N. Higgs. Mechanistic differences in actin bundling activity of two mammalian formins, FRL1 and mDia2. 281(20):14383–14392.

[63] Tomoyuki Hatano, Salvatore Alioto, Emanuele Roscioli, Saravanan Palani, Scott T. Clarke, Anton Kamnev, Juan Ramon Hernandez-Fernaud, Lavanya Sivashanmugam,

Bernardo Chapa-Y-Lazo, Alexandra M. E. Jones, Robert C. Robinson, Karuna Sampath, Masanori Mishima, Andrew D. McAinsh, Bruce L. Goode, and Mohan K. Balasubramanian. Rapid production of pure recombinant actin isoforms in pichia pastoris. 131(8).

[64] Kimihide Hayakawa, Hitoshi Tatsumi, and Masahiro Sokabe. Actin filaments function as a tension sensor by tension-dependent binding of cofilin to the filament. 195(5):721–727.

[65] Jessica L. Henty-Ridilla, Aneliya Rankova, Julian A. Eskin, Katelyn Kenny, and Bruce L. Goode. Accelerated actin filament polymerization from microtubule plus-ends. 352(6288):1004–1009.

[66] Henry N. Higgs and Kevin J. Peterson. Phylogenetic analysis of the formin homology 2 domain. 16(1):1–13.

[67] D. A. Holtzman, K. F. Wertman, and D. G. Drubin. Mapping actin surfaces required for functional interactions in vivo. 126(2):423–432.

[68] J. E. Honts, T. S. Sandrock, S. M. Brower, J. L. O'Dell, and A. E. Adams. Actin mutations that show suppression with fimbrin mutations identify a likely fimbrin-binding site on actin. 126(2):413–422.

[69] Pirta Hotulainen and Pekka Lappalainen. Stress fibers are generated by two distinct actin assembly mechanisms in motile cells. 173(3):383–394.

[70] Jennifer Y. Hsiao, Lauren M. Goins, Natalie A. Petek, and R. Dyche Mullins. Arp2/3 complex and cofilin modulate binding of tropomyosin to branched actin networks. 25(12):1573–1582.

[71] Junqi Huang, Yinyi Huang, Haochen Yu, Dhivya Subramanian, Anup Padmanabhan, Rahul Thadani, Yaqiong Tao, Xie Tang, Roland Wedlich-Soldner, and Mohan K. Balasubramanian. Nonmedially assembled f-actin cables incorporate into the actomyosin ring in fission yeast. 199(5):831–847.

[72] Yinyi Huang, Hongyan Yan, and Mohan K. Balasubramanian. Assembly of normal actomyosin rings in the absence of mid1p and cortical nodes in fission yeast. 183(6):979–988.

[73] H. Isambert, P. Venier, A. C. Maggs, A. Fattoum, R. Kassab, D. Pantaloni, and M. F. Carlier. Flexibility of actin filaments derived from thermal fluctuations. effect of bound nucleotide, phalloidin, and muscle regulatory proteins. 270(19):11437–11444.

[74] Matthew Johnson, Daniel A. East, and Daniel P. Mulvihill. Formins determine the functional properties of actin filaments in yeast. 24(13):1525–1530.

[75] Mini Jose, Sylvain Tollis, Deepak Nair, Romain Mitteau, Christophe Velours, Aurelie Massoni-Laporte, Anne Royou, Jean-Baptiste Sibarita, and Derek McCusker. A quantitative imaging-based screen reveals the exocyst as a network hub connecting endocytosis and exocytosis. 26(13):2519–2534.

[76] Antoine Jégou, Marie-France Carlier, and Guillaume Romet-Lemonne. Formin mDia1 senses and generates mechanical forces on actin filaments. 4:1883.

[77] Antoine Jégou and Guillaume Romet-Lemonne. Single filaments to reveal the multiple flavors of actin. 110(10):2138–2146.

[78] D. A. Kaiser, V. K. Vinson, D. B. Murphy, and T. D. Pollard. Profilin is predominantly associated with monomeric actin in acanthamoeba. 112 (Pt 21):3779–3790.

[79] Tomoko Kamasaki, Ritsuko Arai, Masako Osumi, and Issei Mabuchi. Directionality of f-actin cables changes during the fission yeast cell cycle. 7(9):916–917.

[80] Tomoko Kamasaki, Masako Osumi, and Issei Mabuchi. Three-dimensional arrangement of f-actin in the contractile ring of fission yeast. 178(5):765–771.

[81] Hyeran Kang, Michael J. Bradley, Brannon R. McCullough, Anaëlle Pierre, Elena E. Grintsevich, Emil Reisler, and Enrique M. De La Cruz. Identification of cation-binding sites on actin that drive polymerization and modulate bending stiffness. 109(42):16923–16927.

[82] Eric Karsenti. Self-organization in cell biology: a brief history. 9(3):255–262.

[83] J. B. Keeney and J. D. Boeke. Efficient targeted integration at leu1-32 and ura4-294 in schizosaccharomyces pombe. 136(3):849–856.

[84] Daniel J. Kelpsch and Tina L. Tootle. Nuclear actin: From discovery to function. 301(12):1999–2013.

[85] James Peter Kemp and William M. Brieher. The actin filament bundling protein α-actinin-4 actually suppresses actin stress fibers by permitting actin turnover. page jbc.RA118.004345.

[86] Arminja N. Kettenbach, Lin Deng, Youjun Wu, Suzanne Baldissard, Mark E. Adamo, Scott A. Gerber, and James B. Moseley. Quantitative phosphoproteomics reveals pathways for coordination of cell growth and division by the conserved fission yeast kinase pom1. 14(5):1275–1287.

[87] Seema Khurana and Sudeep P. George. The role of actin bundling proteins in the assembly of filopodia in epithelial cells. 5(5):409–420.

[88] Taekyung Kim, John A. Cooper, and David Sept. The interaction of capping protein with the barbed end of the actin filament. 404(5):794–802.

[89] David R. Kovar, Elizabeth S. Harris, Rachel Mahaffy, Henry N. Higgs, and Thomas D. Pollard. Control of the assembly of ATP- and ADP-actin by formins and profilin. 124(2):423–435.

[90] David R. Kovar, Jeffrey R. Kuhn, Andrea L. Tichy, and Thomas D. Pollard. The fission yeast cytokinesis formin cdc12p is a barbed end actin filament capping protein gated by profilin. 161(5):875–887.

[91] David R. Kovar, Vladimir Sirotkin, and Matthew Lord. Three's company: the fission yeast actin cytoskeleton. 21(3):177–187.

[92] Shusaku Kurisu and Tadaomi Takenawa. The WASP and WAVE family proteins. 10(6):226.

[93] D. J. Kushner. Self-assembly of biological structures. 33(2):302–345.

[94] Damien Laporte, Valerie C. Coffman, I.-Ju Lee, and Jian-Qiu Wu. Assembly and architecture of precursor nodes during fission yeast cytokinesis. 192(6):1005–1021.

[95] Damien Laporte, Nikola Ojkic, Dimitrios Vavylonis, and Jian-Qiu Wu. α-actinin and fimbrin cooperate with myosin II to organize actomyosin bundles during contractile-ring assembly. 23(16):3094–3110.

[96] Shimin Le, Xian Hu, Mingxi Yao, Hu Chen, Miao Yu, Xiaochun Xu, Naotaka Nakazawa, Felix M. Margadant, Michael P. Sheetz, and Jie Yan. Mechanotransmission and mechanosensing of human alpha-actinin 1. 21(10):2714–2723.

[97] I.-Ju Lee, Valerie C. Coffman, and Jian-Qiu Wu. Contractile-ring assembly in fission yeast cytokinesis: Recent advances and new perspectives. 69(10):751–763.

[98] W. L. Lee, M. Bezanilla, and T. D. Pollard. Fission yeast myosin-i, myo1p, stimulates actin assembly by arp2/3 complex and shares functions with WASp. 151(4):789–800.

[99] W. Lehman, R. Craig, and P. Vibert. Ca(2+)-induced tropomyosin movement in limulus thin filaments revealed by three-dimensional reconstruction. 368(6466):65–67.

[100] Daisy W. Leung and Michael K. Rosen. The nucleotide switch in cdc42 modulates coupling between the GTPase-binding and allosteric equilibria of wiskott-aldrich syndrome protein. 102(16):5685–5690.

[101] Fang Li and Henry N. Higgs. The mouse formin mDia1 is a potent actin nucleation factor regulated by autoinhibition. 13(15):1335–1340.

[102] Yujie Li, Jenna R. Christensen, Kaitlin E. Homa, Glen M. Hocky, Alice Fok, Jennifer A. Sees, Gregory A. Voth, and David R. Kovar. The f-actin bundler α-actinin ain1 is tailored for ring assembly and constriction during cytokinesis in fission yeast. 27(11):1821–1833.

[103] T. P. Loisel, R. Boujemaa, D. Pantaloni, and M. F. Carlier. Reconstitution of actin-based motility of listeria and shigella using pure proteins. 401(6753):613–616.

[104] Alexis J. Lomakin, Kun-Chun Lee, Sangyoon J. Han, Duyen A. Bui, Michael Davidson, Alex Mogilner, and Gaudenz Danuser. Competition for actin between two distinct f-actin networks defines a bistable switch for cell polarization. 17(11):1435–1445.

[105] Campion K. P. Loong, Huan-Xiang Zhou, and P. Bryant Chase. Persistence length of human cardiac α-tropomyosin measured by single molecule direct probe microscopy. 7(6):e39676.

[106] J. B. Marchand, D. A. Kaiser, T. D. Pollard, and H. N. Higgs. Interaction of WASP/scar proteins with actin and vertebrate arp2/3 complex. 3(1):76–82.

[107] Sophie G. Martin and Fred Chang. Dynamics of the formin for3p in actin cable assembly. 16(12):1161–1170.

[108] P. Matsudaira. Modular organization of actin crosslinking proteins. 16(3):87–92.

[109] A. McGough, B. Pope, W. Chiu, and A. Weeds. Cofilin changes the twist of f-actin: implications for actin filament dynamics and cellular function. 138(4):771–781.

[110] A. McGough, M. Way, and D. DeRosier. Determination of the alpha-actinin-binding site on actin filaments by cryoelectron microscopy and image analysis. 126(2):433–443.

[111] Yansong Miao, Xuemei Han, Liangzhen Zheng, Ying Xie, Yuguang Mu, John R. Yates, and David G. Drubin. Fimbrin phosphorylation by metaphase cdk1 regulates actin cable dynamics in budding yeast. 7:11265.

[112] Yansong Miao, Catherine C. L. Wong, Vito Mennella, Alphée Michelot, David A. Agard, Liam J. Holt, John R. Yates, and David G. Drubin. Cell-cycle regulation of formin-mediated actin cable assembly. 110(47):E4446–4455.

[113] Alphée Michelot, Michael Costanzo, Ali Sarkeshik, Charles Boone, John R. Yates, and David G. Drubin. Reconstitution and protein composition analysis of endocytic actin patches. 20(21):1890–1899.

[114] Alphée Michelot and David G. Drubin. Building distinct actin filament networks in a common cytoplasm. 21(14):R560–R569.

[115] Tom Misteli. The concept of self-organization in cellular architecture. 155(2):181–186.

[116] Hiroaki Mizuno and Naoki Watanabe. mDia1 and formins: screw cap of the actin filament. 8:95–102.

[117] Rikuri Morita, Masak Takaine, Osamu Numata, and Kentaro Nakano. Molecular dissection of the actin-binding ability of the fission yeast α-actinin, ain1, in vitro and in vivo. 162(2):93–102.

[118] James B. Moseley and Bruce L. Goode. Differential activities and regulation of saccharomyces cerevisiae formin proteins bni1 and bnr1 by bud6. 280(30):28023–28033.

[119] R. D. Mullins, J. A. Heuser, and T. D. Pollard. The interaction of arp2/3 complex with actin: nucleation, high affinity pointed end capping, and formation of branching networks of filaments. 95(11):6181–6186.

[120] Mirco Müller, Ralph P. Diensthuber, Igor Chizhov, Peter Claus, Sarah M. Heissler, Matthias Preller, Manuel H. Taft, and Dietmar J. Manstein. Distinct functional interactions between actin isoforms and nonsarcomeric myosins. 8(7):e70636.

[121] K. Nakano, K. Satoh, A. Morimatsu, M. Ohnuma, and I. Mabuchi. Interactions among a fimbrin, a capping protein, and an actin-depolymerizing factor in organization of the fission yeast actin cytoskeleton. 12(11):3515–3526.

[122] Kentaro Nakano, Jun Imai, Ritsuko Arai, Akio Toh-E, Yasushi Matsui, and Issei Mabuchi. The small GTPase rho3 and the diaphanous/formin for3 function in polarized cell growth in fission yeast. 115:4629–4639.

[123] Kentaro Nakano and Issei Mabuchi. Actin-depolymerizing protein adf1 is required for formation and maintenance of the contractile ring during cytokinesis in fission yeast. 17(4):1933–1945.

[124] Y. Namba, M. Ito, Y. Zu, K. Shigesada, and K. Maruyama. Human t cell l-plastin bundles actin filaments in a calcium-dependent manner. 112(4):503–507.

[125] Francois Nedelec and Dietrich Foethke. Collective langevin dynamics of flexible cytoskeletal fibers. 9(11):427–427.

[126] Erin M. Neidt, Colleen T. Skau, and David R. Kovar. The cytokinesis formins from the nematode worm and fission yeast differentially mediate actin filament assembly. 283(35):23872–23883.

[127] Kien Xuan Ngo, Noriyuki Kodera, Eisaku Katayama, Toshio Ando, and Taro QP Uyeda. Cofilin-induced unidirectional cooperative conformational changes in actin filaments revealed by high-speed atomic force microscopy. 4.

[128] B. J. Nolen, N. Tomasevic, A. Russell, D. W. Pierce, Z. Jia, C. D. McCormick, J. Hartman, R. Sakowicz, and T. D. Pollard. Characterization of two classes of small molecule inhibitors of arp2/3 complex. 460(7258):1031–1034.

[129] Toshiro Oda and Yuichiro Maéda. Multiple conformations of f-actin. 18(7):761–767.

[130] Kyoko Okada, Francesca Bartolini, Alexandra M. Deaconescu, James B. Moseley, Zvonimir Dogic, Nikolaus Grigorieff, Gregg G. Gundersen, and Bruce L. Goode. Adenomatous polyposis coli protein nucleates actin assembly and synergizes with the formin mDia1. 189(7):1087–1096.

[131] Shoichiro Ono and Kanako Ono. Tropomyosin inhibits ADF/cofilin-dependent actin filament dynamics. 156(6):1065–1076.

[132] Takanori Otomo, Chinatsu Otomo, Diana R. Tomchick, Mischa Machius, and Michael K. Rosen. Structural basis of rho GTPase-mediated activation of the formin mDia1. 18(3):273–281.

[133] Takanori Otomo, Diana R. Tomchick, Chinatsu Otomo, Mischa Machius, and Michael K. Rosen. Crystal structure of the formin mDia1 in autoinhibited conformation. 5(9):e12896.

[134] Gábor Papp, Beáta Bugyi, Zoltán Ujfalusi, Szilvia Barkó, Gábor Hild, Béla Somogyi, and Miklós Nyitrai. Conformational changes in actin filaments induced by formin binding to the barbed end. 91(7):2564–2572.

[135] M. Pasquali, V. Shankar, and D. C. Morse. Viscoelasticity of dilute solutions of semiflexible polymers. 64(2):020802.

[136] Aditya S. Paul, Aditya Paul, Thomas D. Pollard, and Thomas Pollard. The role of the FH1 domain and profilin in formin-mediated actin-filament elongation and nucleation. 18(1):9–19.

[137] Aditya S. Paul and Thomas D. Pollard. Review of the mechanism of processive actin filament elongation by formins. 66(8):606–617.

[138] T. D. Pollard. Rate constants for the reactions of ATP- and ADP-actin with the ends of actin filaments. 103(6):2747–2754.

[139] Thomas D. Pollard. Actin and actin-binding proteins. 8(8).

[140] Thomas D. Pollard and John A. Cooper. Quantitative analysis of the effect of acanthamoeba profilin on actin filament nucleation and elongation. 23(26):6631–6641.

[141] M. Pring, A. Weber, and M. R. Bubb. Profilin-actin complexes directly elongate actin filaments at the barbed end. 31(6):1827–1836.

[142] Britta Qualmann and Michael M. Kessels. New players in actin polymerization–WH2-domain-containing actin nucleators. 19(6):276–285.

[143] Margot E. Quinlan, John E. Heuser, Eugen Kerkhoff, and R. Dyche Mullins. Drosophila spire is an actin nucleation factor. 433(7024):382–388.

[144] Aashish Ranjan, Brad T. Townsley, Yasunori Ichihashi, Neelima R. Sinha, and Daniel H. Chitwood. An intracellular transcriptomic atlas of the giant coenocyte caulerpa taxifolia. 11(1):e1004900.

[145] Shmuel Razin. Mycoplasmas. In Samuel Baron, editor, *Medical Microbiology*. University of Texas Medical Branch at Galveston, 4th edition.

[146] Viviana I. Risca, Evan B. Wang, Ovijit Chaudhuri, Jia Jun Chia, Phillip L. Geissler, and Daniel A. Fletcher. Actin filament curvature biases branching direction. 109(8):2913–2918.

[147] Francisco Rivero, Tetsuya Muramoto, Ann-Kathrin Meyer, Hideko Urushihara, Taro Q. P. Uyeda, and Chikako Kitayama. A comparative sequence analysis reveals a common GBD/FH3-FH1-FH2-DAD architecture in formins from dictyostelium, fungi and metazoa. 6:28.

[148] Stéphane Romero, Christophe Le Clainche, Dominique Didry, Coumaran Egile, Dominique Pantaloni, and Marie-France Carlier. Formin is a processive motor that requires profilin to accelerate actin assembly and associated ATP hydrolysis. 119(3):419–429.

[149] Guillaume Romet-Lemonne and Antoine Jégou. Mechanotransduction down to individual actin filaments. 92(10):333–338.

[150] Klemens Rottner, Jan Hänisch, and Kenneth G. Campellone. WASH, WHAMM and JMY: regulation of arp2/3 complex and beyond. 20(11):650–661.

[151] Klemens Rottner, Theresia E. B. Stradal, and Juergen Wehland. Bacteria-host-cell interactions at the plasma membrane: stories on actin cytoskeleton subversion. 9(1):3–17.

[152] Jeremy D. Rotty, Congying Wu, Elizabeth M. Haynes, Cristian Suarez, Jonathan D. Winkelman, Heath E. Johnson, Jason M. Haugh, David R. Kovar, and James E. Bear. Profilin-1 serves as a gatekeeper for actin assembly by arp2/3-dependent and -independent pathways. 32(1):54–67.

[153] André Schönichen and Matthias Geyer. Fifteen formins for an actin filament: A molecular view on the regulation of human formins. 1803(2):152–163.

[154] Bonnie J. Scott, Erin M. Neidt, and David R. Kovar. The functionally distinct fission yeast formins have specific actin-assembly properties. 22(20):3826–3839.

[155] D Sept and J A McCammon. Thermodynamics and kinetics of actin filament nucleation. 81(2):667–674.

[156] Hanshuang Shao, Chuanyue Wu, and Alan Wells. Phosphorylation of alpha-actinin 4 upon epidermal growth factor exposure regulates its interaction with actin. 285(4):2591–2600.

[157] Shashank Shekhar, Mikael Kerleau, Sonja Kühn, Julien Pernier, Guillaume Romet-Lemonne, Antoine Jégou, and Marie-France Carlier. Formin and capping protein together embrace the actin filament in a ménage à trois. 6.

[158] Vladimir Sirotkin, Christopher C. Beltzner, Jean-Baptiste Marchand, and Thomas D. Pollard. Interactions of WASp, myosin-i, and verprolin with arp2/3 complex during actin patch assembly in fission yeast. 170(4):637–648.

[159] Vladimir Sirotkin, Julien Berro, Keely Macmillan, Lindsey Zhao, and Thomas D. Pollard. Quantitative analysis of the mechanism of endocytic actin patch assembly and disassembly in fission yeast. 21(16):2894–2904.

[160] B. Sjöblom, A. Salmazo, and K. Djinović-Carugo. Alpha-actinin structure and regulation. 65(17):2688–2701.

[161] Colleen T. Skau, David S. Courson, Andrew J. Bestul, Jonathan D. Winkelman, Ronald S. Rock, Vladimir Sirotkin, and David R. Kovar. Actin filament bundling by fimbrin is important for endocytosis, cytokinesis, and polarization in fission yeast. 286(30):26964–26977.

[162] Colleen T. Skau and David R. Kovar. Competition between fimbrin and tropomyosin regulates endocytosis and cytokinesis kinetics in fission yeast. 20(16):1415–1422.

[163] Kalomoira Skoumpla, Arthur T. Coulton, William Lehman, Michael A. Geeves, and Daniel P. Mulvihill. Acetylation regulates tropomyosin function in the fission yeast schizosaccharomyces pombe. 120:1635–1645.

[164] J. Victor Small, Theresia Stradal, Emmanuel Vignal, and Klemens Rottner. The lamellipodium: where motility begins. 12(3):112–120.

[165] J. A. Spudich and S. Watt. The regulation of rabbit skeletal muscle contraction. i. biochemical studies of the interaction of the tropomyosin-troponin complex with actin and the proteolytic fragments of myosin. 246(15):4866–4871.

[166] Benjamin C. Stark, Thomas E. Sladewski, Luther W. Pollard, and Matthew Lord. Tropomyosin and myosin-II cellular levels promote actomyosin ring assembly in fission yeast. 21(6):989–1000.

[167] J. Strand, M. Nili, E. Homsher, and L. S. Tobacman. Modulation of myosin function by isoform-specific properties of saccharomyces cerevisiae and muscle tropomyosins. 276(37):34832–34839.

[168] F. B. Straub and G. Feuer. [adenosine triphosphate, the functional group of actin]. 2(2):141–151.

[169] Xiaolei Su, Jonathon A. Ditlev, Michael K. Rosen, and Ronald D. Vale. Reconstitution of TCR signaling using supported lipid bilayers. 1584:65–76.

[170] Cristian Suarez, Robert T. Carroll, Thomas A. Burke, Jenna R. Christensen, Andrew J. Bestul, Jennifer A. Sees, Michael L. James, Vladimir Sirotkin, and David R. Kovar. Profilin regulates f-actin network homeostasis by favoring formin over arp2/3 complex. 32(1):43–53.

[171] Cristian Suarez and David R. Kovar. Internetwork competition for monomers governs actin cytoskeleton organization. 17(12):799–810.

[172] T. M. Svitkina and G. G. Borisy. Arp2/3 complex and actin depolymerizing factor/cofilin in dendritic organization and treadmilling of actin filament array in lamellipodia. 145(5):1009–1026.

[173] Matthew P. Swaffer, Andrew W. Jones, Helen R. Flynn, Ambrosius P. Snijders, and Paul Nurse. Quantitative phosphoproteomics reveals the signaling dynamics of cell-cycle kinases in the fission yeast schizosaccharomyces pombe. 24(2):503–514.

[174] M. Symons, J. M. Derry, B. Karlak, S. Jiang, V. Lemahieu, F. Mccormick, U. Francke, and A. Abo. Wiskott-aldrich syndrome protein, a novel effector for the GTPase CDC42hs, is implicated in actin polymerization. 84(5):723–734.

[175] Haosu Tang, Damien Laporte, and Dimitrios Vavylonis. Actin cable distribution and dynamics arising from cross-linking, motor pulling, and filament turnover. 25(19):3006–3016.

[176] L. G. Tilney and D. A. Portnoy. Actin filaments and the growth, movement, and spread of the intracellular bacterial parasite, listeria monocytogenes. 109(4):1597–1608.

[177] M. Toya, F. Motegi, K. Nakano, I. Mabuchi, and M. Yamamoto. Identification and functional analysis of the gene for type i myosin in fission yeast. 6(3):187–199.

[178] D. Vavylonis, J.-Q. Wu, S. Hao, B. O'Shaughnessy, and T. D. Pollard. Assembly mechanism of the contractile ring for cytokinesis by fission yeast. 319(5859):97–100.

[179] Ana Virel and Lars Backman. Molecular evolution and structure of alpha-actinin. 21(6):1024–1031.

[180] Hui Wang and Dimitrios Vavylonis. Model of for3p-mediated actin cable assembly in fission yeast. 3(12):e4078.

[181] Raymond W Washington and David A Knecht. Actin binding domains direct actin-binding proteins to different cytoskeletal locations. 9(1).

[182] N. Watanabe, P. Madaule, T. Reid, T. Ishizaki, G. Watanabe, A. Kakizuka, Y. Saito, K. Nakao, B. M. Jockusch, and S. Narumiya. p140mdia, a mammalian homolog of drosophila diaphanous, is a target protein for rho small GTPase and is a ligand for profilin. 16(11):3044–3056.

[183] M. D. Welch, J. Rosenblatt, J. Skoble, D. A. Portnoy, and T. J. Mitchison. Interaction of human arp2/3 complex and the listeria monocytogenes ActA protein in actin filament nucleation. 281(5373):105–108.

[184] Alaina H. Willet, Nathan A. McDonald, K. Adam Bohnert, Michelle A. Baird, John R. Allen, Michael W. Davidson, and Kathleen L. Gould. The f-BAR cdc15 promotes contractile ring formation through the direct recruitment of the formin cdc12. 208(4):391–399.

[185] Jonathan D. Winkelman, Colleen G. Bilancia, Mark Peifer, and David R. Kovar. Ena/VASP enabled is a highly processive actin polymerase tailored to self-assemble parallel-bundled f-actin networks with fascin. 111(11):4121–4126.

[186] Jonathan D. Winkelman, Cristian Suarez, Glen M. Hocky, Alyssa J. Harker, Alisha N. Morganthaler, Jenna R. Christensen, Gregory A. Voth, James R. Bartles, and David R. Kovar. Fascin- and α-actinin-bundled networks contain intrinsic structural features that drive protein sorting. 26(20):2697–2706.

[187] D. Winter, T. Lechler, and R. Li. Activation of the yeast arp2/3 complex by bee1p, a WASP-family protein. 9(9):501–504.

[188] Benjamin A. Wolfe and Kathleen L. Gould. Split decisions: coordinating cytokinesis in yeast. 15(1):10–18.

[189] J. Q. Wu, J. Bähler, and J. R. Pringle. Roles of a fimbrin and an alpha-actinin-like protein in fission yeast cell polarization and cytokinesis. 12(4):1061–1077.

[190] Jian-Qiu Wu, Jeffrey R. Kuhn, David R. Kovar, and Thomas D. Pollard. Spatial and temporal pathway for assembly and constriction of the contractile ring in fission yeast cytokinesis. 5(5):723–734.

[191] Jian-Qiu Wu and Thomas D. Pollard. Counting cytokinesis proteins globally and locally in fission yeast. 310(5746):310–314.

[192] Jian-Qiu Wu, Vladimir Sirotkin, David R. Kovar, Matthew Lord, Christopher C. Beltzner, Jeffrey R. Kuhn, and Thomas D. Pollard. Assembly of the cytokinetic contractile ring from a broad band of nodes in fission yeast. 174(3):391–402.

[193] Jingyuan Xu, Denis Wirtz, and Thomas D. Pollard. Dynamic cross-linking by α-actinin determines the mechanical properties of actin filament networks. 273(16):9570–9576.

[194] Helen L. Yin and Paul A. Janmey. Phosphoinositide regulation of the actin cytoskeleton. 65(1):761–789.

[195] Ann Yonetani, Raymond J. Lustig, James B. Moseley, Tetsuya Takeda, Bruce L. Goode, and Fred Chang. Regulation and targeting of the fission yeast formin cdc12p in cytokinesis. 19(5):2208–2219.

[196] Haneul Yoo, Elizabeth A. Roth-Johnson, Batbileg Bor, and Margot E. Quinlan. Drosophila cappuccino alleles provide insight into formin mechanism and role in oogenesis. 26(10):1875–1886.

[197] Michael E. Young, John A. Cooper, and Paul C. Bridgman. Yeast actin patches are networks of branched actin filaments. 166(5):629–635.

[198] Sally H. Zigmond, Marie Evangelista, Charles Boone, Changsong Yang, Arvin C. Dar, Frank Sicheri, Joe Forkey, and Martin Pring. Formin leaky cap allows elongation in the presence of tight capping proteins. 13(20):1820–1823.

[199] Dennis Zimmermann, Kaitlin E. Homa, Glen M. Hocky, Luther W. Pollard, Enrique M. De La Cruz, Gregory A. Voth, Kathleen M. Trybus, and David R. Kovar. Mechanoregulated inhibition of formin facilitates contractile actomyosin ring assembly. 8(1).

[200] Dennis Zimmermann, Alisha N. Morganthaler, David R. Kovar, and Cristian Suarez. In vitro biochemical characterization of cytokinesis actin-binding proteins. 1369:151–179.